Published in final edited form as:
Chem Rev. 2014 April 23; 114(8): 4496–4539. doi:10.1021/cr400477t.

Lanthanide Probes for Bioresponsive Imaging

Marie C. Heffern[‡,a], **Lauren M. Matosziuk**[‡,a], and **Thomas J. Meade**[*,a]

[a]Department of Chemistry, Molecular Biosciences, Neurobiology, Biomedical Engineering, and Radiology, Northwestern University, Evanston, Illinois 60208-3113

1. Introduction

The chemistry of the less familiar elements is a fascinating topic especially for the inorganic minded. The lanthanides, or rare earths, comprise the 5d block of the periodic table and represent a huge array of applications from catalysis to lasers, and of course, imaging agents.[1]

Recent advances in luminescence and magnetic resonance microscopy have, in part, been stimulated by extraordinary success in the development of new lanthanide probes. The unique properties of the lanthanides provide for a deep tool chest for the chemist, biologist and the imaging scientist to exploit, and that exploitation is in full swing.

In this review we focus on two classes of lanthanide probes that are subsets of the larger area of metalloimaging: luminescent and magnetic lanthanides. In Section 2 we discuss the general design and photophysical properties of lanthanides and how these parameters are tuned to develop bioresponsive probes for optical imaging. In Section 3 we provide a brief description of how MR images are acquired and the how MRI contrast agents are engineered to respond to biological events of interest. These guiding principles have driven research that has produced a truly diverse number of new agents that are target specific and bioresponsive (or bioactivatable). While other imaging modalities utilize lanthanide-based probes, these topics are beyond the scope of this review. We direct the reader to explore some excellent reviews in the important areas of radiometals and multimodal imaging.[2–5]

2. Lanthanide Probes for Optical Imaging

Optical imaging is a high resolution and sensitive technique with fast response times that when coupled with magnetic resonance imaging (MRI) can provide researchers with a truly powerful one-two punch.[3,4] As with MRI, optical imaging uses non-ionizing radiation and the signal or contrast can be designed for modulation in response to biological events.[6–8] While optical imaging does not possess the high spatial resolution or depth penetration of MRI, the technique is highly sensitive and semi-quantitative, requiring low concentrations of the probe to produce high contrast images and cellular and subcellular resolution.[3,9]

[*]CORRESPONDING AUTHOR: Thomas J. Meade, Department of Chemistry, Molecular Biosciences, Neurobiology, Biomedical Engineering, and Radiology, Northwestern University, Evanston, Illinois 60208-3113, Phone: 847-491-2841, Fax: 847-491-3832, tmeade@northwestern.edu.
[‡]These authors contributed equally to this work.

Lanthanide-based luminescent probes are particularly attractive for their long luminescence lifetimes. The long decay times offer a tremendous advantage for the time-gated detection of biological samples (such as in time-resolved luminescence microscopy) wherein interfering short-lived autofluorescence and scattering is suppressed, drastically improving signal-to-noise ratio and increasing overall probe sensitivity.[10–12]

Lanthanides possess intrinsic luminescence that originates from f-f electron transitions in the $4f^n$ shell of the $[Xe]5s^25p^6$ configuration and offer unique properties for optical imaging contrast agents that address current limitations of their organic counterparts.[1,13,14] First, due to shielding by the 5s and 5p orbitals, the 4f orbitals do not directly participate in chemical bonding. The emission wavelengths of lanthanides are thus minimally perturbed by the surrounding matrix and ligand field, resulting in sharp, line-like emission bands with the same fingerprint wavelengths and narrow peak widths of the corresponding free Ln(III) salts. Second, the f-f transitions are formally forbidden by the spin and Laporte rule and feature long excited state lifetimes in the milli- to microsecond range.[13,15] This property lends luminescent lanthanides to time-gated or time-resolved live-cell or in vivo imaging that enhance signal-to-noise ratios through elimination of interferences from scattering and short-lived autofluorescence of biological constituents. Finally, since the differences in electronic properties between the different Ln(III) ions reside in the shielded 4f orbitals, varying the metal center imposes minor effects on the chemical properties of the Ln(III) complex, allowing for facile multiplexing for ratiometric or multimodal applications.

2.1 Introduction to Luminescent Lanthanides as Optical Contrast Agents

2.1.1 The Antenna Effect—Although the excited state lifetimes of Ln(III) complexes are long, the forbidden f-f transitions suffer the consequence of weak intrinsic luminescence due to low molar absorptivity.[1,13] Intense light sources such as lasers are required to populate the excited states of Ln(III) ions by direct excitation and are impractical for the majority of biological imaging.[14,16,17] Attachment of a light-harvesting antenna circumvents this limitation by sensitizing the Ln(III) ion in what has been termed as the antenna effect (Figure 1A).[7,14,18–20] Light absorbed to the short-lived singlet excited state of the antenna (S0 → S1) can undergo intersystem crossing to the longer-lived triplet excited state (S1 → T1). Sensitization occurs by population of the lowest ^5D_J excited state of the lanthanide through energy transfer from the T_1 state of the antenna. Energy transfer can also occur from the S_1 state, but energy transfer from the T_1 state is generally accepted as the mechanism due to its longer lifetime.[7,13,19] Electronic transitions from the ^5D_J excited state to the ^7F_J ground state of the lanthanide emits photons characterized by a series of bands in the visible (Eu(III) and Tb(III)) and near-IR (Dy(III) and Sm(III)) wavelengths. Figure 1B depicts $^5D_0 \rightarrow {}^7F_J$ transitions (ΔJ = 0, 1, 2, 3, 4, and 5) for Eu(III) and from the $^5D_4 \rightarrow {}^7F_J$ transitions (ΔJ = 2, 3, 4, 5, 6) for Tb(III) with commonly observed wavelengths. Based on this mechanism, most existing lanthanide-based optical probes comprise three major components: a luminescent metal center, a protective chelate, and a sensitizing antenna.[8,21]

2.1.2 Designing Luminescent Lanthanides for Biological Imaging—The emission intensity or brightness (B) of an emissive lanthanide can be expressed in simplified form as:

$$B = \varepsilon \phi_{Tot} \quad (2.1)$$

where ε is the molar extinction coefficient of the system and Φ_{Tot} is the total quantum yield.[23,24] In a sensitized lanthanide system, Φ_{Tot} can be expressed in terms of the intrinsic quantum yield of the lanthanide ion (Φ_{Ln}) and the sensitization efficiency (η_{sens}). The ε term is primarily based on molar absorptivity of the $S_0 \rightarrow S_1$ transition of the antenna (ε_{Ant}). In simplified form, η_{sens} can be further expressed as a product of the efficiency of intersystem crossing (ISC) between the antenna excited states (η_{ISC}) and the $T_1 \rightarrow {}^5D_J$ energy transfer (η_{ET}), so that the total quantum yield and brightness can be described as:

$$\phi_{Tot} = \phi_{Ln} \eta_{ISC} \eta_{ET} \quad (2.2)$$

$$B = \varepsilon_{Ant} \phi_{Ln} \eta_{ISC} \eta_{ET} \quad (2.3)$$

The discrete components of sensitized lanthanide chelates must be carefully designed to cooperatively maximize these terms while displaying stability and compatibility with biological media.[25]

2.1.2.1 Lanthanide Metal Center: The choice of metal center influences luminescence intensity, emission wavelength, and excited state lifetime. The luminescence intensity is directly related to Φ_{Ln} and is influenced by the competitiveness of radiative versus non-radiative energy decay. The intrinsic emission intensity of a given Ln(III) ion is based on the energy gap between the lowest excited state and highest ground state level. This criterion dictates that Gd(III) is the most luminescent; however, it emits in the far-UV region (around 310 nm), making Gd(III) chelates impractical for biological applications.[13,18] In contrast, Sm(III) and Dy(III) display favorable emission wavelengths in the near-IR region. However, their lower excited state energies make them susceptible to energy dissipation through non-radiative processes, decreasing emission intensity and luminescence lifetimes.

Eu(III) and Tb(III) chelates have received considerable attention due to several factors. 1) The emission intensities are higher than Sm(III) and Dy(III) while displaying biologically appropriate emission wavelengths in the visible region (Figure 1B).[18] 2) Eu(III) and Tb(III) probes display long luminescent lifetimes in the millisecond range, in contrast to the nanosecond lifetimes of most organic fluorophores and microsecond lifetimes of Sm(III) and Tb(III) complexes, making them extremely advantageous for time-resolved luminescence.[1,13,26,27] 3) Compared to the near-IR emitting lanthanides, Eu(III) and Tb(III) show less sensitivity to quenching by singlet oxygen and by vibrational energy transfer to X-H (X = C, N, O) of the surrounding ligands and matrix. 4) The non-degeneracy of the ${}^5D_0$ emissive states of Eu(III) confers an additional advantage in that it results in well-defined spectra for facile interpretation.[1,14] This is especially useful in the development of responsive probes described in Section 2.2. Subsequent discussions will focus on current progress with Eu(III) and Tb(III) probes, though it should be noted that advances have been made in recent years to address the challenges of near-IR emitting Ln(III) probes.[28–31]

2.1.2.2 Lanthanide Chelates: For biological imaging, lanthanides are typically chelated with multidentate ligands to attenuate the toxicity of free lanthanide ions.[4,6,7,18,32] In luminescent applications, chelation serves an additional role of protecting the metal center from solvent coordination. Coordination of water molecules shorten the excited state lifetimes of the Ln(III) ions through non-radiative vibrational energy transfer to the high-frequency O-H oscillator (this is in contrast to the beneficial effects on relaxivity with MRI contrast agents, as will be discussed in Section 3.1).[25,33,34] Thus, *q*, the number of water molecules coordinated to the Ln(III) center (i.e. inner sphere water molecules) highly influences lanthanide emission. This parameter can be quantified using the luminescence lifetimes in H_2O and D_2O:

$$q = \mathrm{A}(1/\tau_{\mathrm{H2O}} - 1/\tau_{\mathrm{D2O}} - \mathrm{B}) \quad (2.4)$$

where A and B are intrinsic properties of the Ln(III) ion.[35,36] Chelates minimize *q* via coordinative saturation or steric crowding of the metal center, thereby attenuating solvent quenching and maximizing the Φ_{Ln} term.

For use as cellular probes, the chelate must form a complex that stably saturates the Ln(III) coordination sphere over wide pH range and resists hydrolysis.[25] Given the hard-acid nature of lanthanide ions, hard bases, such as carboxylic acids, amides, and pyridines are typically implemented as ligands. Macrocycles (such as DOTA derivatives) and open nona- or octadentate chelates (such as DTPA derivatives) equipped with sterically bulky arms are commonly used for luminescent applications.[7,19] Increasing the rigidity of the chelate itself can further minimize energy loss through other X-H (X = C, N, O) vibrations of the chelate.[37]

2.1.2.3 Sensitizing Antennae: The antenna should possess a high molar absorptivity (high ε_{Ant}) for the $S_0 \rightarrow S_1$ transition. Ideal excitation wavelengths (λ_{ex}) should be >340 nm to permit the use of quartz optics and minimize interfering excitation by chromophores in biological media (such as tryptophan and NADH).[19,25] Antennae for luminescent lanthanides are generally limited to excitations <420 nm due to energy requirements, namely a sufficiently small singlet-triplet state energy gap for efficient ISC and a triplet state energy that is greater than the excited state of the Ln(III) excited state.[38]

Upon absorption, ISC from the S_1 into the T_1 state must be favored over competing radiative (antenna fluorescence) and non-radiative relaxation back to the S_0 ground state to achieve a high η_{ISC}. This is most efficient when the ΔE between the T_1 and S_1 is <7000 cm^{-1}.[7] The Ln(III) ion in the chelate serves as a sensitizer for ISC to the triplet state (in addition to being an energy acceptor) due to the increased spin-orbit coupling from the heavy-atom effect, making ISC faster in a chelated lanthanide than with the free chromophore.[39]

The η_{ET} of the T_1(antenna) → ^5D_J(Ln) is determined by the energy gap between the two states. The energy of this triplet state must be slightly higher in energy than the ^5D_J of the lanthanide (20,400 cm^{-1} for the $^5D_4$ of the Tb(III) ion and 17,200 cm^{-1} for the $^5D_0$ of the Eu(III) ion) but with sufficiently large ΔE to minimize back-energy transfer.[1,14] Such thermal repopulation of the T_1 manifold can be avoided with ΔE ≥ 1850 cm^{-1}.[40] Electron

transfer must be favored over competing $T_1 \rightarrow S_0$ phosphorescence or non-radiative energy dissipation. Beyond the energy requirements, both excited states of the antenna should be resilient to quenching through electron or charge transfer from singlet oxygen, anions and electron rich species.[15,25]

The majority of luminescent lanthanide probes covalently attach the antenna to a chelate (such as the aforementioned DOTA and DTPA) through a linker or spacer, termed here as a *pendant antenna* (Figure 2). Pendant antennae are generally believed to sensitize the lanthanide ion through Förster resonance energy transfer.[19] This mechanism is governed by dipole-dipole coupling (between the T_1 of the antenna and the 4f orbitals of the lanthanide) with an efficiency of $1/r^6$, where r is the distance between the antenna and lanthanide. The pendant antenna design is attractive for ensuring stable coordinative saturation, as modular changes in the antenna and linker can be made for the desired application with minimal effect on the protective chelate.

Pendant antennae are often derived from existing organic chromophores with well-defined fluorescence profiles that are appropriate for the sensitization energy requirements.[41–45] The photophysical properties of Eu(III) and Tb(III) sensitizers such as azaxanthone, phenanthridine, and tetracycline, have been extensively studied in the context of lanthanide probes for time-resolved luminescent bioassays and are being applied to cellular imaging applications (Figure 2B).[1,7,19,42,46–48] While translation of these lanthanide probes into cellular systems is still in its early stages, the Parker group has recently performed extensive evaluation on the cellular localization and uptake profiles of pendant antennae systems with various sensitizers and linkers. These studies have provided valuable design principles for targeting probes to the desired biological compartments.[46,49,50] We refer the reader to excellent reviews and articles that have been recently published on this subject.[7,25,46,49–52]

Improving sensitization efficiency of pendant antennae has focused on increasing η_{ET} through either decreasing linker length or using antennae that can directly coordinate to the metal center.[53] In addition to improving Förster energy transfer through decreased r, coordinating pendant antennae can undergo energy transfer via the Dexter mechanism. The Dexter (or exchange) mechanism is a double electron transfer that occurs through orbital overlap with an efficiency proportional to $1/e^r$.[19] The photophysical benefits of these antennae have been exemplified with tetraazatriphenylene. Tetraazatriphenylene contains a Ln(III)-coordinating nitrogen and possesses fast η_{ISC} (T_1 = 24000 cm^{-1}, S_1=29000 cm^{-1}). Furthermore, it is difficult to oxidize since it is electron poor, making it a promising antenna for producing bright luminescence.[38]

In addition to decreasing distance, the overall η_{Sens} can be improved by increasing the number of pendant antennae attached to a single chelate.[19,54–56] Walton et al. recently investigated cellular imaging properties of highly luminescent Eu(III) probes that incorporated three pendant pyridylalkynyl antennae into a chelate derived from triaazacyclononane (Figure 3).[54] Coordinative saturation was achieved by direct antenna coordination through the pyridine nitrogens and *p*-substitution of the pyridyl moiety with Eu(III)-coordinating phosphinate or carboxylate arms. At λ_{ex} values between 310–340 nm, exceptional brightness was observed with reported ε values of 55–60,000 $M^{-1}cm^{-1}$ (more

than 10 times higher than any previously reported 1:1 EuL system where L = chelate derivatized with pendant antenna) and Φ_{Tot} as high as 59%. Further, these probes were efficiently taken up in NIH 3T3 cells and localized in the mitochondria. This highly emissive platform was extended to responsive probes (as discussed in Section 2.2.1), and demonstrates the promise of such a design in developing bright probes with pendant antennae.

Higher absorbing antennae with efficient ISC have been achieved with d-f bimetallic complexes where d-metal complexes can serve as the sensitizing pendant antenna. Due to the heavy atom effect, ISC is highly efficient and several transitions can be accessed from intraligand transfers to metal-to-ligand charge transfer (MLCT) transitions.[57–65] However, little progress has been made in translating these systems to cellular applications and will not be discussed in detail here. We refer the reader to two reviews on the progress of these bimetallic systems.[63,64]

An alternative approach to pendant antennae for achieving bright emission is the use of chromophores that simultaneously serve as the protective multidentate chelates, termed here as *chelating antennae* (Figure 4).[19] As with coordinating antennae, chelating antennae can sensitize Ln(III) luminescence by both Förster and Dexter energy transfer. Since the first introduction of their class by Lehn et al. with bipyridine- and 1,10-phenanthroline-containing cryptands, many chelating antennae have been developed for biological applications, some of which are shown in Figure 4B.[22,66] In addition to energy matching, their use in biological applications require that they be kinetically inert to hydrolysis, saturate the metal center to prevent water access, water-soluble, and taken up by cells for cellular imaging. These requirements have limited these sensitizers to derivatives of simple aromatic structures, such as pyridines and isophthalamides.

In recent years, Raymond and coworkers have developed chelating antennae based on 2-hydroxyisophthalamide (IAM) as a binding unit to sensitize Tb(III).[19,70,71] Coordination of IAM occurs through the phenolate oxygen and the adjacent carbonyl oxygen (salicylate-type binding as shown in Figure 4B, top left). The amide of the other carbonyl forms a hydrogen bond with the phenolic oxygen and stabilizes a favorable ligand conformation for metal coordination. Initial evaluations of the sensitization efficiency of IAM binding units observed remarkably high Φ_{Tot}. This led to the development of octadentate ligands comprising a series of connected IAM binding units.[72] While favorable properties of the free IAM unit, such as high molar absorptivity and quantum yield (ε = 26800 $M^{-1}cm^{-1}$, φ = 59%, τ = 2.6) were retained, the first generation of octadentate IAM derivatives were not water-soluble.

Samuel et al. improved solubility without compromising spectroscopy by substituting the amide methyl with methoxyethyl and retained excellent photophysical properties ($\varepsilon \approx$ 27000, φ = 56%, τ = 2.6).[71] The Raymond group has similarly developed 1-hydroxy-pyridine-2-one (HOPO) for Eu(III) sensitization.[19,73,74] Generally, the HOPO-derived ligands (which coordinate to the metal center in a catecholate-type manner) are more stable than the IAM ligands. However, HOPO-type ligands display lower quantum yields and are incapable of sensitizing Tb(III) due their energies being too close to the excited state of

Tb(III). As with most chelating antennae, HOPO and IAM based chelates are currently confined to bioassays (not intracellular applications).

Yuan and coworkers have explored the use of polyacid-based chelating antennae for cellular applications.[69] These probes sensitize Tb(III) and Ln(III) through pyridine and pyrazole moieties incorporated into the chelate backbone (Figure 4B, bottom). As probes of this type have been developed primarily for bioresponsive applications (where R = the bioresponsive unit), these will be discussed in more detail in Section 2.2.3. Briefly (for intracellular analyte detection), pro-chelates in which the acetates are protected with esters are added to cells alongside the free lanthanide salt. Upon cleavage of the esters with intracellular esterases, the probes self-assemble to form the chelated lanthanide complex with sensitized emission.[75,76]

While stringent requirements on stability, solubility, and photophysical properties have limited advances of chelating antenna systems in intracellular applications, the examples highlighted here can inform future design. Such prospects are highly attractive for the remarkable sensitization efficiencies and circularly polarized luminescence applications as described in the next section (Section 2.1.2.4).

2.1.2.4 Circularly Polarized Luminescence: Circularly polarized luminescence (CPL) has emerged as another important parameter in the design of luminescent lanthanides.[77–81] CPL is the luminescence analogue of circular dichroism. It is the measurement of chiroptical activity of excited state emission, (i.e. the differential emission of left and right circularly polarized light). At a given wavelength of emission (λ_{em}) CPL is measured in terms of the dissymmetry factor, g_{em} as:

$$g_{em}=\frac{2(I_L - I_R)}{I_L+I_R} \quad (2.5)$$

where I_L and I_R are the right and left circularly polarized components of the radiation. The CPL signal is influenced by the chirality imposed by the coordination environment of the chelate about the Ln(III) center, or other structural factors of the chelate such as helicity from side arms.[81]

Much recent work has sought to develop chiral and enantiopure lanthanide complexes that can produce well-defined CPL signals.[77,79,81] In particular, Raymond and coworkers have explored enantiopure forms of the IAM and HOPO ligands that possess both high Φ_{Tot} and strong CPL activity. While the earlier reported chiral IAM complexes retained brightness of the parent complexes, modest CPL activity was observed. CPL activity was improved by increasing the rigidity of the complex to produce cyLI-IAM the complex as a chiral Tb(III) sensitizer (Figure 5).[70] While cyLI-IAM is tetradentate (to form ML_2 complexes with Tb(III)) and likely less stable than an octadentate counterpart, its fairly straightforward synthesis made it a good model to evaluate the effects of minor structural changes of the chelate on CPL activity.

Another rigid tetradentate IAM derivative was evaluated alongside cyLI-IAM that incorporated phenyl groups on the chiral ethylenediamine region of the ligand (dpenLI-

IAM) rather than the cyclohexyl modification of cyLI-IAM. The Tb(III) complex of cyLI-IAM complex retained the high quantum yield of its octadentate counterpart (Φ_{Tot} = 60%) whereas dpenLI-IAM exhibited a decrease in quantum yield ($\Phi_{To\tau}$ = 32%). This was attributed to differential solvent access, with cyLI-IAM efficiently blocking water coordination (q = 0) and dpenLI-IAM resulting in a mixture of complexes with q = 0 and q = 1. Both ligands displayed an increase in CPL activity in contrast to previously reported IAM ligands, demonstrating the importance of rigidity in enhancing chiroptical activity.[77,79] The use of CPL in biological reporting has advanced in the recent years and will be discussed in detail in Section 2.2.4.

2.2 Bioresponsive Modulation of Lanthanide Luminescence

The last decade has seen major advances in bioresponsive luminescent lanthanides that can sense biological analytes or environments through alterations in photophysical behavior of the probe.[4,8,25,82] Researchers have taken advantage of the number of required components in sensitized lanthanides to modulate luminescence intensity, excited state lifetimes, and emission profiles (λ_{em}) in response to biological stimuli. The high sensitivity and fast imaging time of optical imaging makes these types of lanthanide complexes ideal for the detection of low concentration analytes and dynamic cellular processes. While early examples of responsive probes focused primarily on their use for bioassays (e.g. immunoassays), this work has ushered in promising developments in lanthanide-based optical sensors for intracellular imaging.[19,23]

Particular focus has been placed on using lanthanide probes for quantitative analysis.[21,83] Many existing luminescent probes rely on short-lived fluorescence emission at single wavelengths.[23,55,84] These probes can suffer from inaccurate quantitation due to various interferences such as photobleaching, background absorbance or emission, scattering, and reliance on probe concentration. Analyte binding or chemical alterations to the probe may further contribute to unreliable quantitation by altering uptake efficiency and localization. As previously discussed, the long-lived luminescence of lanthanides addresses some of these challenges by the use of time-resolved luminescence whereby short-lived fluorescence and scattering interferences are minimized. The well-defined sharp emission bands of lanthanide complexes lend themselves to an additional means of accurate quantitation, namely ratiometric analysis.

Ratiometric analysis utilizes an internal calibration process to isolate quantitation from probe concentration. [85–87] As previously mentioned, due to shielding of the 4f orbitals, the Ln(III) center can be interchanged with little change in solubility and biological behavior, but with detectable photophysical differences.[33,75,86,88,89] This property has been harnessed for ratiometric detection using “cocktails” of different lanthanides in a common chelate structure, particularly for detection of analytes that alter coordination properties.[33,75,82,90] For instance, in a “cocktail” of coordinatively unsaturated Eu(III) and Tb(III) complexes, bound water molecules can be displaced with more polarizable anionic analytes. This results in perturbations in the hypersensitive bands of the Eu(III) analogues that can be calibrated against the less sensitive bands of the Tb(III) analogue. Through developing a ratiometric calibration curve, the “cocktail” can measure analyte concentration. An early example of

this approach was demonstrated in the measurement of anions such as urate in biological fluids.[33,91,92]

Alternatively, “cocktails” can be used for ratiometric detection of analytes that alter the antenna to produce differential energy transfer efficiency to the various lanthanide excited states.[86] An early example by Tremblay and coworkers demonstrated this concept with a systematic study of antennae derived from a carbostyril core.[86] Derivatives were synthesized with varying biologically relevant functional groups and their sensitization bias, defined as

$$(\mathrm{I_{Tb}} - \mathrm{I_{Eu}})/(0.5(\mathrm{I_{Tb}} + \mathrm{I_{Eu}})$$

(where I_{Tb} from 530–560 nm and I_{Eu} from 605–630 nm, respectively) were compared (Figure 6). Pairs of derivatives with distinguishable sensitization biases and potential application for bioresponsive switches were identified. The ethoxyester (derivative **19**) and carboxylic acid (derivative **28**) derivatives were selected for a proof-of-concept ratiometric study wherein hog liver esterase hydrolysis activity was measured.

Another common approach to ratiometric analysis uses intensity ratios of selected emission bands in a single Ln(III) complex. The symmetry-forbidden, lanthanide f-f transitions become allowed by induction of magnetic dipole (MD) transitions that are independent of the surrounding ligand, electronic dipole (ED) transitions that are sensitive to the surrounding ligand field and solvent, or a mixture of the two (MD/ED).[13] ED-allowed transitions (and to a lesser extent, ED/MD-allowed transitions) are considered “hypersensitive” to the polarizability of the Ln(III) ligands, and the intensity and form of these bands can inform the coordination environment of the lanthanide. The intensity ratios of hypersensitive bands to the comparatively insensitive MD-allowed bands can thus permit quantitation of analytes that are detected by ligand exchange mechanisms.[26,33,90] The approach is especially useful for Eu(III) probes since the degeneracy of the $^5D_0$ state leads to relatively simple spectra where the ΔJ=2 and ΔJ=4 bands are hypersensitive.[26]

Guided by these principles, four major modes of luminescent signaling to biological analytes have emerged for emissive lanthanide complexes: 1) modulation of bound water molecules 2) altering the distance between the Ln(III) and the antenna to modulate efficiency of energy transfer 3) altering the excited states of the antenna, and 4) affecting the complex chirality that is monitored by CPL.

2.2.1 Modulation of q—The number of waters coordinated to the lanthanide metal center (*q*) influences emission intensity, luminescence lifetime and spectral form.[33] The first two result from vibrational quenching from non-radiative energy dissipation through the O-H oscillator as discussed in Section 2.1.2.2 (Figure 7). The latter stems from the sensitivity of Ln(III) centers to ligand polarizability that can induce asymmetric transformation and allow otherwise forbidden transitions. Hard anionic analytes can coordinatively exchange with Ln(III)-bound waters to relieve quenching and alter spectral form, affording *q*-modulated emissive lanthanide complexes. In fact, the first reported examples of responsive luminescent lanthanide sensors utilized this approach.[82,92,93] The *q*-modulated response by

the presence of an analyte can occur through intramolecular or intermolecular ligand exchange.

Bioresponsive luminescent agents have been designed that rely on *intramolecular q*-modulation. In this strategy, a side arm is attached to the chelate that can reversibly coordinate the metal center.[8] The presence of an analyte alters the coordination propensity of the side arm. Parker et al. have made several advances in probes with this design that can monitor changes in pH through a substituted sulfonamide moiety.[94,95] The sulfonamide reversibly coordinates to the lanthanide center in response to pH. In neutral to high pH, the deprotonated sulfonamide coordinates the Ln(III) center, blocking water access. Low pH environments favor the protonated sulfonamide, making coordination unfavorable and promoting the coordination of one water molecule to the Ln(III) center (Figure 8). Consequently, the coordination environment, and thus, the intensity and spectral form, is altered by changes in pH. While some interference is observed from proteins and endogenous anions such as bicarbonate with this class of Ln(III) complexes, selected emission band ratios have been successfully calibrated against pH for the successful measurement of intracellular pH. The first generation of these probes with azaxanthone and azathioxanthone sensitizers localized in the nucleolus and measured a neutral pH (pH 7.4), as expected, using a calibration curve.

To direct intracellular compartmentalization of the probe, pH-sensitive probes were designed based on insight from localization profile studies of azaxanthone and azathioxanthone lanthanide chelates.[49,50] Based on these studies, an amide spacer was selected to link the azaxanthone sensitizer to promote localization in the lysosomes through macropinocytotic uptake. The Eu(III) and Tb(III) complexes retained the pH-dependent response in the intensity ratios of selected bands and protonation constants were calculated.

Fast and irreversible localization in the lysosomes were observed, and the pH of the lysosomes of live cells was successfully measured with a Tb(III)/Eu(III) “cocktail.”[95] The green/red ratio from the images, corresponding to the Tb and Eu emissions, was used to evaluate pH. Comparable values to a commercial organic dye, LysoSensor Probe (Invitrogen), were obtained. The pH detection with these probes was validated by observed increases in pH in time-course measurements in the presence of the K^+/H^+ ionophore nigericin.

To enhance emission brightness, the pH-sensitive sulfonamide moiety was incorporated into a nonadentate scaffold with two pydridylalkenylaryl pendant chromophores (Figure 9).[96] The complex was derived from a bright luminescent parent molecule that localized in the mitochondria through macropinocytotic processing (Section 2.1.2.3, Figure 9).[54] While retaining the same pH-response through the sulfonamide ligation mechanism, the complex achieved a much higher molar absorptivity and quantum yield (~60000 $M^{-1}cm^{-1}$ and 38%, versus <6000 $M^{-1}cm^{-1}$ and <6% of the azaxanthone-sensitized probe). However, cell uptake was altered from the parent molecule with the probe localizing in endoplasmic reticulum rather than the lysosomes or mitochondria. Nonetheless, the probe was applied to monitor pH changes in the ER (which correlates to cytoplasmic pH given the high proton permeability of the ER) using intensity ratios of selected bands [$\Delta J=2/(\Delta J=1+\Delta J=2)$].

Additionally, pH-response was accompanied by changes in luminescence lifetime, likely due to altered favorability of protein binding. Consequently, luminescence lifetime could be used to measure cytosolic pH with proper calibration.

In addition to intramolecular ligation, *q*-modulation through intermolecular ligation has been demonstrated most prevalently with oxyanions.[33,90,97] These analytes readily bind tricationic Ln(III) centers and undergo ligand exchange with bound water to form ternary complexes with the chelates. Oxyanions (Figure 10) are key metabolites, and detection of their levels in biological fluids and cellular compartments can be used to diagnose cell states and understand biological signaling mechanisms.[33,51] The design of these anion-binding probes must carefully take selectivity and pH-dependence of analyte speciation and binding affinity into consideration. Additionally, as with pH, the utility of the probe is directly affected by its localization profile. Researchers use sterics around the metal center, electrostatics, and linker design to direct molecular selectivity and uptake behavior.[50,98]

Systematic studies of varying lanthanide probes have been used to gain insight into the parameters that govern selectivity and aid development of similar *q*-modulated probes. Pal et al. evaluated a series of azaxanthone- and azathiaxanthone-sensitized Eu(III) macrocyclic complexes that varied by charge and steric crowding (Figure 11).[99] The 3+ charge of the Eu(III) center was modulated with neutral ethyl-esters, negatively charged carboxylates, and glutarates on the macrocyclic side arms to give total charges of 3+, 1+, and 1−, respectively. Steric demand was varied by the side-arm substituents (derived from either alanine or phenylalanine, subsituent R in Figure 11) or by methylation of the secondary amine of the macrocycle (substituent R’ in Figure 11).

Through ratiometric analysis of selected Eu(III) emission bands, binding constants and calibration curves were obtained. Figure 11 represents the ratios of the citrate to lactate binding constants (log K_a) calculated from the reported values. Selectivity for the tri-anionic citrate over the mono-anionic lactate increases with increasing positive charge, consistent with binding through coulombic interactions. Further, increased steric crowding about the metal center increases selectivity for lactate over the larger citrate anion. Using these probes according to the desired selectivity, citrate and lactate levels were measured in biological fluids (urine, seminal, and prostate).[99,100] In contrast to the multicomponent enzymatic methods that are currently available, the detection was fast (< 5 min) and time-gated fluorescence could be used to improve signal-to-noise ratios and consequential quantitation.

While initial use of the probes in quantifying anionic analytes focused on sensors for biological fluids, progress has been made towards applying these probes to cellular and subcellular imaging, such as in the measurement of intracellular bicarbonate concentrations.[8,33] The Parker lab designed a Ln(III) chelate with an amide-linked azaxanthone sensitizer/linker unit that promotes cell internalization by macropinocytosis and directs traffic into the mitochondria (Figure 12).[101,102] In the absence of bicarbonate, the probe was shown to have a *q*=2. Displacement of water by bicarbonate yields a *q*=0 complex with alleviation of the water-induced quenching. In turn, the bicarbonate-bound ternary complex displays increased luminescence and altered spectral form due to changes in the polarizability of the bound axial ligand. While other oxyanions interfered with bicarbonate

binding, bicarbonate exists at relatively high concentrations, making its detection favorable by this mechanism. The exception to this is ATP; rather than increasing luminescence intensity like bicarbonate, ATP-binding decreases emission. The decrease in emission is likely due to antenna quenching by adenosine charge transfer to the triplet state of the electron-poor azaxanthone. Significant protein (serum albumin) binding was also observed and quenched fluorescence (likely through charge transfer with electron-rich aromatic residues, e.g. tyrosine), but did not change spectral form.

With these considerations, a calibration curve in simulated biological media (high concentrations of albumin and ATP) was obtained using ratios of the $\Delta J=2/\Delta J=1$ band intensities, and bicarbonate levels were accurately measured. The Tb(III) analogue served as an emissive calibrant since little change is observed in the emission intensities with carbonate binding (10% versus 250% of Eu). Estimations were made for the equilibrium bicarbonate concentrations in serum and cells with pCO_2 cycling, specifically in the mitochondria. The measurements were validated by a detected reduction in bicarbonate levels in the presence of acetazolamide, a carbonic anhydrase inhibitor.

Several more examples have emerged that demonstrate the potential of intermolecular *q*-modulated agents in biological applications that are not discussed here. We refer the reader to additional examples provided in a recent review by Parker et al.[33]

2.2.2 Modulation of Sensitization by Antenna-Ln Distance—Sensitization of lanthanide complexes occurs via energy transfer from the triplet excited state of the antenna to the metal ion. Researchers have exploited the distance-dependence of this energy transfer process to modulate luminescence through altering the distance between the antenna and the metal center (Figure 13).

The lanthanide-antenna distance has been altered through modulation of the linker upon interacting with the analyte of interest. Pierre et al. designed a Tb(III) probe with a spacer consisting of a crown ether linked to an aryl group for potassium ion (K^+) detection by cation-π interactions.[97] Aryl groups have been shown to complex to potassium ions bound in crown ethers with selectivity over sodium ions (Na^+) due to steric constraints with the latter.[103,104] In the original design, the lanthanide center and an azaxanthone antenna were separated with a crown ether and a phenyl group serving as a flexible linker. In the presence of K^+, simultaneous complexation of the ether and the phenyl to the potassium brings the antenna closer to the lanthanide, resulting in a “turn-on” response with increased luminescence. However, this system showed little effectiveness in aqueous solutions.

A water-soluble europium probe, termed Eu-KPhen was subsequently designed that utilized a phenanthridine group as both the K^+ complexing aryl group and the antenna (Figure 14).[105] The potassium probe exhibited the expected “turn-on” response due to decreased distance between the antenna and the lanthanide, mediated by the cation-π interaction. At biologically relevant concentrations for extracellular detection, (0–12.5 mM K^+), an 83% luminescence increase was observed. At the same concentrations, negligible changes in luminescence were observed for Na^+. At higher concentrations of Na^+ (137 mM) closer to the expected extracellular concentrations, only a 35% increase in intensity was observed.

Time-gated ratiometric detection was performed using the emission from excitation at 267 nm that is sensitive to K^+ concentration and emission from excitation at 400 nm that is sensitive to probe concentration but not K^+ concentration.

Work by Schneider et al. reported a redox sensor that altered antenna-Ln distance through modulating the conformation of a peptidic linker between a Tb(DTPA) chelate and a carbostyril antenna.[106] The linker contained a peptide sequence with a moderate propensity for β-sheet formation with cysteines that could respond to the environment. In reducing conditions, the cysteines remained protonated and the peptide adopted a flexible conformation, resulting in a long antenna-Ln distance and thus, a weakly luminescent species. In contrast, oxidizing conditions induced disulfide bond formation between the cysteines and stabilized a β-sheet conformation, thereby bringing the antenna near the lanthanide and producing a highly luminescent species.

A more drastic change has been observed in the case where the antenna is attached to the lanthanide in the presence of the analyte. Viguier and Hulme took advantage of the catalytic role of copper(I) in Huisgen 1,3-dipolar cycloaddition (“click”) reactions to attach an alkyne-containing europium complex to a dansyl azide antenna (Figure 15).[107] Addition of 10 μM glutathione-coordinated copper(I) to an equimolar mixture of the antenna and lanthanide chelate catalyzed the cycloaddition reaction. The covalent attachment of the antenna near the metal ion produced a 10-fold enhancement in luminescence relative to the unreacted Eu(III) chelate. This sensor is a promising example of how components of existing synthetic methodologies can be manipulated for imaging applications.

Antenna-lanthanide distance can be modulated by the reversible coordination of the antenna to a coordinatively unsaturated lanthanide complex (Figure 16). Reversible antenna coordination modulates both *q* and metal-antenna distance. While “switch on” probes of this class were introduced several decades ago, they are generally limited to the detection of chromophoric analytes such as salicylate and benzoic acid (Figure 16A).[108–110] Modified approaches to “switch on” strategy rely on analyte-driven reactions that assemble the coordinating antenna to then form the sensitized ternary complex with the Ln(III) chelate. Meyer and Karst exemplified this approach for the detection of peroxidase activity. In the presence of peroxidase, *p*-hydroxyphenylpropionic acid served as an enzyme substrate and dimerized to form a biphenol that could coordinate to and sensitize the Tb(III) EDTA complex (Figure 17A).[111] Page and coworkers recently reported a similar strategy to detect hydroxyl radicals by reaction with the pro-antenna, trimesate, to form the coordinating Tb(III) sensitizer 2-hydroxytrimesic acid (Figure 17B).[112]

“Switch off” probes have been developed using the reverse strategy wherein the analyte displaces or catalyzes the dissociation of a coordinating antenna (Figure 16B).[110,113–117] Gunnlaugsson and co-workers have extensively studied this approach for the detection of anions such as tartaric acid.[110,113–115] However, the displacement approach suffers from selectivity as with similar *q*-modulated sensors. Recently, a similar design was implemented in the detection of transition metals that did not solely rely on competitive interactions with the Ln(III) center. Rather, selectivity was driven by competitive coordination of the antenna to the Ln(III) and the transition metal analyte (Figure 18). A substituted phenanthroline that

is known to coordinate metals such as iron was attached to the lanthanide as a sensitizer. In the presence of certain metal ions, such as Fe(II) and Co(II), the phenanthroline dissociates from the lanthanide and coordinates the transition metal (Figure 18).[116]

The approach was translated to the design of a zinc sensor using an 8-hydroxyquinoline antenna.[117] In addition to having a decrease in the near-IR emission of the lanthanide-hydroxyquinoline (Yb form, 800–1100 nm), the resulting Zn-hydroxyquinoline complex exhibited orthogonal spectroscopic emission (400–700 nm), permitting the monitoring of Zn(II) ion concentration by dual emission. To a degree, while the selectivity of the lanthanide was somewhat limited, the dual emission capability of the system confers another degree of control for selective data encoding.

While antenna coordination provides dramatic changes in luminescence through drastic alterations in antenna-Ln(III) distance, these strategies are currently limited to bioassays. The multi-component requirements of the procedures may complicate the cellular localization profiles, hindering progress for live-cell imaging applications.

2.2.3 Modulation of the Antenna Excited State—While *q*-modulation can be useful for anions, altering the antenna excited state through chemoselective reactions with analytes is a promising approach for detecting reactive small molecules.[8,97,118–120] Reactive small molecules such as singlet oxygen, hydrogen peroxide, and nitric oxide are vital for understanding biological processes and signaling molecules.[121–125] Perturbing the antenna excited state is a popular strategy for detecting metals, since metal binding to chromophores can alter their photochemical properties.[116,126] Additionally, antenna transformation has been used to detect enzyme activity.[127,128] In these scenarios sensitizers that have altered photophysical properties upon cleavage of peptide bonds can be used for enzyme-responsive lanthanide sensors.

Advances in bioresponsive organic fluorophores have catalyzed progress in the development of these probes, as insight to the behavior of these chromophores can be translated to the organic antenna. Two major modes have emerged whereupon antenna modulation can alter lanthanide emission: 1) analyte reaction with a caged or pro-antenna to produce a sensitizing antenna, 2) controlling sensitization with electron transfer through switches appended to the antenna or direct analyte interactions with the antenna.

2.2.3.1 Analyte-Triggered Antenna Formation: Lanthanide probes have been developed with pro-antennae that are masked by reactive cages. In this construct the target analyte can react with a caged antenna to then activate the formation of the sensitizer (Figure 19A).[97,128,129] This borrows from analyte-triggered formation approaches of organic fluorophores while conferring advantages of the lanthanide systems, such as long luminescence lifetimes and large Stokes shifts.

Recently, Lippert et al. developed a Tb(III) probe relying on reaction-based sensitization of the lanthanide (Figure 19B).[129] Previous probes for the direct detection of hydrogen peroxide, (such as Eu(III) tetracycline complexes) relied on the exchange of water with hydrogen peroxide, a weaker oscillator and thus a less efficient quencher of lanthanide

luminescence.[130–132] While these probes showed high sensitivity to hydrogen peroxide and exhibited long luminescent lifetimes, they showed poor selectivity against phosphate and citrate, prohibiting live-cell imaging. This challenge was addressed with the reaction-based Tb(III) probes through employing a boronate ester that is chemoselective for hydrogen peroxide to cage or mask the antenna. Reaction of the caged antenna with the analyte produced either an aniline or phenol that could sensitize and switch on the Tb(III) luminescence. These probes were successfully used to detect stimulated hydrogen peroxide production in live cells.

In a similar approach, Pershagen and coworkers reported caged coumarin antennae for bioresponsive sensitization of an array of analytes.[128] Using a coumarin as the antenna core, the cage was varied for the detection of the desired analytes. Specifically phenylboronic acid, triisopropylsilane, allyl, and galactose cages were employed to detect hydrogen peroxide, fluoride, palladium ($Pd^{0/2+}$) and β-galactosidase, respectively. Each caged antenna precursor was synthesized as alkyne-modified building blocks that could be attached to an azide-modified Ln(III) DO3A chelate through facile “click” chemistry. The target analytes could be detected at nano to micromolar concentrations. While selectivity for hydrogen peroxide, fluoride, and the enzyme were not explicitly tested, the palladium probe was selective over other transition metals. Further, the authors demonstrated the simultaneous detection of hydrogen peroxide and fluoride with a mixture of the respective probes with no detectable cross interference.

2.2.3.2 Electron Transfer Switches to Modulate Antenna Sensitization: The sensitization efficiency of antennae can be controlled by appending a switch that is driven by charge or electron transfer.[84,97] In recent years, many of these probes have incorporated photo-induced electron transfer (PeT) switches to control emission derived from PeT-switchable organic fluorophores.[84] In the “off” state of a PeT-switchable emissive lanthanide system, the HOMO of the PeT switch is higher in energy than the S_0 ground state of the antenna. On photo-excitation of the antenna to the S_1 state, the PeT switch donates an electron to pair with the remaining unpaired electron in S_0 ground state of the antenna. The electron transfer process competes with radiative decay and reduces the sensitizing efficiency and, consequently, lanthanide luminescence. To “switch” the probe on, the PeT switch is chemically altered by the analyte so as to decrease the energy of the HOMO to a state lower than the S_0 ground state of the antenna, inhibiting the electron transfer. This, in turn, restores the sensitizing capacity of the antenna, and thus, lanthanide luminescence (Figure 21).

The earliest example of this type of Ln(III) sensor was reported by Terai et al.[127] The feasibility of the approach was demonstrated with a series of DTPA-chelated lanthanide complexes that contained organic moieties (potential PeT switches) of varying HOMO levels (as calculated by DFT) attached to a quinolinone antenna.[127] The quantum yield of luminescence of the different chelates showed a dependence on the HOMO levels of the organic moieties, with higher quantum yields corresponding to the lower HOMO energies.

As a proof-of-concept, a probe for microsomal leucine aminopeptidase (LAP) was designed that utilized aniline as a donor for PeT switching of the quinolinone antenna. In the absence of LAP, the aniline amine was masked as an amide-bonded valine, rendering it a poor PeT

donor (PeT switch “off”) and the quinolinone an efficient sensitizer for lanthanide luminescence. Upon cleavage of the valine-aniline bond by LAP to unmask the aniline, the PeT switch was turned “on”, turning luminescence “off” as a result of antenna quenching via PeT from the aniline. Using this PeT-switchable lanthanide complex, LAP activity could be measured with time-resolved fluorescence measurements. The concept of a switch driven by PeT or alternative electron transfer mechanisms like intramolecular charge transfer (ICT) for controlling Ln(III) luminescence has since advanced towards “turn-on” lanthanide luminescent probes.

Work in the Yuan group has extensively shown the use of antenna switches through PeT or ICT for the detection of reactive small molecules (Figure 23).[75,76,118,133–140] The general design utilizes a polyacid chelating antenna consisting of trispyridinyl-tetrakisacetate (for Eu(III) complexes or Tb(III)/Eu(III) cocktails) or a bispyrazolepyridine-tetrakisacetate for Tb(III) complexes (Figure 4B, bottom, previously discussed in Section 2.1.2.3). The chelating antenna is derivatized with an electron transfer switch on the central pyridine ring that responds to the analyte of interest.

The first of this class was a sensor for singlet oxygen ($^1O_2$) through incorporation of an anthracene switch.[118,135] Previous work had shown that certain organic fluorophores were quenched by covalent attachment to anthracene.[141,142] Quenching was alleviated upon reaction of the anthracene with $^1O_2$ to form an endoperoxide.[141–144] By appending anthracene to the pyridine of the sensitizing polyacid chelate, the resulting Ln(III) complex responds with an increase in luminescence intensity in the presence of $^1O_2$. The system was specific for $^1O_2$ over other reactive oxygen species.

While the probe could not permeate the cell membrane, successful cellular studies were achieved upon administration of the probe in two components: the ester-protected chelate (with the antenna) and the free Ln(III) salt. As outlined in Section 2.1.2.3, upon internalization of the two components, the esters are cleaved by intracellular esterases exposing the polyacids which can then coordinate the lanthanide salt to form the emissive probe (Figure 23A).

Similar switchable chelate platforms were used for other small reactive molecules including HOCl and NO (Figure 23B and C).[75,76,133,134,136–140] Ratiometric cellular detection of the analytes was achieved with Eu(III)/Tb(III) cocktail formulations.[75,134] Additionally, this design was extended to the detection of pH and metal ions.[133,134] While the current method of probe administation may not be ideal for *in vivo* applications, these switchable chelates are promising tools for understanding biological processes at the cellular level.

In some cases, the analyte itself may directly interact with the antenna and alter sensitization through electron transfer processes. Pierre et al. developed a probe for Tb(III) nucleoside phosphates that relies on electron transfer between the analytes and the antenna.[145] The aromatic phenanthridine antenna governed selectivity for nucleoside phosphates over anionic phosphates through **π-π** stacking interactions (Figure 24). Furthermore, the adenosine served as a PeT switch to the phenanthridine antenna, decreasing Tb(III) luminescence. The complex showed differential affinity for the different phosphates (ATP,

ADP, and AMP) due to the tricationic charge of the complex, with highest affinity for the highly negative ATP. The probe was successfully used for the time-gated luminescence detection of ATP at millimolar concentrations relevant to biological conditions.

Antennae-analyte electron transfer can be catalyzed by derivitizing the antenna with a receptor unit specific for the analyte. McMahon & Gunnlaugson recently employed this strategy for the detection of d-metal ions.[146] A phenyl sensitizer of a Tb(III) chelate was derivatized with an iminodiacetate receptor unit. The acetate arms coordinated a series of dicationic transition metals, but only Cu(II) and Hg(II) altered luminescence, quenching overall emission by 65% and 40% respectively. These complexes were used in aqueous environments, making this approach attractive for future d-metal ion detection by luminescent lanthanides.

2.2.4 Modulation of CPL for Analyte Detection—While the majority of lanthanide agents respond to analytes through change in spectral form and emission intensity, recent research is evaluating the chiroptical properties as a means of producing a signal, namely circularly polarized luminescence (CPL).[81] As outlined in Section 2.1.2.4, CPL is measured by the dissymmetry factor, g_{em}. CPL spectroscopy combines the sensitivity of luminescence imaging and the specificity of chiroptical response, and one can envision that the advancement on polarized microscopy will accelerate the use of CPL of lanthanide complexes either in combination with or independent of optical imaging techniques.

Current work in bioresponsive lanthanide probes with CPL detection is limited to biological assays, primarily for sensing protein binding.[81] Since proteins consist of a series of organized chiral structures, CPL is sensitive to protein conformation (Figure 26). While this work was limited to detection of various amino acids, probes have recently emerged that bind to proteins, and by doing so, induce fingerprint signals.[78,81,147]

Carr et al. developed chiral probes for the identification of serum proteins (Figure 27).[147] In earlier work, a europium complex with two axazanthone moieties was shown to bind to serum albumin, likely through hydrophobic interactions between the antenna and the protein surface.[46] This study was extended to evaluate interactions with “acute-phase” proteins involved in inflammatory responses. The complex was shown to bind strongly with α-1-acid glycoprotein to produce a strong CPL signal. CPL was also observed upon binding to α-1-antitrypsin, though with a relatively lower binding affinity. The strong interaction with α-1-acid glycoprotein was suggested to occur through a combination of amino acid (likely glutamate) coordination to the metal center, as indicated by a change in *q*, and non-covalent interactions between the protein and azaxanthone. The CPL signals differed between the two protein binders demonstrating the possibility to differentiate proteins with lanthanide probes through CPL “fingerprints.”

In a slightly different approach, Yuasa et al. used CPL fingerprints to differentiate between proteins covalently labeled with a self-assembling europium complex (Figure 28).[78] *Staphylococcus aureus* nuclease (SNase), bovine serum albumin, and insulin were each labeled with a succinimidyl ester of a β-diketonate ligand through amide bond formation with lysine residues on the proteins. When combined with $EuCl_3$, the β-diketonate ligand

(bound to protein) coordinates to the metal center to produce the sensitized europium complex. Distinct CPL spectra were observed for each protein-bound Eu-β-diketonate complex. The J=2 to J=1 signal was used for ratiometric determination of specific protein conformations of SNase, since the electric dipole-induced J=2 signal is sensitive to the surrounding ligand field whereas the magnetic dipole-derived J=1 signal is not. Thermal denaturation of SNase was detectable by changes in CPL using these ratios, in agreement with the changes in circular dichroism, suggesting applications of such probes in evaluating protein conformation.

3. Lanthanide Probes for MR Imaging

Medical imaging has revolutionized the field of diagnostic medicine. Physicians have a wide array of imaging modalities at their disposal, including positron emission tomography (PET), computed tomography (CT), optical imaging, ultrasound, and magnetic resonance imaging (MRI). There are both advantages and disadvantages to each of these modalities. For example, the excellent spatial resolution and unlimited penetration depth of MRI make it an excellent tool for in vivo studies. MRI does not require the use of ionizing radiation, allowing researchers and clinicians to perform long-term studies requiring multiple scans while minimizing side effects.

A MR image is acquired by inserting a specimen within an external magnetic field and applying a short RF pulse thereby exciting the water protons. Over time, the water protons relax to equilibrium where this process occurs at different rates within different types of environments such as cells or tissue. These relaxation times can be recorded and spatially encoded to generate an image of internal anatomy. Tissues with faster relaxation rates produce greater signal intensity, appearing brighter in the resulting image. To improve the sensitivity of MRI, Gd(III)-based contrast agents are employed to differentiate between regions of interest that are histologically distinct, but magnetically similar. The magnetic field generated by the unpaired electrons of Gd(III) interacts with water molecules to increase their relaxation rate, improving signal intensity.

3.1 Introduction to MRI Contrast Agents

Protons possess the quantum mechanical property of spin angular momentum, $\boldsymbol{I}$. Because the nucleus is positively charged, this angular momentum gives rise to a magnetic moment, $\boldsymbol{\mu}$. Application of an external magnetic field ($\boldsymbol{B}_0$) to a sample of protons gives rise to two possible nuclear states: one in which the nuclear spins (and consequently the *z*-component of the angular momentum, μ_z) are aligned in the direction of the field, and the other in which they are aligned against the field.[148] The energy difference between these two states is proportional to the magnitude of $\boldsymbol{B}_0$, with the state aligned with the direction of the field being the more energetically favorable. Transitions from one state to the other occur when the nucleus absorbs or emits energy of the appropriate frequency, ω_0 (Figure 29).

In a macroscopic sample, the vector sum of the magnetic moments produced by individual nuclei gives rise to a measurable quantity of macroscopic magnetization, $\boldsymbol{M}$. Because the individual spins do not rotate about $\boldsymbol{B}_0$ in phase, the *x* and *y* components of $\boldsymbol{\mu}$ produced by each individual nucleus will have a random distribution, negating the *x* and *y* components of

the macroscopic magnetization, M_x and M_y, respectively.[148] However, because the two orientations of μ_z are not equal in energy, slightly more nuclei will occupy the more energetically favorable state, making the *z*-component of ***M***, M_z, non-zero (Figure 30B).

The application of an RF pulse along the *x*-axis creates a secondary magnetic field ($\boldsymbol{B}_1$) which interacts with the nuclei in such a way that the net magnetization vector is tipped away from the *z*-axis, toward the *xy* plane (Figure 30C). The flip angle (i.e. the degree to which ***M*** is rotated away from the *z*-axis) is related to the duration of the pulse. If a 90° pulse is applied, ***M*** is tipped entirely into the *xy* plane. In such a case, M_x and M_y become non-zero while M_z vanishes (Figure 30D).

Once $\boldsymbol{B}_1$ is removed, M_x, M_y, and M_z return to their equilibrium values with characteristic time constants T_1 and T_2, respectively (Figure 30E). These recovery times can be measured, forming the basis for the signal intensity in MRI.[149,150] The recovery of the M_z component, mediated by spin-lattice (or T_1) relaxation processes, occurs as the distribution of nuclear spins returns to its initial state, in which a greater proportion of spins align with the field (Figure 31). This requires nuclei to transition from the high to low energy state via stimulated emission. Such transitions are mediated by the presence of nearby magnetic fields fluctuating at the Larmor frequency.

The unpaired electrons of paramagnetic metals, such as Gd(III) and Mn(II), generate their own magnetic fields. Thus their presence in solution has a dramatic effect on T_1 and T_2 relaxation times, making such complexes useful as MR contrast agents. Solomon, Bloembergen, and Morgan developed the basic theory (SBM theory) describing the acceleration of T_1 relaxation in the presence of a paramagnetic complex.[149,151–153] Within this framework, the observed T_1 relaxation rate ($T_{1,obs}$) is the sum of two terms, the diamagnetic rate ($T_{1,d}$, or the T_1 relaxation rate in the absence of the paramagnetic ion) and the paramagnetic rate ($T_{1,p}$, the rate enhancement imparted by the paramagnetic component).

$$\frac{1}{T_{1,obs}} = \frac{1}{T_{1,d}} + \frac{1}{T_{1,p}} \quad (3.1)$$

The paramagnetic component of the observed relaxation rate is a linear function of the concentration of the paramagnetic complex in solution. Thus Equation 3.1 can be rewritten as follows:

$$\frac{1}{T_{1,obs}} = \frac{1}{T_{1,d}} + r_1[Gd] \quad (3.2)$$

where r_1 is termed the relaxivity of the paramagnetic complex, a measure of how effectively the contrast agent reduces the T_1 relaxation rate of the surrounding solvent. The signal produced in an MR image is determined by water proton relaxation rate; faster T_1 relaxation results in greater signal. Thus, complexes displaying a high r_1 will increase the brightness of an MR image more effectively.

A significant portion of research in the field of contrast agent development is devoted to controlling the relaxivity of Gd(III) complexes.[148] Due to the toxicity of free Gd(III), clinical contrast agents chelate this ion using a macrocyclic, polyaminocarboxylate ligand such as 1,4,7,10-tetraazacyclododecane-1,4,7,10-tetraacetic acid (DOTA, Figure 32). The structure of the chelate determines the interaction between the ion and the surrounding water molecules, and consequently the relaxivity of the complex. There are a number of parameters that control relaxivity; however, only a few can be modified by chemical changes to the chelate structure (Figure 33).

The first of these parameters is *q*, the number of water molecules bound directly to the Gd(III) center at a given time. As mentioned above, water molecules in the first coordination sphere of Gd(III) experience the most pronounced T_1 rate enhancement, thus a larger *q* value corresponds to a higher r_1. However, an increase in *q* is typically achieved by decreasing the coordination number of the chelating ligand. This can decrease the kinetic stability of the complex, increasing the risk of toxicity resulting from free Gd(III).

The second parameter is τ_m (the mean residence lifetime of the bound water molecule) or the inverse of the water exchange rate (k_{ex}). The principle T_1 rate enhancement comes through water molecules directly bound to Gd(III) ion. The faster the bound water exchanges with surrounding water molecules, the more rapidly the rate enhancement effect can be transmitted to the bulk and the brighter the signal will be. However, if water exchange occurs too rapidly, each bound water molecule is not coordinated to Gd(III) long enough for full relaxation to occur. The counterbalancing of these factors leads to an optimal τ_m value of approximately 10–20 ns for clinical strength magnets (1–3 T), and will be discussed in more detail below.[154]

The third parameter that can be manipulated to optimize relaxivity is τ_r (the rotational correlation time) or how rapidly the molecule tumbles in solution. The τ_r of small molecule Gd(III)-chelates is typically far below that of optimal values.[154] This is often the limiting factor for increasing r_1 at clinically relevant field strengths. Current strategies for increasing τ_R values focus on increasing the molecular weight (MW) of the complexes, as larger molecules tend to tumble more slowly in solution.

This section of the review is not intended to present a comprehensive survey of the very large number of MR contrast agents that have been recently reported. Rather, we will focus on the key chemical and physical parameters that guide the development of new probes. The field of small molecule MRI contrast agents has seen rapid development in many areas including the development of a number of Mn(II)-based agents,[155–161] Eu(II) probes for high-field imaging,[162,163] and the conjugation of Gd(III)-chelates to a wide variety of targeting domains.[164–175]

The focus of the following sections is to describe and provide examples for the optimization of relaxivity: arguably the most widely studied area of MR contrast agent research. Section 3.2 discusses current methods for improving relaxivity through optimization of τ_m and τ_R while Section 3.3 focuses on the development of bioresponsive probes that transform the agent from low to high relaxivity in response to physiological events.

3.2 Improving Relaxivity

Theoretically, at 0.5 T the maximum relaxivity for a Gd(III)-based contrast agent with one inner sphere water molecule is near 100 $mM^{-1}s^{-1}$.[148] Contrast agents used in clinical diagnosis have relaxivities between 4–5 $mM^{-1}s^{-1}$, leaving significant room for improvement. As discussed in Section 3.1, three parameters govern the relaxivity of a complex: the number of inner sphere water molecules, their rate of exchange with the bulk solvent, and the tumbling rate of the complex in solution (Figure 33). An increase in the number of inner sphere water molecules is typically accompanied by a reduction in the coordination number of the ligand, and consequently the kinetic and thermodynamic stability may be compromised.

Therefore, we have focused on discussing strategies for the optimization of τ_m and τ_R. However, it is important to note that Raymond and co-workers have developed a class of high-relaxivity complexes based on the HOPO ligand class which possess higher *q* values (2 and 3), without adversely affecting complex stability. The agents are exquisitely designed to preserve in vivo stability of the complex and significantly increasing the observed r_1 of the agent.[176–183]

The relationship between *q* and r_1 is both linear and field independent; however, the relationship between τ_R, τ_m, and r_1 is more complex. At clinically relevant field strengths (≥ 1.5 T), the primary mechanism of T_1 relaxation enhancement by Gd(III) contrast agents is the dipole-dipole interaction between the paramagnetic metal and the water protons.[154] The correlation time for this mechanism is the sum of several processes: rotational motion of the Gd(III)-proton vector, the longitudinal electronic relaxation time (T_{1e}), and the water exchange rate:

$$\frac{1}{\tau_{1c}}=\frac{1}{\tau_R}+\frac{1}{T_{1e}}+\frac{1}{\tau_m} \quad (3.3)$$

T_1 relaxation is characterized by transitions from the high to low energy spin state that occur in response to the presence of nearby magnetic fields fluctuating at the Larmor frequency (ω_0). Consequently, r_1 is optimized when the inverse of the correlation time, τ_{c1}, is equal to the Larmor frequency and this has two important implications.[154] First τ_m and τ_R must be optimized simultaneously to achieve maximum relaxivity. Second, because the Larmor frequency varies with the strength of the external magnetic field, the optimal values of τ_m and τ_R will be field-dependent.

At field strengths ≥ 1.5T electronic relaxation is slow with respect to rotational tumbling; thus the $1/T_{1e}$ term in Equation 3.3 becomes negligible, and the expression can be reduced to:

$$\frac{1}{\tau_{1c}}=\frac{1}{\tau_R}+\frac{1}{\tau_m} \quad (3.4)$$

At these field strengths, improvements to clinically approved agents can be achieved by decreasing the rotational tumbling rate and increasing the water exchange rate (i.e.,

increasing τ_R and decreasing τ_m). The τ_R values of these small molecule chelates are approximately 100 *picoseconds*, while the τ_m values range from tens to hundreds of *nanoseconds*.[154] Consequently the $1/\tau_R$ term dominates Equation 3.4, and increases in τ_R will have a more dramatic impact on relaxivity than decreases in τ_m. However, once the rotational tumbling rate has been slowed by several orders of magnitude, increases in the water exchange rate of the complexes significantly affect relaxivity. Researchers have employed a variety of strategies to optimize both of these parameters over a range of field strengths.[154,184] Many of these strategies require a detailed understanding of the coordination chemistry of the lanthanide-chelate complex, and will be discussed in the following sections.

3.2.1 Optimization of τ_R—At low-to mid-field strengths (3T and below), the most effective way to increase the relaxivity of a complex is to increase τ_R.[154] Because larger molecules tumble more slowly in solution, τ_R optimization strategies focus on increasing the MW of contrast agents. To accomplish this, the chelate can be attached to a large macromolecule such as a protein, or multiple chelates can be either appended to a central scaffold or self-assembled to create a high-MW, multimeric structure.[185] It should be noted that the rigidity of the linkage between the chelate and either the macromolecule or the scaffold is *crucial* for effective r_1 enhancement.[184] If the linkage is too flexible, the local rotation of the chelate (τ_{Rl}) about the linkage will be decoupled from the global rotation of the larger structure (τ_{Rg}), limiting the effect of τ_R enhancement of r_1.[154]

The most widely known (and clinically approved) example of a macromolecule-binding contrast agent is MS-325, a small molecule DTPA derivative that binds to human serum albumin (HSA, Figure 34) with an affinity of 85 μM.[186] Upon binding to HSA, the τ_R of the complex increases from 115 ps to 10.1 ns, resulting in a 9-fold increase in r_1[186].

A great deal of work has been devoted to optimizing the performance of MS-325 and determining its mechanism of action.[184,186–188] Moreover, a number of studies have utilized similar structures to target various agents to the hydrophobic binding site of HSA. Chang et al. developed a derivative of 3,6,10-tri(carboxymethyl)-3,6,10-triazadodecanedioic acid (TTDA) containing a cyclobutane ring and a benzyl group (Bz-CB-DDTA, Figure 35).[189] While this complex has a lower affinity for HSA than MS-325, its relaxivity following protein binding is significantly higher (66.7 $mM^{-1}s^{-1}$ at 20 MHz, as compared to 47 $mM^{-1}s^{-1}$ for MS-325) owing to faster water exchange properties imparted by the cyclobutyl moiety.

Complexes that bind to proteins other than HSA have been reported.[184,185] A series of Gd(III) probes have been developed that bind to HaloTag (HT: a reporter protein) which forms a covalent attachment to long chain haloalkanes.[190] This series of complexes (*n*-CHTGd) is composed of a Gd(III)-DO3A derivative conjugated to a chloroalkane chain, where the distance between the chelate and the haloalkane was systematically altered (Figure 36). The complexes with shorter linkages showed the largest increases in r_1 upon binding to HT, underscoring the importance of maintaining a rigid linkage between the chelate and the macromolecule to prevent local rotation of the complex. At 60 MHz, 2-

CHTGd showed a 6-fold increase in r_1 upon HT binding (from 3.8 $mM^{-1}s^{-1}$ to 22 $mM^{-1}s^{-1}$).

A number of groups have explored the conjugation of Gd(III) chelates to other macromolecular structures, including nanodiamonds or nanoparticles,[191–194] viral capsids,[195–197] and DNA.[198,199] Meade and co-workers peptide coupled an amine functionalized derivative of Gd(III) DOTA to the carboxylated surface of a nanodiamond to achieve a relaxivity of 58.8 $mM^{-1}s^{-1}$ per Gd(III) at 60 MHz, one of the highest values per Gd(III) ion reported thus far.[191]

Raymond and co-workers have performed a number of studies exploring the attachment of Gd(III) chelates to both the interior and exterior surface of MS2 viral capsids. The MS2 capsid contains 180 copies of the coat protein, arranged into an icosahedral structure.[179,196] Lysine (Lys) residues on the exterior of the capsid or tyrosine (Tyr) residues on the interior of the capsid were selectively functionalized with a reactive aldehyde using an NHS ester or diazonium salt, respectively (Figure 37). The aldehyde was reacted with an alkoxyamine derivative of the HOPO ligand, and metalated with Gd(III). The internally-modified capsids exhibited significantly higher relaxivity than those modified on the exterior (30.7 $mM^{-1}s^{-1}$ as compared to 41.6 $mM^{-1}s^{-1}$ at 30 MHz), indicating that i) water access to the interior of the protein coat is sufficient to produce high T_1 contrast and ii) complexes conjugated to the surface with more rigid linkers resulted in higher relaxivity due to decreased local motion. This second point was confirmed by a more recent study where Francis et al. conjugated a malemide derivative of HOPO to internal cysteine residues (resulting in an even more rigid linkage) achieving a relaxivity of 38.2 $mM^{-1}s^{-1}$, even at 60 MHz.

Meade and Mirkin et al. developed a novel strategy for the attachment of Gd(III)-DO3A based chelates to DNA-functionalized gold nanoparticles (AuNPs).[198] An alkyne-modified DO3A chelate was coupled to a 24-mer poly-dT sequence containing five azide-modified nucleotides using copper-catalyzed click chemistry. The DNA strands were immobilized onto citrate- stabilized AuNPs of two different sized particles: either 13 nm or 30 nm. The effect of MW on relaxivity can be clearly seen in this study: at 60 MHz, the alkyne modified chelate by itself has an r_1 of 3.2 $mM^{-1}s^{-1}$ per Gd(III) ion; following attachment to the DNA strand, r_1 increases to 8.7 $mM^{-1}s^{-1}$; conjugation to the 13 nm particles further increases r_1 to 16.9 $mM^{-1}s^{-1}$, while conjugation to the 30 nm particles results in a r_1 of 20.0 $mM^{-1}s^{-1}$ (Figure 38).

Hamilton et al. utilized DNA to increase the molecular weight of small molecule chelates and relied on self-assembly of a higher-order quadruplex structure rather than covalent attachment to a large scaffold (Figure 39).[199] One of two Gd(III)-DOTA derivatives were peptide coupled to the 5’ end of quadruplex-forming oligonucleotides (Gd-dTGGGGGGTTTT). Upon quadruplex assembly, the relaxivity of oligo-conjugated chelates increased from 6.4 to 11.7 $mM^{-1}s^{-1}$ (4 T), resulting from both the increased MW of the macromolecular structure and the increased rigidity imparted by quadruplex structure. This approach has several advantages: i. the scaffold is composed of DNA reducing the risk of toxicity; ii. the system is modular; substitution of a shorter, more rigid linker, between the chelate and the oligo would be a straight forward modification to further increase relaxivity;

iii. functionalized quadruplexes have been shown to selectively associate with specific proteins allowing for the development of targeted, high-relaxivity probes.

A number of groups have conjugated long alkyl chains to Gd(III) chelates to facilitate either self-assembly into micellular structures or incorporation into liposomes.[156,200–206] The most recent work in this area has focused on the attachment of two separate alkyl chains to a macrocyclic Gd(III)-DO3A chelate.[205,206] Botta et al. compared the relaxation properties of two chelates: one with a single alkyl chain extending from the acetate arm of Gd(III)-DOTA, the other with two alkyl chains on adjacent acetate arms.[205] It was hypothesized that upon formation of a micellular structure or incorporation into a liposome, the complex with two alkyl chains would be anchored in place, restricting local rotation of the chelate and enhancing both τ_R and relaxivity (Figure 40). This hypothesis was confirmed by nuclear magnetic resonance dispersion (NMRD) and relaxometric studies. At 0.5 T, the relaxivity values of the single chain and dual chain complexes were 15.4 and 34.8 $mM^{-1}s^{-1}$, respectively.[205] Extensive NMRD analysis allowed for decoupling of local (τ_{Rl}) and global (τ_{Rg}) rotational correlation times. The complex with a single alkyl chain had much shorter values of both τ_{Rl} and τ_{Rg} (210 and 2900 ps, respectively) than the dual chain complex (820 and 4700 ps).[205] Desreux et al. employed a similar strategy but appended the alkyl chains to adjacent carbons on the ethylene bridge of the cyclen backbone of Gd(III)-DOTA rather than to the acetate arms, developing a complex with a relaxivity of 35 $mM^{-1}s^{-1}$.[206]

Covalent attachment of multiple chelates to smaller organic or inorganic scaffolds is an attractive strategy for τ_R optimization. Several modular systems that rely on click chemistry to attach either azide or alkyne modified Gd(III) chelates to various organic cores including cyclodextrin,[207] fluorescent porphyrazines,[208] or a central benzene ring[209] have been developed (Figure 41). The benzene-based system, which contains three chelates and displays a relaxivity of 15.4 $mM^{-1}s^{-1}$ per Gd(III), is particularly attractive as it contains an additional functional handle for subsequent attachment to a targeting group, fluorophore, or cellular transduction domain.[209] Hawthorne et al. employed click chemistry to attach 11 or 12 Gd(III) chelates to an inorganic, icosahedral boronate scaffold.[210,211] Using a linear Gd(III)-DTTA (q = 2), they obtained an impressively high relaxivity of 13.8 $mM^{-1}s^{-1}$, even at high field strength (7 T).[211] While the per Gd(III) relaxivity of the scaffold containing macrocyclic Gd(III)-DO3A chelates (q = 1) was notably lower (6.2 $mM^{-1}s^{-1}$), this still represents a significant improvement over the monomeric complexes.[210]

Metal ions can serve as a central scaffold for multimeric Gd(III) complexes. Merbach and Tóth pioneered the development of metallostars, multinuclear complexes in which a Gd(III) chelate is conjugated to a multidentate ligand such as bipyridine (bpy) or phenanthroline that subsequently forms an octahedral coordination complex with a transition metal such as Fe(II) or Ru(II).[212] Such complexes offer a number of advantageous characteristics including the possibility of multimodal imaging using transition metal fluorescence and an intermediate MW that is ideal for increasing relaxivity over a broad range of field strengths. A variety of metallostar complexes have been developed, differing in the structure of Gd(III) chelate, the multidentate ligand, the transition metal to Gd(III) ratio, and the identity of the central transition metal (Figure 42).[174,212–220]

In summary, a primary strategy for increasing the rotational correlation time of small molecule contrast agents is to increase their molecular weight. This can be accomplished by coupling the agent to a larger macromolecule such as a protein or nanoparticle, or by complexing multiple Gd(III) contrast agents to a central molecular scaffold.

3.2.2 τ_m optimization—The optimization of water exchange rates ($1/\tau_m$ or k_{ex}) requires a thorough understanding of the coordination chemistry of the lanthanide complex (including the mechanism of water exchange), the conformation of the chelate and the steric compression that this imparts, and the hydrogen bonding network created by the chelating atoms of the ligand.

For Gd(III) complexes with octadentate ligands and a single inner sphere water, the primary mechanism of water exchange is dissociative.[221] Gd(III) favors a nine-coordinate geometry and the rigidity of the chelate prevents the geometric rearrangements required to accommodate the ten-coordinate transition structure of an associative mechanism. Since there is no incoming ligand to assist in weakening the Gd-O_{water} bond, the rate-determining step of water dissociation has a high activation barrier. Therefore, any factor that weakens this bond will accelerate the rate of water exchange.

The partial charge of the chelating oxygen on the pendant back-binding arms has a dramatic effect on τ_m[222] Carboxylates and other negatively charged groups accelerate the exchange process compared to neutral chelating groups such as amides.[223–227] As measured by ^{17}O NMR the τ_m of Gd(III) DOTA is 244 ns,[228] while the τ_m of the tetramethylamide analogue (DTMA) is two orders of magnitude longer (19 μs).[223] Merbach and Tóth et al. determined that each carboxylate substitution reduces k_{ex} by approximately a factor of four.[224] Presumably, the negative charge of the carboxylates reduces the electropositive nature of the Gd(III) center, weakening the interaction between the metal and the O_{water} lone pair.

Based on density functional theory (DFT) calculations which showed that the oxygen atom of a chelating ketone is more electropositive than that of an amide, Sherry et al. hypothesized that the introduction of a ketone-based pendant arm would slow water exchange even more so than an amide group (Figure 44).[229] To evaluate this hypothesis, a series of chelates was synthesized and the τ_m values measured. Within the series of complexes the ratio of amide-based to ketone-based pendant arms was systematically varied. Results were consistent with the initial hypothesis; each amide-to-ketone substitution resulted in slower water exchange.[229] It is likely that the reduced partial charge of the ketone-based pendant arm makes it a weaker donor. This results in a more electropositive metal that interacts more strongly with a coordinated water molecule, *increasing* the activation barrier for water dissociation and *decreasing* the water exchange rate.

To systematically explore how the identity of the pendant arm affects water exchange, Napolitano et al. used a combinatorial approach to synthesize a library of 80 peptoid-modified Eu(III)-DOTA tetraamide derivatives and developed a PARACEST-based assay (see Section 3.3 for an explanation of PARACEST) to rapidly screen their water exchange rates (Figure 45).[230]

Increasing the degree of steric compression about the metal center destabilizes Gd-O_{water} bond, decreasing τ_m. There are two primary strategies for introducing steric compression. The first, pioneered by Merbach et al., involves the incorporation of an additional methylene group into either the cyclen backbone [Gd(III)-TRITA] or one of the carboxylate arms (Gd-DOTAN-prop) of a DOTA-based chelate (Figure 46).[231–233] Crystal structure analysis of the first coordination sphere of the metal in the Gd(III)-TRITA complex provided conformation of increased steric compression; the O-Gd-O angles of Gd(III)-TRITA complex are significantly compressed compared to those of Gd(III)-DOTA. Interestingly, the Gd-O_w distance is unaffected by the introduction of the additional methylene group. However, the distance between the plane of the chelating oxygens and the metal center is significantly longer in Gd(III)-TRITA than Gd(III)-DOTA (0.83 Å compared to 0.7 Å). As a result, the coordinated water molecule is significantly closer to the highly anionic plane of carboxylates, facilitating water dissociation.

The second, more widely studied strategy for increasing steric compression focuses on controlling the isomeric distribution of the chelates.[234,235] Macrocyclic chelates can exist in two diastereomeric conformations, square antiprismatic (SAP) and twisted-square antiprismatic (TSAP), which differ dramatically in water exchange rate. Geometrically, the two isomers are distinguished by the twist angle between the plane defined by the chelating oxygen atoms and the chelating nitrogen atoms; the SAP isomer has a twist angle of ~40° while twist angle of the TSAP is closer to ~25° (Figure 47).[236] For Gd(III)-DOTA, the SAP conformation is the major isomer, the TSAP conformation is the minor isomer.[236] Consequently the SAP and TSAP conformations are also referred to as the M (major) and m (minor) conformations, respectively.

For symmetric macrocycles such as Gd(III)-DOTA, two sources of chirality define the SAP and TSAP isomers: the gauche orientation of each of the ethylene bridges between the nitrogen atoms of the cyclen backbone (δ δ δ δ or λ λ λ λ), and the helicity of the pendant carboxylate groups [Δ (clockwise arrangement) or Λ (counter clockwise arrangement)].[234,235,237] The TSAP isomer has the same stereochemistry at both positions [Δ(δ δ δ δ) or Λ(λ λ λ λ)], while the SAP isomer has the opposite stereochemistry at the two positions [Δ(λ λ λ λ) or Λ(δ δ δ δ)]. Interconversion between the two isomers occurs by one of two mechanisms: i) ring inversion – a concerted inversion of the gauche conformation of all four ethylene bridges (δ δ δ δ ↔ λ λ λ λ) or ii) arm rotation – concerted movement of all four pendant carboxylate arms (Δ ↔ Λ) (Figure 48). Successive or concerted occurrence of both arm rotation and ring inversion leads to an enantiomerization process.

It is well established that water exchange occurs much more rapidly for the TSAP isomer of DOTA derivatives. The most common explanation for this discrepancy is the increased steric crowding about the water coordination site in the TSAP isomer. As a result of steric repulsion between the chelating nitrogen and oxygen atoms, the distance between the N_4 and O_4 plane is significantly greater in the TSAP isomer.[238] It has been proposed that this geometric feature makes the metal center less accessible to the coordinated water molecule.[239] To account for this, the inner sphere water molecule must come in closer proximity to the negatively charged O_4 plane or the Gd-O_w bond distance must increase.

Either event will reduce the activation barrier for water dissociation, leading to the faster water exchange rate observed for such complexes. It should be noted that while the TSAP conformation may reduce the accessibility of the Gd(III) center to surrounding water molecules, the increased O_4-N_4 distance allows this isomer to accommodate larger lanthanide metals as well as more sterically demanding pendant arms. In fact, studies examining the SAP/TSAP ratio of a given ligand for a variety of lanthanides indicate that the earlier lanthanides display a preference for the TSAP geometry. As the ionic radius increases across the period this preference steadily shifts toward the SAP isomer until reaching Er(III); at which point the equilibrium begins to shift back toward the TSAP isomer.[239–242]

The exchange kinetics of DOTAM are slow enough to allow for the identification of two separate NMR resonances for the bound water on the two different isomers.[225,243] Consequently Dunand et al. were able to determine the SAP:TSAP ratio of isomers of DOTAM present in solution as well the τ_m values of the individual isomers.[225,244] The τ_m of the SAP isomer is 120 μs which is nearly 50 times longer than the 3 μs τ_m of the TSAP isomer. Though the SAP isomer is the major conformation in solution ([SAP]/[TSAP] = 4.5) the rapidly exchanging TSAP isomer contributes 90% of the overall water exchange rate.[225]

A later study by Woods et al. further confirmed that water exchange on the TSAP isomer occurs more rapidly.[150] By introducing a carboxyethyl substituent α to the macrocycle, they were able to alter both the SAP/TSAP ratio and the τ_m of the overall solution. Three different derivatives were examined, differing only in the absolute stereochemistry of the carboxyethyl substituent. Each derivative yielded a different SAP/TSAP ratio that correlated well with the τ_m values of the complexes; the complexes that had a higher proportion of TSAP isomer had significantly lower τ_m values (Figure 49).

The difference in water exchange rate between the two isomers is magnified when two of the amide groups are replaced by carboxylates. Sherry et al. examined two such DOTA derivatives, Gd(III)-DOTA-2DMA and Gd(III)-DOTA-2APA, and found that the exchange rates of the TSAP isomers were 100 and 1000 times faster than the SAP isomers, respectively (Figure 50).[226]

The short τ_m of the TSAP isomer make this molecular conformation more useful as a MR contrast agent. Consequently, it is important to understand and exert control over the coordinating arm rotation and ring inversion processes that lead to interconversion of the two isomers. NMR techniques can be used to determine the mechanism of isomerization, as well as the rates at which the two processes are occurring.

^{1}H NMR spectra of the Eu(III) and Yb(III) analogues of DOTA-like ligands contain separate resonances for the protons located in the axial and equatorial positions on the ring. The protons of the SAP and TSAP isomers can also be distinguished from one another; for a given resonance, the protons of the SAP isomer display a larger paramagnetic shift.[150] Moreover, the two possible isomerization processes result in the exchange of different protons. During arm rotation the axial protons of one isomer exchange with the axial protons of the other, while ring inversion results in the exchange of the axial protons of one isomer

with the equatorial protons of the other (Figure 51).[150] Consequently, NMR experiments that are used to identify exchange processes (such as 2D EXSY and magnetization transfer studies) can be used to determine which processes are occurring, and at what rate.[150,225,242,245–248]

For both Gd(III)-DOTA and DOTAM (the tetraamide derivative) each of these processes contribute to isomerization.[225,236,237,247,249–253] However, the introduction of further substituents to the ligand can effectively restrict these processes. Substitution on the pendant back-binding arms slows or completely eliminates the arm rotation process,[244,246,254,255] while substitution on the cyclen backbone restricts the ring inversion motion (Figure 52).[242,245,248,256] Substitution at both positions effectively locks the macrocycle into a single conformation. Further, by defining the absolute stereochemistry at the site of substitution, researchers are able to synthesize complexes that exist solely in the TSAP conformation.

For example, Sherry et al. determined that setting the stereochemistry of NB-DOTMA such that the nitrophenyl substituent on the macrocycle and the methyl substituents of the pendant acetates have the same absolute configuration (*S-SSSS*), locks the complex into the desired TSAP geometry (Figure 52).[237,242,245,249,250] When the substituents have the opposite absolute configuration (*S-RRRR*), the chelate is locked in the SAP geometry. Further characterization of the two complexes confirmed that the water-exchange rate of the TSAP-locked complex is significantly faster than that of the SAP-locked complex (τ_m = 15 and 120 ns, respectively).[245]

The SAP/TSAP ratio is affected by the steric requirements of the pendant arms of the chelate. Phosphonate pendant arms are more sterically demanding than carboxylate groups. Substitution of all four carboxylates of DOTA with phosphonate groups (DOTP) leads to a structure that is sterically crowded enough to eliminate the inner-sphere water molecule (i.e., $q = 0$), limiting the utility of such chelates as MR contrast agents.[257] However, a single phosphonate-carboxylate substitution (DO3AP) imparts enough steric bulk to shift the isomeric composition in favor of the more open TSAP conformation, while still maintaining a $q = 1$.[258–260]

Recently, several groups have used DFT calculations in conjunction with NMR data to improve understanding of the dynamical conversion between the various isomers in solution, as well as the reasons behind the accelerated water exchange of the TSAP isomer.[235,251,252,261] Purgel et al. performed a DFT study to further examine the SAP/TSAP preference of phosphonate derivatives of DOTA, DO3AP and DO2A2P.[252] Their results showed both qualitative and quantitative agreement with experiment. As discussed above, replacement of the carboxylate arms of Ln(III) DOTA with phosphonate arms increases the chelate preference for the TSAP conformation. Using the B3LYP hybrid functional in conjunction with a 6–31G(d) basis set for the ligand atoms and the effective core potential (ECP) developed by Dolg et al. for the metal,[262] Purgel et al. were able to accurately reproduce this trend. Moreover, the method successfully predicted the relative energy difference between the two conformations within ~ 1.1 kcal/mol. The accuracy of this

method implies that computational calculations may prove to be a valuable tool for the design of new ligands that prefer the TSAP geometry.

Pollet et al. performed ab initio molecular dynamics simulations on Gd(III) HP-DO3A (Prohance) in explicit solvent to investigate the difference in the water exchange properties of the two conformations.[261] As discussed above, the most common explanation for the discrepancy asserts that in the TSAP conformation, the Gd(III) center is less sterically accessible to water molecules, weakening the Gd-O_w bond and lowering the activation barrier to water dissociation. However, the results presented by Pollet et al. suggest that the explanation may be related to the interactions between the chelate and the second sphere water molecules (those that form hydrogen bonds directly to the ligand or to the inner sphere water of the complex).

The solvation shell of Ln(III)-DOTA complexes is highly anisotropic – the face about the plane of chelating oxygen atoms (herein referred to as the 'top' face) is strongly hydrophilic, while the face below the plane of chelating nitrogen atoms is composed of methylene groups and is thus strongly hydrophobic. Consequently, the top face of the complex is well solvated by surrounding water molecules. For Gd(III)-HPDO3A, calculations indicate that the non-coordinating oxygen of each carboxylate group is solvated by two water molecules in both the SAP and TSAP conformation. However, in the TSAP conformation, two of the *coordinating* oxygen atoms are also solvated by a water molecule, placing two second-sphere waters in close proximity to the inner-sphere water. This in turn reduces the hydrogen bonding capabilities of the inner-sphere water in the TSAP conformation, as the coordinated water must compete with the two nearby second-sphere waters. The stronger hydrogen bonds formed by the SAP isomer induce a significant polarization of the O-H bond in the inner sphere water, increasing the electrostatic attraction between the oxygen atom of the inner sphere water molecule and the Gd(III) center, and in turn increasing the strength of the Gd-O_w bond and decreasing the exchange rate.

In summary, much work has been devoted to modulating the water exchange rates of Gd(III) chelates. Because the mechanism of water exchange is dissociative, any factor that weakens the Gd-O_w bond will accelerate the exchange process, including the incorporation of negatively charged pendant arms, the introduction of steric compression to the complex, or an increase in the TSAP/SAP isomeric ratio of the chelate. Of these three, the latter has been studied the most extensively with a number of groups seeking to understand and control the mechanism of isomer interconversion.

3.3 Bioresponsive MR contrast agents

Research regarding the optimization of relaxivity of Gd(III) agents prepared the way for the development of bioresponsive MR contrast agents. These complexes were designed to be conditionally activated by a biochemical or physiological event.[263] Such probes are of great use for molecular imaging applications allowing researchers to monitor physiological processes in vivo using a non-invasive imaging modality. Since the introduction of the first bioresponsive MR contrast agent (enzyme-activated EGad)[264–266] more than 50 examples of this class of probes have been developed.[267] These agents are capable of responding to a wide variety of stimuli (or are conditionally activated) and can be activated by several

different mechanisms. This section focuses on the development of probes that respond to changes in ion concentration, enzyme activity, and pH. However, it should be noted that recent progress in this area has been made in the development of probes that respond to temperature fluctuations,[268–271] glucose concentration,[272,273] singlet oxygen,[6,264,265,268,274,275] and hypoxic conditions.[6,272,274]

3.3.1 Mechanisms of Bio-activation—Several mechanisms can be used to control the response of bioresponsive MR probes; the most common include τ_R modulation, *q*-modulation, and PARACEST. τ_R-modulation is the simplest mechanism of activation. τ_R modulated probes undergo an increase in molecular weight (MW) in response to the event of interest (EOI), resulting in an increased τ_R, and thus an increased r_1. Such increases in MW typically occur as a result of either protein binding or EOI-induced self-assembly (Figure 53). For example, a small molecule Gd(III) chelate can be labeled with a binding domain that is selective for a large molecule or protein (Figure 53B). Upon binding, the molecular weight of the agent is dramatically increased with subsequent increase in τ_r

The design of *q*-modulated probes is focuses on manipulating the coordination environment of the chelate (Figure 54). Such probes consist of three primary domains: a macrocyclic Gd(III) chelate, a bio-responsive domain, and a molecular linker between the two. Prior to the EOI, the bio-responsive domain is associated with the Gd(III) chelate in such a way that it restricts water access to the metal center, creating a low-relaxivity, $q = 0$ state. The association between the bio-responsive domain and the Gd(III) chelate typically involves the back-binding of a functional group on the bio-responsive domain to the metal center, rendering it coordinatively saturated.

In response to the EOI, the complex undergoes a structural change that results in the dissociation of the bio-responsive domain from the Gd(III) center, opening a coordination site for water binding and creating a high-relaxivity, $q = 1$ state (Figure 54). This dissociation can happen in one of two ways. The back-binding functional group can selectively bind to the substrate being detected (as is the case for ion-responsive agents) or the bio-responsive domain is cleaved entirely, as is the case for enzyme-activated probes.[6,264,265,274–276]

For both τ_R-modulated and *q*-modulated MR probes, the efficacy of the agent can be quantified by the change in relaxivity that is produced upon activation (Δr_1). The greater this change in relaxivity, the more sensitive the agent is to the EOI which will facilitate differentiation between activated and un-activated agent. Consequently, optimization of this class of probes focuses on minimizing relaxivity in the pre-activated state while maximizing relaxivity following activation.

3.3.2 CEST and PARACEST Agents—Understanding of PARACEST-based bioresponsive probes requires an explanation of the principles behind chemical exchange saturation transfer (CEST) imaging, which can be understood within the context of NMR spectroscopy.[267,276] For an extensive description of this class of probes we direct the reader to an excellent tutorial review published by Sherry et al.[276] As discussed in Section 3.1, the application of an external magnetic field causes spin-active nuclei to align with or against

the field. Because the population of the two states is determined by the Boltzmann distribution, the lower-energy state in which the nuclear spin is aligned with the field is more populated, giving rise to a net magnetic moment in the direction of the field. The application of an RF pulse alters this distribution; thus, pulse sequences can be developed to investigate the local environment of the nuclei by monitoring the changes to the magnetization vectors in the *x*, *y* and *z* directions.[153]

CEST can occur in a sample containing two pools of protons, A and B, which are in distinct environments and undergo chemical exchange with one another (Figure 55). If an NMR acquisition pulse is applied to the sample without any prior magnetic perturbations, the resulting spectrum will display two distinct signals at different frequencies, ω_a and ω_b (Figure 56, left).[222,249,277]

If the frequency difference between the signals ($\Delta\omega$) is sufficiently large, a pre-saturation pulse can be selectively applied to pool B prior to the acquisition pulse. This pulse promotes nuclei in Pool B from the lower-energy state to the higher-energy state (Figure 56, bottom center). As the population difference between the two states decreases, the net magnetization vector in the *z* direction is reduced. Because the signal intensity in an NMR spectrum is related to the magnitude of the magnetization vector, subsequent application of an NMR acquisition pulse produces a spectrum in which the signal from pool B is greatly diminished.[276]

When chemical exchange between the protons of Pool A and Pool B occurs following pre-saturation of Pool B, some portion of the magnetization saturation will be transferred to Pool A. During the chemical exchange process, protons in the high-energy states of the two pools will exchange with one another.[277] Because the pre-saturation pulse selectively increased the number of high-energy protons in Pool B, this exchange process will *increase* the population of the *high-energy state* of Pool A at the expense of the high-energy state of Pool B. Protons in the low-energy states of the two pools will also exchange with one another. However, because the pre-saturation pulse selectively depleted the population of the low-energy state of Pool B, the exchange process will *decrease* the number of *low-energy protons* in Pool A, so as to increase the number of low-energy protons in Pool B.[276]

The end result of the two exchange processes is that the population difference between the high and low energy states of Pool A is reduced. Subsequent application of an NMR acquisition pulse will then produce a spectrum in which the signals from both Pool A and Pool B are reduced. Thus, the signal from Pool A can be indirectly saturated by direct saturation of Pool B, a principle that can easily be extended to imaging applications.[276,277]

Water protons represent the primary source of signal in an MR image. Consequently, image contrast can be produced by indirectly altering water signal intensity via application of a saturation pulse to exchangeable protons. As with MRI, CEST imaging can be performed without the use of exogenous contrast media.[277] However, the use of paramagnetic metal complexes as contrast agents (PARACEST) both improves the sensitivity of the technique and extends its utility to molecular imaging applications, facilitating non-invasive detection of physiological changes in pH, ion concentration, or enzyme activity.

Several conditions must be met for CEST to occur. These requirements explain the mechanism of PARACEST sensitivity enhancement. First, the exchange rate must be faster than the T_1 relaxation rate of A and B:

$$k_{ex} \geq \frac{1}{T_1}$$

In the limits of fast T_1 relaxation, Pool B will return to equilibrium before the exchange process occurs and the effect of the pre-saturation pulse will not be transferred to Pool A (Figure 56, center top). Thus, faster rates of k_{ex} produce stronger CEST effects, as a greater proportion of magnetization saturation can be transferred within a given timeframe.[276,277] However, this must be tempered by the second condition, namely that the exchange process must be slow on the NMR timescale. That is, the exchange rate (k_{ex}) must be less than or equal to the difference in frequency between the two signals A and B:

$$k_{ex} \leq \Delta\omega$$

This ensures that one pool can be selectively saturated, and that the exchange process will not result in coalescence of the two signals (Figure 56, right). Thus, Δω serves as an upper limit to the exchange rate, which in turn determines magnitude of the CEST signal.[276,277]

Paramagnetic complexes significantly alter the chemical shift of protons in the near vicinity, making them excellent contrast agents for CEST imaging (PARACEST). Specifically, for Eu(III) complexes of polyaminocarboxylate ligands containing one inner sphere water molecule, the proton signal from the coordinated water is shifted ~50 ppm from that of the bulk water.[267,276,278] Such a large value of Δω increases the maximum exchange rate that allows for observation of CEST, and consequently the maximum intensity of the resulting CEST signal. However, the water exchange of lanthanide complexes typically employed as MR contrast agents, such as Gd(III)-DOTA, occurs too rapidly for these complexes to act as effective PARACEST agents. However, as discussed in Section 3.2.2, the chemical structure of macrocyclic, polyaminocarboxylate ligands has a dramatic effect on their water exchange properties.[222] Replacement of the carboxylate groups of DOTA with amide groups slows the water exchange rate by several orders of magnitude, making complexes such as Eu(III)-DOTAM useful as PARACEST agents.[222,278]

The effectiveness of a PARACEST agent can be assessed by measuring the intensity of the bulk water signal after the application of a pre-saturation pulse; a CEST spectrum is generated by plotting the bulk water signal intensity as a function of the frequency of the pre-saturation pulse (measured as the off-set from the direct saturation frequency), and is indicative of the PARACEST capabilities of the complex.[267,276,278] In a solution of the paramagnetic complex, direct saturation (i.e. application of a pulse at the frequency of the bulk water frequency) will eliminate the bulk water signal entirely. However, application of a pre-saturation pulse at the frequency of the coordinated water molecule (in the case of Eu(III)-DOTMA, +50 ppm) will also reduce the bulk water signal, due to CEST (Figure 57). The magnitude of this decrease indicates the PARACEST capabilities of the agent.[276,278]

Several features make PARACEST complexes particularly useful as bioresponsive contrast agents.[267,279] First, the magnitude of the PARACEST effect is largely determined by the water exchange rate. As long as the system remains in the slow exchange regime (i.e., $k_{ex} \leq \Delta\omega$), increases in the exchange rate will enhance the observed PARACEST effect. Because the exchange rate is strongly dependent on both pH and temperature, these complexes inherently report variations in both of these biologically relevant quantities.

Moreover, the magnitude of the hyperfine shift of the coordinated water molecule (i.e., the value of $\Delta\omega$) depends on the ligand field strength, which is in turn a function of the identity of the lanthanide. Thus a series of isostructural complexes of the same ligand can be prepared that utilize the same ligand but contain different metal centers. These complexes will have very different $\Delta\omega$ values and can thus be activated separately using pre-saturation pulses of two different frequencies, as shown by Aime et al.[278,279] Because the biodistribution of these isostructural complexes should be identical, one can be used as a bioresponsive agent, while the other is used as a concentration marker, allowing for quantitative determination of biologically relevant quantities such as pH.

Pagel et al. have reported an intriguing new example of a this class of probes termed "catalyCEST".[279,280] The probe is designed to detect enzyme activity (transglutaminase) and the subsequent formation of a covalent bond by CEST. The agent is prepared by coupling a cadaverine derivative with Tm(III)-DO3A (Figure 58). In mixtures containing the CEST agent a covalent bond was formed between the probe and a glutamine residue of the protein albumin. After conjugation, changes were detected in the CEST spectrum where the MR frequencies and amplitudes were dependent on the peptide sequence. These promising results suggest that the CEST agent could be used to detect the presence of transglutaminase in complex mixtures.

3.3.3 Ion-Activated Probes—In addition to their association with natural biological processes, fluctuations in the concentration of ions such as Zn(II), Ca(II), Fe(II), and Cu(II) are implicated in a number of pathologies.[281,282] Consequently, a non-invasive method for monitoring changes in the concentration of various ions would be advantageous. To this end, a number of groups have developed ion-activated MR contrast agents and a few examples of this class probes are discussed here. For an extensive overview of ion-activated MR contrast agents we direct the reader to an excellent review by Chang et al.[280,283]

The Meade lab developed the first ion-activated MR contrast agent (DOPTA-Gd) which is a *q*-modulated Ca(II)-sensitive probe.[275] The Ca^{2+} binding domain is comprised of a tetraaminoacetate Ca(II)-binding ligand known as BAPTA (Figure 59). A Gd(III)-DO3A chelate is conjugated to either side of this ion-binding core. In the absence of Ca(II), the acetate groups of BAPTA are believed to bind to the Gd(III) center, restricting water access. In the presence of Ca(II), these acetate groups will preferentially coordinate to Ca(II), opening a site on the lanthanide for water coordination.[283–286] The agent shows a 75% increase in relaxivity in response to the presence of physiologically relevant concentrations of Ca(II), i.e. 0.1–10 μM.[275,284]

Since the development of DOPTA-Gd several other examples of Ca(II)-sensitive agents have been developed, in an effort to improve both the increase in relaxivity upon Ca(II) addition and the Ca(II) binding affinity.[275,283–286] While most of these recently developed Ca(II)-sensitive probes are *q*-modulated, Peters et al. developed a bisphosphonate modified chelate that undergoes metal-induced oligomeriztion, increasing the τ_R and thus the relaxivity of the complex.[284,287]

A number of Zn(II)-activated probes have been developed in recent years. Sherry et al. developed the τ_r modulated Zn(II)-activated contrast agent, Gd-DOTA-diBPEN (Figure 60), which contains two dipicolylamine groups which have a high affinity for Zn(II) ions.[274,287,289,290] In the absence of Zn(II), the complex has no affinity for HSA. In the presence of Zn, however, the agent forms a 1:2 Gd-DOTA-diBPEN:Zn(II) adduct that readily binds to HSA, increasing the τ_R and thus the relaxivity of the complex. Specifically, in the presence of HSA, at 23 MHz, the relaxivity changes from 6.6 to 17.4 $mM^{-1}s^{-1}$ upon the addition of two equivalents of Zn(II), a 165% increase. Moreover, the complex has a high affinity for Zn(II) (K_d = 33.6 nM), making it an excellent candidate for in vivo studies of fluctuations in Zn(II) concentration.

Consequently, Sherry et al. performed several subsequent studies with this agent to explore how the addition of insulin-stimulating levels of glucose affects the release of Zn(II) from β-islet cells. Their initial experiments involved an ex vivo study utilizing freshly isolated islets. In the presence of both HSA and Gd-DOTA-diBPEN, the islets subjected to a high, insulin-stimulating concentration of glucose (17.5 mM) exhibited much lower T_1 values than those subjected to a low, non-insulin stimulating level of glucose (2.5 mM) (Figure 61). Subsequently, they performed an in vivo study with 12-week old mice. Following an intraperitoneal (IP) injection of glucose (50 μL of a 20% glucose solution, designed to reach the target blood glucose concentration of 17 mM), 25 μL of Gd-DOTA-diBPEN (25 mM) was administered via tail vein injection. After 10 minutes, MR images showed significant T_1 contrast enhancement only in areas associated with the pancreas, i.e. insulin producing β-islet cells (Figure 62). No such contrast enhancement was observed when Gd-HPDO3A (a non-bioresponsive, commercially available contrast agent) was administered under the same conditions, indicating that Gd-DOTA-diBPEN is capable of detecting in vivo changes in Zn(II) concentration associated with insulin release. Further efforts to develop analogues of Gd-DOTA-diBPEN that optimize the affinity of the Zn(II) bound form for HSA are currently underway.[280,288,291]

Several *q*-modulated, Zn(II)-activated contrast agents have also been developed. The Gd-daa-*n* series developed by Meade et al. has been studied in detail (Figure 63).[274,289,290,293–296] The agent consists of three primary domains: a Gd-DO3A chelate, a Zn(II)-binding domain, and an aliphatic linker between the two. Similar to the mechanism utilized by the Ca(II)-sensitive DOPTA-Gd, in the absence of Zn(II), one of the acetate groups of the Zn(II) binding domain coordinates back to the Gd(III) center, restricting water access to create a low-relaxivity state with $q = 0$. In the presence of Zn(II), both acetate groups preferentially coordinate the divalent transition metal, leaving a coordination site open on the lanthanide for water access, creating a high relaxivity, $q = 1$ state.

A recent study performed a systematic structural optimization of the agent, showing that the change in relaxivity upon the addition of Zn(II) strongly depends on the length of the aliphatic linker, *n*. Complexes with intermediate linker lengths (*n* = 4 or 5 carbons) exhibit the largest change in relaxivity upon the addition of Zn(II). Specifically, the relaxivity changed from 2.5 to 7.8 $mM^{-1}s^{-1}$ at 1.5 T upon the addition of Zn(II), a 200% increase. When the linker is too short (*n* = 2 or 3 carbons), neither acetate group of the Zn(II) binding domain is able to bind back to the Gd(III) center in the absence of Zn(II), and the complex cannot effectively restrict water access. Conversely if the linker is too long (*n* = 6 or 7 carbons), the acetate groups of the Zn(II) binding domain are able to bind back, but the two acetates undergo a rapid coordinative exchange with one another, limiting the water restricting capabilities of the complex. In addition to optimizing a specific Zn(II)-activated contrast agent, this study elucidated key principles for the design of future generations of *q*-modulated contrast agents.

The Chang lab has developed a series of *q*-modulated, Cu-activated MR contrast agents containing thioether-based copper-binding domains. The most effective of these agents are CG2, CG3, and CG7 (Figure 64), which display more than a 300% increase in relaxivity in response to the presence of Cu(I).[263–266,280,291,297–301] In the absence of copper, the nitrogen of the pyridine ring separating the copper-binding domain from the Gd(III) chelate coordinates to the Gd(III) center, restricting water access. Once copper is added to the system the nitrogen (and the thioether moieties) bind the copper eliminating the steric obstruction from the Gd(III) center and facilitating water access. In addition to the increase in relaxivity displayed by these agents, CG2, CG3 and CG7 are highly selective for Cu over other biologically relevant metal cations such as Zn(II), Ca(II), and Mg(II) and show extraordinarily high affinity for Cu, with binding constants below the picomolar range. Such high affinity and selectivity is necessary for agents designed to detect fluctuations in Cu, as the concentration of free Cu in vivo is significantly lower than that of other metal cations such as Zn(II).

Several groups have focused on the development of anion-responsive probes, particularly those that are activated by the presence of phosphate groups.[293–296,304,305] The Morrow Lab has performed extensive studies with Ln(*S*-THP)$^{3+}$: a complex that exhibits significantly enhanced PARACEST effects at neutral pH in the presence of several biologically relevant anions, including citrate, acetate, and diethyl phosphate (Figure 65).[293–295] Anions modulate the exchange rate of the alcohol protons through innersphere and outersphere interactions. While future work is required to improve the selectivity of these complexes, initial results are promising.

3.3.4 Enzyme-Activated Probes—A number of enzyme-activated MR contrast agents have been developed in the past two decades. A large fraction of these probes are activated by reporter proteins, such as β- galactosidase (β-gal),[263–266,297–301,306–309] while others are activated by proteases (MMPs)[263,304,305] or peroxidases.[263,306–309]

The first reported enzyme-activated MRI contrast agent, EGad, was developed by the Meade lab (Figure 66).[263–266] This *q*-modulated agent is activated by β-gal, the enzymatic product of the LacZ reporter gene.[263,265,266,310,311] In the absence of β-gal activity, the sugar moiety

is positioned in such a way as to inhibit water access to the Gd(III) ion. Because the original agent displayed only a 30% increase in r_1 in response to β-gal activity, two structural analogues were developed – α- and β-EGadMe (Figure 66).[264–266,297] These agents contain an additional methyl group in the linkage between the Gd(III) chelate and the sugar moiety, either α or β to the macrocycle. Both α- and β-EGadMe show a 40–50% increase in relaxivity in the presence of β-gal, highlighting the fact that subtle structural changes can have profound effects on the efficacy of *q*-modulated contrast agents.[264–266,297]

Despite favorable changes in relaxivity in the presence of β-gal, the enzyme kinetics of the EGad series was not optimal. To address this issue, a new generation of enzyme-activated agents was developed which contain an extended, self-immolative linkage between the sugar and the Gd(III) chelate (Figure 67).[297–300] In the presence of β-glucoronidase the sugar moiety is cleaved, initiating an electron cascade, which causes the rest of the linkage to dissociate from the chelate.[297,299] This new design successfully improved the kinetics of enzymatic cleavage compared to the EGad series.

Several other groups have developed τ_R modulated, β-gal-responsive contrast agents.[298–300,306–309] The Wang lab developed Gd(DOTA-FPG), which, upon cleavage of the β-gal moiety, rearranges to form a highly reactive electrophile that is attacked by a nucleophilic site on HSA (or by another available protein with a nucleophilic site) to form a covalent adduct with the contrast agent, increasing both the τ_R (from 228 ps to 1068 ps) and the relaxivity (from 7.6 to 15.5 $mM^{-1}s^{-1}$) of the complex (Figure 68).[299,308,309] Using a similar strategy, Hanaoka et al. developed a DTPA derivative in which a biphenyl moiety connects the chelate to a β-gal substrate[298] In the absence of β-gal, the complex has little affinity for HSA; however, following enzymatic cleavage of the sugar substrate, the complex terminates in a hydrophobic aromatic group and the affinity of the complex for HSA increases dramatically (Figure 69). Subsequent formation of a non-covalent adduct between the complex and HSA increases the relaxivity from 6 to 9.5 $mM^{-1}s^{-1}$.

Weissleder and Bogdanov et al. developed a class of τ_R-modulated, enzyme-activated MR contrast agents that respond to the presence of peroxidase enzymes such as myeloperoxidase (MPO), an enzyme that is activated during inflammatory responses and is capable of generating reactive oxygen species.[306–309] These probes consist of an easily oxidized phenolic alcohol (such as a tyramido- or 5-hydroxytryptamido- (5-HT) group) conjugated to either Gd(III)-DTPA[308,309] or Gd(III)-DO3A.[308] In the presence of MPO, the tyramido or 5-HT moiety becomes oxidized, forming a free radical. These radical complexes subsequently combine with one another, forming high molecular weight oligomers up to five units long. These oligomers exhibit a high propensity for protein binding, further increasing the molecular weight, and consequently the τ_R and relaxivity of the contrast agents. The bis-5-HT modified DTPA complex, Gd-MPO, (Figure 70) has been studied extensively.[308,309] Upon MPO-induced oligomerization, the r_1 of the complex increases from 4.5 to 9 $mM^{-1}s^{-1}$.[308,309] Crosslinking of the oligomers with other proteins further increases the relaxivity to nearly 25 $mM^{-1}s^{-1}$.[308,312] Using an animal stroke model, Weissleder et al. confirmed that this agent is capable of reporting on the oxidative activity of MPO in vivo, illustrating its potential as both a research and diagnostic tool.[309,312]

1.3.4 pH-activated probes—The polyornithine-based MR contrast agent developed by Aime et al. is an excellent example of a pH responsive MR probes.[312] This agent is composed of 114 ornithine residues, 30 of which are modified with Gd(III)-DO3A derivatives (Figure 71). At low pH, the free amines of the unmodified ornithine residues are protonated and fully hydrated, and the complex displays a reasonable amount of rotational freedom. Consequently, the local rotation of the chelates is decoupled from the global rotation of the molecule. As the pH increases, these amines become deprotonated and form intramolecular hydrogen bonds, rigidifying the structure. This increases the local τ_R of the chelate, and in turn the relaxivity. As the pH increases from 4 to 8, the relaxivity of the complex increases from 23 to 32 $mM^{-1}s^{-1}$.[312–315]

A number of Gd(III)-based, pH-responsive contrast agents have been developed that rely on the pH-dependence of either pendant arm coordination to the metal center (i.e. *q*modulation)[270,313–315,318–320] or water exchange acceleration.[316,317,319,320] However, PARACEST agents are especially well suited for pH monitoring applications, as they offer the possibility for quantitative pH mapping.[270,318–320] As discussed in Section 3.3.2, the magnitude of the effect produced by a given PARACEST agent is determined by the rate at which the proton of interest exchanges with the protons of the bulk water molecule, a property that is inherently pH dependent. Moreover, due to their different values of Δω, multiple pH-responsive PARACEST agents containing different metal centers can be administered simultaneously to allow for ratiometric pH determination. Further, PARACEST agents may contain more than one pool of exchangeable protons.

For example, the pH-responsive agent Ln(III)-DOTAM-Gly (Ln(III) = Eu, Pr, Nd) developed by Aime et al. contains two different pools of exchangeable protons, those of the coordinated water molecule and those of the amide groups on the pendant arms (Figure 72).[318–320] These two pools of protons display distinct values of Δω, and can thus be independently activated by applying presaturation pulses of two different frequencies. In the pH range of 6–8, only the amide proton exchange rate displays a strong pH dependence and the water exchange rate is largely pH independent. Consequently, a concentration independent measure of pH can be acquired by measuring the ratio of the intensities of these two separate PARACEST signals.

One challenge posed by the Ln(III)-DOTAM-Gly system is that it entails the measurement of a PARACEST signal that is not significantly shifted from the bulk water resonance (Δω of pendant amide protons is typically only ~15 ppm), which may confound results with partial off-resonance saturation. Sherry et al. improved upon this design by replacing one of the pendant amide arms of Eu(III)-DOTAM-Gly with a ketone donor conjugated to an ionizable phenol (Figure 73).[318] As the pH increases, the phenol becomes deprotonated (pKa ~ 6.5–6.7) and the complex adopts a quinone-like resonance structure in which the former ketone donor becomes negatively charged. Such a change in the coordination environment of the lanthanide changes the intensity, and more interestingly the frequency, of the PARACEST signal arising from the coordinated water. Between pH 6.0 and 7.6, Δω of the coordinated water shifts from 49 – 55 ppm.[318] Moreover, within this pH range, the ratio of the PARACEST intensities measured after activation at 49 and 55 ppm is both linear and concentration independent.[318] Thus, this agent can be used to quantitatively determine

pH using only a single pool of protons whose PARACEST signal is sufficiently shifted from the bulk water resonance.

4. Summary

Substantial progress has been made toward the design and development of lanthanide-based probes that are both biocompatible and bioresponsive. These efforts have given rise to a large number of promising new probes for optical imaging and MRI.

Luminescent lanthanide sensors are quickly progressing towards time-gated, live-cell imaging applications, permitting quantification of specific analytes with ratiometric detection. The examples highlighted here describe the principles for tuning the selectivity, localization, and photophysical properties of emissive lanthanide sensors. These advances, coupled with the remarkable progress in luminescence microscopy, offer exciting prospects for the use of lanthanide-based probes for dynamic cellular and whole animal imaging applications.

The remarkable advances in the preparation of new MR imaging agents over the last 2 decades is making a significant impact in basic science applications and diagnostic radiology. Whole animal imaging provides a unique window into the fundamental questions of developmental and very recently, molecular biological questions that we face.

Major strides in understanding the basic chemical and physical properties of lanthanide coordination complexes have uncovered their vast potential as diagnostic tools. Probes can be rationally tailored to the desired application, offering scientists across multiple disciplines exciting tools to tackle complex biological problems from the basic science to clinical endpoints.

Acknowledgments

The authors are grateful to Sarah Kamper, Christiane Carney, Victoria Harrison, and Daniel J. Feld for reviewing the manuscript. M. C. H. and L. M. M. would like to acknowledge the National Science Foundation Graduate Research Fellowship. The authors gratefully acknowledge funding from National Institute of Health under Grant R01EB005866, and the Center for Cancer Nanotechnology Excellence (CCNE) initiative of the National Institutes of Health's National Cancer Institute under Award U54CA151880.

References

1. Bünzli, J-CG.; Eliseeva, SV. Springer Series on Fluorescence. Lanthanide Luminescence: Photophysical, Analytical and Biological Aspects. Hänninen, P.; Härmä, H., editors. Vol. Vol. 7. Springer Verlag: Verlag Berlin Heidelberg; 2011. p. 1-46.
2. Ramogida CF, Orvig C. Chem. Commun. 2013; 49:4720.
3. Laurent S, Vander Elst L, Muller RN. Q. J. Nucl. Med. Mol. Imaging. 2009; 53:586. [PubMed: 20016451]
4. Hanaoka K. Chem. Pharm. Bull. 2010; 58:1283. [PubMed: 20930392]
5. Louie A. Chem. Rev. 2010; 110:3146. [PubMed: 20225900]
6. Major JL, Meade TJ. Acc. Chem. Res. 2009; 42:893. [PubMed: 19537782]
7. Montgomery CP, Murray BS, New EJ, Pal R, Parker D. Acc. Chem. Res. 2009; 42:925. [PubMed: 19191558]
8. Thibon A, Pierre VC. Anal. Bioanal. Chem. 2009; 394:107. [PubMed: 19283368]

9. Weissleder R, Ntziachristos V. Nat. Med. 2003; 9:123. [PubMed: 12514725]
10. Vereb G, Jares-Erijman E, Selvin PR, Jovin TM. Biophysical Journal. 1998; 74:2210. [PubMed: 9591648]
11. Gahlaut N, Miller LW. Cytometry A. 2010; 77A:1113. [PubMed: 20824630]
12. Connally RE, Piper JA. Ann. N. Y. Acad. Sci. 2008; 1130:106. [PubMed: 18596339]
13. Werts MHV. Sci. Prog. 2005; 88:101. [PubMed: 16749431]
14. Bünzli J-CG. Acc. Chem. Res. 2006; 39:53. [PubMed: 16411740]
15. Bünzli J-CG, Chauvin A-S, Kim HK, Deiters E, Eliseeva SV. Coord. Chem. Rev. 2010; 254:2623.
16. Leif RC, Vallarino LM, Becker MC, Yang S. Cytometry A. 2006; 69:767. [PubMed: 16969794]
17. Spangler, C.; Schäferling, M. Springer Series on Fluorescence. Lanthanide Luminescence: Photophysical, Analytical and Biological Aspects. Hänninen, P.; Härmä, H., editors. Vol. Vol. 7. Berlin, Germany: Springer Series on Fluorescence; Springer Verlag; 2010. p. 235-262.
18. Hemmilä I, Laitala V. J. Fluoresc. 2005; 15:529. [PubMed: 16167211]
19. Moore EG, Samuel APS, Raymond KN. Acc. Chem. Res. 2009; 42:542. [PubMed: 19323456]
20. Weissman SI. J. Chem. Phys. 1942; 10:214.
21. Bünzli J-CG. Chem. Rev. 2010; 110:2729. [PubMed: 20151630]
22. Alpha B, Ballardini R, Balzani V, Lehn J-M, Perathoner S, Sabbatini N. Photochem. Photobiol. 1990; 52:299.
23. Hagan AK, Zuchner T. Anal. Bioanal. Chem. 2011; 400:2847. [PubMed: 21556751]
24. De Sa GF, Malta OL, de Mello Donegá C, Simas AM, Longo RL, Santa-Cruz PA, da Silva EF Jr. Coord. Chem. Rev. 2000; 196:165.
25. Parker D. Aust. J. Chem. 2011; 64:239.
26. Werts MHV, Jukes RTF, Verhoeven JW. Phys. Chem. Chem. Phys. 2002; 4:1542.
27. Ziessel R, Ulrich G, Asfari Z, Lehn JM. Pure Appl. Chem. 1995; 67:135.
28. Law G-L, Pham TA, Xu J, Raymond KN. Angew. Chem. Int. Ed. 2012; 51:2371.
29. Werts MHV, Woudenberg RH, Emmerink PG, van Gassel R, Hofstraat JW, Verhoeven JW. Angew. Chem. Int. Ed. 2000; 112:4716.
30. Beeby A, Faulkner S, Williams JAG. Dalton Trans. 2002:1918.
31. Werts MHV, Verhoeven JW, Hofstraat JW. J. Chem. Soc. Perkin Trans. 2000:433.
32. Hess BA, Kedziorski A, Smentek L, Bornhop DJ. J. Phys. Chem. A. 2008; 112:2397. [PubMed: 18298101]
33. Butler SJ, Parker D. Chem. Soc. Rev. 2013; 42:1652. [PubMed: 22760156]
34. Kielar F, Montgomery CP, New EJ, Parker D, Poole RA, Richardson SL, Stenson PA. Org. Biomol. Chem. 2007; 5:2975. [PubMed: 17728864]
35. Horrocks WD Jr, Sudnick DR. J. Am. Chem. Soc. 1979; 101:334.
36. Beeby A, Clarkson IM, Dickins RS, Faulkner S, Parker D, Royle L, de Sousa AS, Williams JAG, Woods M. J. Chem. Soc. Perkin Trans. 1999:493.
37. Bünzli J-CG, Piguet C. Chem. Soc. Rev. 2005; 34:1048. [PubMed: 16284671]
38. Poole RA, Bobba G, Cann MJ, Frias J-C, Parker D, Peacock RD. Org. Biomol. Chem. 2005; 3:1013. [PubMed: 15750644]
39. Santos, dos CM, Harte AJ, Quinn SJ, Gunnlaugsson T. Coord. Chem. Rev. 2008; 252:2512.
40. Latva M, Takalo H, Mukkala V-M, Matachescu C, Rodríguez-Ubis JC, Kankare J. J. Lumin. 1997; 75:149.
41. Montgomery CP, Parker D, Lamarque L. Chem. Commun. 2007:3841.
42. Atkinson P, Findlay KS, Kielar F, Pal R, Parker D, Poole RA, Puschmann H, Richardson SL, Stenson PA, Thompson AL, Yu J. Org. Biomol. Chem. 2006; 4:1707. [PubMed: 16633563]
43. Ge P, Selvin PR. Bioconjugate Chem. 2004; 15:1088.
44. van der Tol EB, van Ramesdonk HJ, Verhoeven JW, Steemers FJ, Kerver EG, Verboom W, Reinhoudt DN. Chem. Eur. J. 1998; 4:2315.
45. Bassett AP, Magennis SW, Glover PB, Lewis DJ, Spencer N, Parsons S, Williams RM, De Cola L, Pikramenou Z. J. Am. Chem. Soc. 2004; 126:9413. [PubMed: 15281834]

46. Murray BS, New EJ, Pal R, Parker D. Org. Biomol. Chem. 2008; 6:2085. [PubMed: 18528570]
47. Beeby A, Bushby LM, Maffeo D, Williams JAG. J. Chem. Soc. Perkin Trans. 2000:1281.
48. Pandya S, Yu J, Parker D. Dalton Trans. 2006:2757. [PubMed: 16751883]
49. New EJ, Congreve A, Parker D. Chem. Sci. 2010; 1:111.
50. New EJ, Parker D. Org. Biomol. Chem. 2009; 7:851. [PubMed: 19225664]
51. New EJ, Parker D, Smith DG, Walton JW. Curr. Opin. Chem. Biol. 2010; 14:238. [PubMed: 19884038]
52. Baggaley E, Weinstein JA, Williams JAG. Coord. Chem. Rev. 2012; 256:1762.
53. Parker D. Chem. Soc. Rev. 2004; 33:156. [PubMed: 15026820]
54. Walton JW, Bourdolle A, Butler SJ, Soulie M, Delbianco M, McMahon BK, Pal R, Puschmann H, Zwier JM, Lamarque L, Maury O, Andraud C, Parker D. Chem. Commun. 2013; 49:1600.
55. Hemmilä I, Mukkala V-M, Takalo H. J. Alloys Compd. 1997; 249:158.
56. Takalo H, Hemmil I, Sutela T, Latva M. Helv. Chim. Acta. 1996; 79:789.
57. Kaczmarek M, Lis S. Analyst. 2011; 136:2592. [PubMed: 21519592]
58. Sénéchal-David K, Leonard JP, Plush SE, Gunnlaugsson T. Org. Lett. 2006; 8:2727. [PubMed: 16774242]
59. Nonat AM, Quinn SJ, Gunnlaugsson T. Inorg. Chem. 2009; 48:4646. [PubMed: 19400563]
60. Pope SJ, Coe BJ, Faulkner S, Bichenkova EV, Yu X, Douglas KT. J. Am. Chem. Soc. 2004; 126:9490. [PubMed: 15291523]
61. Feng X, Feng Y-Q, Liu L, Wang L-Y, Song H-L, Ng S-W. Dalton Trans. 2013; 42:7741. [PubMed: 23549773]
62. Kaczmarek M, Idzikowska A, Lis S. J. Fluoresc. 2008; 18:1193. [PubMed: 18454308]
63. Chen F-F, Chen Z-Q, Bian Z-Q, Huang C-H. Coord. Chem. Rev. 2010; 254:991.
64. Ward MD. Coord. Chem. Rev. 2010; 254:2634.
65. Klink SI, Keizer H, van Veggel FC. Angew. Chem. Int. Ed. 2000; 39:4319.
66. Alpha B, Lehn J-M, Mathis G. Angew. Chem. Int. Ed. 1987; 26:266.
67. Yuan J, Wang G. J. Fluoresc. 2005; 15:559. [PubMed: 16167214]
68. Yuan J, Wang G, Majima K, Matsumoto K. Anal. Chem. 2001; 73:1869. [PubMed: 11338604]
69. Yuan J, Tan M, Wang G. J. Lumin. 2004; 106:91.
70. Samuel APS, Lunkley JL, Muller G, Raymond KN. Eur. J. Inorg. Chem. 2010; 2010:3343. [PubMed: 20730030]
71. Samuel APS, Moore EG, Melchior M, Xu J, Raymond KN. Inorg. Chem. 2008; 47:7535. [PubMed: 18671388]
72. Petoud S, Cohen SM, Bünzli J-CG, Raymond KN. J. Am. Chem. Soc. 2003; 125:13324. [PubMed: 14583005]
73. Moore EG, Xu J, Jocher CJ, Castro-Rodriguez I, Raymond KN. Inorg. Chem. 2008; 47:3105. [PubMed: 18311915]
74. Moore EG, Xu J, Jocher CJ, Werner EJ, Raymond KN. J. Am. Chem. Soc. 2006; 128:10648. [PubMed: 16910637]
75. Song C, Ye Z, Wang G, Yuan J, Guan Y. Chem. Eur. J. 2010; 16:6464. [PubMed: 20486239]
76. Chen Y, Guo W, Ye Z, Wang G, Yuan J. Chem. Commun. 2011; 47:6266.
77. Seitz M, Moore EG, Ingram AJ, Muller G, Raymond KN. J. Am. Chem. Soc. 2007; 129:15468. [PubMed: 18031042]
78. Yuasa J, Ohno T, Tsumatori H, Shiba R, Kamikubo H, Kataoka M, Hasegawa Y, Kawai T. Chem. Commun. 2013; 49:4604.
79. Petoud S, Muller G, Moore EG, Xu J, Sokolnicki J, Riehl JP, Le UN, Cohen SM, Raymond KN. J. Am. Chem. Soc. 2007; 129:77. [PubMed: 17199285]
80. Bünzli J-CG, Comby S, Chauvin A-S, Vandevyver CDB. J. Rare Earths. 2007; 25:257.
81. Carr R, Evans NH, Parker D. Chem. Soc. Rev. 2012; 41:7673. [PubMed: 22895164]
82. Parker D, Senanayake PK, Gareth Williams JA. J. Chem. Soc. Perkin Trans. 1998:2129.
83. Eliseeva SV, Bünzli J-CG. Chem. Soc. Rev. 2010; 39:189. [PubMed: 20023849]

84. Callan JF, de Silva AP, Magri DC. Tetrahedron. 2005; 61:8551.
85. Demchenko AP. J. Fluoresc. 2010; 20:1099. [PubMed: 20358283]
86. Tremblay MS, Halim M, Sames D. J. Am. Chem. Soc. 2007; 129:7570. [PubMed: 17518468]
87. Terai T, Ito H, Kikuchi K, Nagano T. Chem. Eur. J. 2012; 18:7377. [PubMed: 22573453]
88. Manning HC, Goebel T, Thompson RC, Price RR, Lee H, Bornhop DJ. Bioconjugate Chem. 2004; 15:1488.
89. Xiao Y, Ye Z, Wang G, Yuan J. Inorg. Chem. 2012; 51:2940. [PubMed: 22356217]
90. Parker D. Coord. Chem. Rev. 2000; 205:109.
91. Poole RA, Kielar F, Richardson SL, Stenson PA, Parker D. Chem. Commun. 2006:4084.
92. Bruce JI, Dickins RS, Govenlock LJ, Gunnlaugsson T, Lopinski S, Lowe MP, Parker D, Peacock RD, Perry JJB, Aime S, Botta M. J. Am. Chem. Soc. 2000; 122:9674.
93. Dickins RS, Aime S, Batsanov AS, Beeby A, Botta M, Bruce JI, Howard JAK, Love CS, Parker D, Peacock RD, Puschmann H. J. Am. Chem. Soc. 2002; 124:12697. [PubMed: 12392417]
94. Pal R, Parker D. Org. Biomol. Chem. 2008; 6:1020. [PubMed: 18327327]
95. Smith DG, McMahon BK, Pal R, Parker D. Chem. Commun. 2012; 48:8520.
96. McMahon BK, Pal R, Parker D. Chem. Commun. 2013; 49:5363.
97. Thibon A, Pierre VC. J. Am. Chem. Soc. 2008; 131:434. [PubMed: 19113859]
98. Bretonnière Y, Cann MJ, Parker D, Slater R. Org. Biomol. Chem. 2004; 2:1624. [PubMed: 15162215]
99. Pal R, Parker D, Costello LC. Org. Biomol. Chem. 2009; 7:1525. [PubMed: 19343236]
100. Pal R, Beeby A, Parker D. J. Pharm. Biomed. Anal. 2011; 56:352. [PubMed: 21680129]
101. Smith DG, Law G-L, Murray BS, Pal R, Parker D, Wong K-L. Chem. Commun. 2011; 47:7347.
102. Smith DG, Pal R, Parker D. Chem. Eur. J. 2012; 18:11604. [PubMed: 22865800]
103. Gokel GW, Barbour LJ, Ferdani R, Hu J. Acc. Chem. Res. 2002; 35:878. [PubMed: 12379140]
104. Meadows ES, De Wall SL, Barbour LJ, Gokel GW. J. Am. Chem. Soc. 2001; 123:3092. [PubMed: 11457020]
105. Weitz EA, Pierre VC. Chem. Commun. 2011; 47:541.
106. Lee K, Dzubeck V, Latshaw L, Schneider JP. J. Am. Chem. Soc. 2004; 126:13616. [PubMed: 15493909]
107. Viguier RFH, Hulme AN. J. Am. Chem. Soc. 2006; 128:11370. [PubMed: 16939257]
108. Bailey MP, Rocks BF, Riley C. Anal. Chim. Acta. 1987; 201:335.
109. Gunnlaugsson T, Harte AJ, Leonard JP, Niewenhuyzen M. Supramol. Chem. 2003; 15:505.
110. Harte AJ, Jensen P, Plush SE, Kruger PE, Gunnlaugsson T. Inorg. Chem. 2006; 45:9465. [PubMed: 17083248]
111. Meyer J, Karst U. Analyst. 2000; 125:1537.
112. Page SE, Wilke KT, Pierre VC. Chem. Commun. 2010; 46:2423.
113. Plush SE, Gunnlaugsson T. Org. Lett. 2007; 9:1919. [PubMed: 17447771]
114. Gunnlaugsson T, Stomeo F. Org. Biomol. Chem. 2007; 5:1999. [PubMed: 17581643]
115. Gunnlaugsson T, Leonard JP. Chem. Commun. 2005:3114.
116. Kotova O, Comby S, Gunnlaugsson T. Chem. Commun. 2011; 47:6810.
117. Comby S, Tuck SA, Truman LK, Kotova O, Gunnlaugsson T. Inorg. Chem. 2012; 51:10158. [PubMed: 22974321]
118. Song B, Wang G, Tan M, Yuan J. J. Am. Chem. Soc. 2006; 128:13442. [PubMed: 17031957]
119. Wang S, Li N, Pan W, Tang B. Trends Anal. Chem. 2012; 39:3.
120. Lim MH, Lippard SJ. Acc. Chem. Res. 2007; 40:41. [PubMed: 17226944]
121. Miller EW, Tulyanthan O, Isacoff EY, Chang CJ. Nat. Chem. Biol. 2007; 3:263. [PubMed: 17401379]
122. Szabo C. Sci. Transl. Med. 2010; 2:59ps54.
123. Moody BF, Calvert JW. Medical Gas Research. 2011; 1:3. [PubMed: 22146243]
124. Miller EW, Chang CJ. Curr. Opin. Chem. Biol. 2007; 11:620. [PubMed: 17967434]

125. Schäferling M, Grögel DBM, Schreml S. Microchim. Acta. 2011; 174:1.
126. McMahon B, Mauer P, McCoy CP, Lee TC, Gunnlaugsson T. J. Am. Chem. Soc. 2009; 131:17542. [PubMed: 19916488]
127. Terai T, Kikuchi K, Iwasawa S-Y, Kawabe T, Hirata Y, Urano Y, Nagano T. J. Am. Chem. Soc. 2006; 128:6938. [PubMed: 16719474]
128. Pershagen E, Nordholm J, Borbas KE. J. Am. Chem. Soc. 2012; 134:9832. [PubMed: 22339236]
129. Lippert AR, Gschneidtner T, Chang CJ. Chem. Commun. 2010; 46:7510.
130. Dürkop A, Wolfbeis OS. J. Fluoresc. 2005; 15:755. [PubMed: 16341794]
131. Wolfbeis OS, Dürkop A, Wu M, Lin Z. Angew. Chem. Int. Ed. 2002; 41:4495.
132. Schäferling M, Wolfbeis OS. Chem. Eur. J. 2007; 13:4342. [PubMed: 17323391]
133. Ye Z, Wang G, Chen J, Fu X, Zhang W, Yuan J. Biosens. Bioelectron. 2010; 26:1043. [PubMed: 20846845]
134. Liu M, Ye Z, Xin C, Yuan J. Anal. Chim. Acta. 2013; 761:149. [PubMed: 23312326]
135. Song B, Wang G, Yuan J. Chem. Commun. 2005:3553.
136. Liu M, Ye Z, Wang G, Yuan J. Talanta. 2012; 99:951. [PubMed: 22967648]
137. Xiao Y, Zhang R, Ye Z, Dai Z, An H, Yuan J. Anal. Chem. 2012; 84:10785. [PubMed: 23190019]
138. Liu M, Ye Z, Wang G, Yuan J. Talanta. 2012; 91:116. [PubMed: 22365689]
139. Cui G, Ye Z, Zhang R, Wang G, Yuan J. J. Fluoresc. 2012; 22:261. [PubMed: 21853255]
140. Ye Z, Chen J, Wang G, Yuan J. Anal. Chem. 2011; 83:4163. [PubMed: 21548628]
141. Olea AF, Wilkinson F. J. Phys. Chem. 1995; 99:4518.
142. Wilkinson F, McGarvey DJ, Olea AF. J. Am. Chem. Soc. 1993; 115:12144.
143. Corey EJ, Taylor WC. J. Am. Chem. Soc. 1964; 86:3881.
144. Gandin E, Lion Y, Van de Vorst A. Photochem. Photobiol. 1983; 37:271.
145. Weitz EA, Chang JY, Rosenfield AH, Pierre VC. J. Am. Chem. Soc. 2012; 134:16099. [PubMed: 22994413]
146. McMahon BK, Gunnlaugsson T. Tetrahedron Lett. 2010; 51:5406.
147. Carr R, Di Bari L, Piano, Lo S, Parker D, Peacock RD, Sanderson JM. Dalton Trans. 2012; 41:13154. [PubMed: 23023320]
148. Caravan P, Ellison JJ, McMurry TJ, Lauffer RB. Chem. Rev. 1999; 99:2293. [PubMed: 11749483]
149. Bloembergen N. J. Chem. Phys. 1957; 27:572.
150. Woods M, Aime S, Botta M, Howard JAK, Moloney JM, Navet M, Parker D, Port M, Rousseaux O. J. Am. Chem. Soc. 2000; 122:9781.
151. Solomon I, Bloembergen N. J. Chem. Phys. 1956; 25:261.
152. Solomon I. Phys. Rev. 1955; 99:559.
153. Bloembergen N, Purcell EM, Pound RV. Phys. Rev. 1948; 73:679.
154. Caravan P, Farrar CT, Frullano L, Uppal R. Contrast Media Mol. Imaging. 2009; 4:89. [PubMed: 19177472]
155. Drahoš B, Lukeš I, Tóth É. Eur. J. Inorg. Chem. 2012; 2012:1975.
156. Parac-Vogt TN, Kimpe K, Laurent S, Piérart C, Elst LV, Muller RN, Binnemans K. Eur. J. Inorg. Chem. 2004; 2004:3538.
157. Zhang G, Liu Y, Yuan Q, Zong C, Liu J, Lu L. Nanoscale. 2011; 3:4365. [PubMed: 21904751]
158. Drahoš B, Kubíček V, Bonnet CS, Hermann P, Lukeš I, Tóth É. Dalton Trans. 2011; 40:1945. [PubMed: 21274464]
159. Kálmán FK, Tircsó G. Inorg. Chem. 2012; 51:10065. [PubMed: 22974437]
160. Loving GS, Mukherjee S, Caravan P. J. Am. Chem. Soc. 2013; 135:4620. [PubMed: 23510406]
161. Zhang Q, Datta A, Gorden JD, Hooker JM, Beyers RJ, Botta M, Goldsmith CR, Francis MB, Aime S, Raymond KN. Inorg. Chem. 2011; 50:9365. [PubMed: 21888331]
162. Garcia J, Neelavalli J, Haacke EM, Allen MJ. Chem. Commun. 2011; 47:12858.

163. Garcia J, Kuda-Wedagedara ANW, Allen MJ. Eur. J. Inorg. Chem. 2012; 2012:2135. [PubMed: 22639543]
164. Sukerkar PA, Macrenaris KW, Meade TJ, Burdette JE. Mol. Pharm. 2011; 8:1390. [PubMed: 21736390]
165. Sukerkar PA, Macrenaris KW, Townsend TR, Ahmed RA, Burdette JE, Meade TJ. Bioconjugate Chem. 2011; 22:2304.
166. Matosziuk LM, Harney AS, Macrenaris KW, Meade TJ. Eur. J. Inorg. Chem. 2012; 2012:2099. [PubMed: 23626484]
167. Frullano L, Wang C, Miller RH, Wang Y. J. Am. Chem. Soc. 2011; 133:1611. [PubMed: 21265506]
168. Vithanarachchi SM, Allen MJ. Chem. Commun. 2013; 49:4148.
169. Geninatti Crich S, Alberti D, Szabo I, Aime S, Djanashvili K. Angew. Chem. Int. Ed. 2013; 52:1161.
170. Lee J, Burdette JE, Macrenaris KW, Mustafi D, Woodruff TK, Meade TJ. Chem. Biol. 2007; 14:824. [PubMed: 17656319]
171. Niers JM, Chen JW, Lewandrowski G, Kerami M, Garanger E, Wojtkiewicz G, Waterman P, Keliher E, Weissleder R, Tannous BA. J. Am. Chem. Soc. 2012; 134:5149. [PubMed: 22397453]
172. Park J-A, Kim JY, Lee YJ, Lee W, Lim SM, Kim T-J, Yoo J, Chang Y, Kim KM. ACS Med. Chem. Lett. 2013; 4:216.
173. Uppal R, Ciesienski KL, Chonde DB, Loving GS, Caravan P. J. Am. Chem. Soc. 2012; 134:10799. [PubMed: 22698259]
174. Verwilst P, Eliseeva SV, vander Elst L, Burtea C, Laurent S, Petoud S, Muller RN, Parac-Vogt TN, de Borggraeve WM. Inorg. Chem. 2012; 51:6405. [PubMed: 22583122]
175. Zhang Z, Kolodziej AF, Greenfield MT, Caravan P. Angew. Chem. Int. Ed. 2011; 50:2621.
176. Werner EJ, Kozhukh J, Botta M, Moore EG, Avedano S, Aime S, Raymond KN. Inorg. Chem. 2009; 48:277. [PubMed: 19032045]
177. Werner EJ, Datta A, Jocher CJ, Raymond KN. Angew. Chem. Int. Ed. 2008; 47:8568.
178. Mendonça AC, Martins AF, Melchior A, Marques SM, Chaves S, Villette S, Petoud S, Zanonato PL, Tolazzi M, Bonnet CS, Tóth É, Di Bernardo P, Geraldes CFGC, Santos MA. Dalton Trans. 2013; 42:6046. [PubMed: 23296398]
179. Datta A, Raymond KN. Acc. Chem. Res. 2009; 42:938. [PubMed: 19505089]
180. Thompson MK, Botta M, Nicolle G, Helm L, Aime S, Merbach AE, Raymond KN. J. Am. Chem. Soc. 2003; 125:14274. [PubMed: 14624565]
181. Garimella PD, Datta A, Romanini DW, Raymond KN, Francis MB. J. Am. Chem. Soc. 2011; 133:14704. [PubMed: 21800868]
182. Floyd WC III, Klemm PJ, Smiles DE, Kohlgruber AC, Pierre VC, Mynar JL, Fréchet JMJ, Raymond KN. J. Am. Chem. Soc. 2011; 133:2390. [PubMed: 21294571]
183. Doble DM, Botta M, Wang J, Aime S, Barge A, Raymond KN. J. Am. Chem. Soc. 2001; 123:10758. [PubMed: 11674017]
184. Caravan P. Acc. Chem. Res. 2009; 42:851. [PubMed: 19222207]
185. Shen C, New EJ. Curr. Opin. Chem. Biol. 2013; 17:158. [PubMed: 23141598]
186. Caravan P, Cloutier NJ, Greenfield MT, McDermid SA, Dunham SU, Bulte JWM, Amedio JC, Looby RJ, Supkowski RM, Horrocks WD, McMurry TJ, Lauffer RB. J. Am. Chem. Soc. 2002; 124:3152. [PubMed: 11902904]
187. Caravan P, Parigi G, Chasse JM, Cloutier NJ, Ellison JJ, Lauffer RB, Luchinat C, McDermid SA, Spiller M, McMurry TJ. Inorg. Chem. 2007; 46:6632. [PubMed: 17625839]
188. Henrotte V, vander Elst L, Laurent S, Muller RN. J. Biol. Inorg. Chem. 2007; 12:929. [PubMed: 17558523]
189. Chang Y-H, Chen C-Y, Singh G, Chen H-Y, Liu G-C, Goan Y-G, Aime S, Wang Y-M. Inorg. Chem. 2011; 50:1275. [PubMed: 21247114]
190. Strauch RC, Mastarone DJ, Sukerkar PA, Song Y, Ipsaro JJ, Meade TJ. J. Am. Chem. Soc. 2011; 133:16346. [PubMed: 21942425]

191. Manus LM, Mastarone DJ, Waters EA, Zhang X-Q, Schultz-Sikma EA, Macrenaris KW, Ho D, Meade TJ. Nano Lett. 2010; 10:484. [PubMed: 20038088]
192. Warsi MF, Adams RW, Duckett SB, Chechik V. Chem. Commun. 2009; 46:451.
193. Lim YT, Cho MY, Choi BS, Lee JM, Chung BH. Chem. Commun. 2008:4930.
194. Taylor KML, Kim JS, Rieter WJ, An H, Lin W, Lin W. J. Am. Chem. Soc. 2008; 130:2154. [PubMed: 18217764]
195. Hooker JM, Datta A, Botta M, Raymond KN, Francis MB. Nano Lett. 2007; 7:2207. [PubMed: 17630809]
196. Datta A, Hooker JM, Botta M, Francis MB, Aime S, Raymond KN. J. Am. Chem. Soc. 2008; 130:2546. [PubMed: 18247608]
197. Qazi S, Liepold LO, Abedin MJ, Johnson B, Prevelige P, Frank JA, Douglas T. Mol. Pharm. 2013; 10:11. [PubMed: 22656692]
198. Song Y, Xu X, Macrenaris KW, Zhang X-Q, Mirkin CA, Meade TJ. Angew. Chem. Int. Ed. 2009; 48:9143.
199. Cai J, Shapiro EM, Hamilton AD. Bioconjugate Chem. 2009; 20:205.
200. Torres S, Martins JA, André JP, Geraldes CFGC, Merbach AE, Tóth É. Chem. Eur. J. 2006; 12:940. [PubMed: 16224764]
201. André JP, Tóth É, Fischer H, Seelig A, Mäcke HR, Merbach AE. Chem. Eur. J. 1999; 5:2977.
202. Accardo A, Tesauro D, Morelli G, Gianolio E, Aime S, Vaccaro M, Mangiapia G, Paduano L, Schillén K. J. Biol. Inorg. Chem. 2006; 12:267. [PubMed: 17143622]
203. Kimpe K, Parac-Vogt TN, Laurent S, Piérart C, Elst LV, Muller RN, Binnemans K. Eur. J. Inorg. Chem. 2003; 2003:3021.
204. Nicolle GM, Tóth É, Eisenwiener K-P, Mäcke HR, Merbach AE. J. Biol. Inorg. Chem. 2002; 7:757. [PubMed: 12203012]
205. Kielar F, Tei L, Terreno E, Botta M. J. Am. Chem. Soc. 2010; 132:7836. [PubMed: 20481537]
206. Vanasschen C, Bouslimani N, Thonon D, Desreux JF. Inorg. Chem. 2011; 50:8946. [PubMed: 21859074]
207. Song Y, Kohlmeir EK, Meade TJ. J. Am. Chem. Soc. 2008; 130:6662. [PubMed: 18452288]
208. Song Y, Zong H, Trivedi ER, Vesper BJ, Waters EA, Barrett AGM, Radosevich JA, Hoffman BM, Meade TJ. Bioconjugate Chem. 2010; 21:2267.
209. Mastarone DJ, Harrison VSR, Eckermann AL, Parigi G, Luchinat C, Meade TJ. J. Am. Chem. Soc. 2011; 133:5329. [PubMed: 21413801]
210. Goswami LN, Ma L, Cai Q, Sarma SJ, Jalisatgi SS, Hawthorne MF. Inorg. Chem. 2013; 52:1701. [PubMed: 23391150]
211. Goswami LN, Ma L, Chakravarty S, Cai Q, Jalisatgi SS, Hawthorne MF. Inorg. Chem. 2013; 52:1694. [PubMed: 23126285]
212. Livramento JB, Weidensteiner C, Prata MIM, Allegrini PR, Geraldes CFGC, Helm L, Kneuer R, Merbach AE, Santos AC, Schmidt P, Tóth É. Contrast Media Mol. Imaging. 2006; 1:30. [PubMed: 17193598]
213. Livramento JB, Sour A, Borel A, Merbach AE, Tóth É. Chem. Eur. J. 2006; 12:989. [PubMed: 16311990]
214. Livramento JB, Tóth É, Sour A, Borel A, Merbach AE, Ruloff R. Angew. Chem. Int. Ed. 2005; 44:1480.
215. Moriggi L, Aebischer A, Cannizzo C, Sour A, Borel A, Bünzli J-CG, Helm L. Dalton Trans. 2009:2088. [PubMed: 19274286]
216. Dehaen G, Verwilst P, Eliseeva SV, Laurent S, vander Elst L, Muller RN, de Borggraeve WM, Binnemans K, Parac-Vogt TN. Inorg. Chem. 2011; 50:10005. [PubMed: 21913641]
217. Dehaen G, Eliseeva SV, Kimpe K, Laurent S, vander Elst L, Muller RN, Dehaen W, Binnemans K, Parac-Vogt TN. Chem. Eur. J. 2012; 18:293. [PubMed: 22139970]
218. Dehaen G, Eliseeva SV, Verwilst P, Laurent S, vander Elst L, Muller RN, de Borggraeve W, Binnemans K, Parac-Vogt TN. Inorg. Chem. 2012; 51:8775. [PubMed: 22839679]
219. Ruloff R, Koten GV, Merbach AE. Chem. Commun. 2004:842.

220. Costa J, Ruloff R, Burai L, Helm L, Merbach AE. J. Am. Chem. Soc. 2005; 127:5147. [PubMed: 15810849]
221. Helm L, Merbach AE. Chem. Rev. 2005; 105:1923. [PubMed: 15941206]
222. Sherry AD, Wu Y. Curr. Opin. Chem. Biol. 2013; 17:167. [PubMed: 23333571]
223. Aime S, Barge A, Botta M, Parker D, de Sousa AS. J. Am. Chem. Soc. 1997; 119:4767.
224. Tóth É, Burai L, Brücher E, Merbach AE. Dalton Trans. 1997:1587.
225. Dunand FA, Aime S, Merbach AE. J. Am. Chem. Soc. 2000; 122:1506.
226. Zhang S, Kovacs Z, Burgess S, Aime S, Terreno E, Sherry AD. Chem. Eur. J. 2001; 7:288. [PubMed: 11205022]
227. Zhang S, Jiang X, Sherry AD. Helv. Chim. Acta. 2005; 88:923.
228. Micskei K, Helm L, Brücher E, Merbach AE. Inorg. Chem. 1993; 32:3844.
229. Green KN, Viswanathan S, Rojas-Quijano FA, Kovacs Z, Sherry AD. Inorg. Chem. 2011; 50:1648. [PubMed: 21306137]
230. Napolitano R, Soesbe TC, de León-Rodríguez LM, Sherry AD, Udugamasooriya DG. J. Am. Chem. Soc. 2011; 133:13023. [PubMed: 21793515]
231. Jászberényi Z, Sour A, Tóth É, Benmelouka M, Merbach AE. Dalton Trans. 2005:2713. [PubMed: 16075110]
232. Laus S, Ruloff R, Tóth É, Merbach AE. Chem. Eur. J. 2003; 9:3555. [PubMed: 12898682]
233. Ruloff R, Tóth É, Scopelliti R, Tripier R, Handel H, Merbach AE. Chem. Commun. 2002:2630.
234. Miller KJ, Saherwala AA, Webber BC, Wu Y, Sherry AD, Woods M. Inorg. Chem. 2010; 49:8662. [PubMed: 20812752]
235. Mayer F, Platas-Iglesias C, Helm L, Peters JA, Djanashvili K. Inorg. Chem. 2012; 51:170. [PubMed: 22128872]
236. Aime S, Botta M, Ermondi G. Inorg. Chem. 1992; 31:4291.
237. Tircsó G, Webber BC, Kucera BE, Young VG, Woods M. Inorg. Chem. 2011; 50:7966. [PubMed: 21819053]
238. Hermann P, Kotek J, Kubíček V, Lukeš I. Dalton Trans. 2008:3027. [PubMed: 18521444]
239. Aime S, Botta M, Garda Z, Kucera BE, Tircsó G, Young VG, Woods M. Inorg. Chem. 2011; 50:7955. [PubMed: 21819052]
240. Delli Castelli D, Caligara MC, Botta M, Terreno E, Aime S. Inorg. Chem. 2013; 52:7130. [PubMed: 23738541]
241. Aime S, Botta M, Fasano M, Marques MPM, Geraldes CF, Pubanz D, Merbach AE. Inorg. Chem. 1997; 36:2059. [PubMed: 11669824]
242. Woods M, Kovacs Z, Kiraly R, Brücher E, Zhang S, Sherry AD. Inorg. Chem. 2004; 43:2845. [PubMed: 15106971]
243. Aime S, Barge A, Botta M, de Sousa AS, Parker D. Angew. Chem. Int. Ed. 1998; 37:2673.
244. Dunand FA, Dickins RS, Parker D, Merbach AE. Chem. Eur. J. 2001; 7:5160. [PubMed: 11775689]
245. Woods M, Kovacs Z, Zhang S, Sherry AD. Angew. Chem. Int. Ed. 2003; 42:5889.
246. Howard JK, Kenwright A, Moloney J. Chem. Commun. 1998:1381.
247. Jacques V, Desreux JF. Inorg. Chem. 1994; 33:4048.
248. Ranganathan RS, Raju N, Fan H, Zhang X, Tweedle MF, Desreux JF, Jacques V. Inorg. Chem. 2002; 41:6856. [PubMed: 12470084]
249. Woods M, Botta M, Avedano S, Wang J, Sherry AD. Dalton Trans. 2005:3829. [PubMed: 16311635]
250. Webber BC, Woods M. Inorg. Chem. 2012; 51:8576. [PubMed: 22809081]
251. Platas-Iglesias C. Eur. J. Inorg. Chem. 2012; 2012:2023.
252. Purgel M, Baranyai Z, de Blas A, Rodríguez-Blas T, Bányai I, Platas-Iglesias C, Tóth I. Inorg. Chem. 2010; 49:4370. [PubMed: 20369836]
253. Shukla RB. Journal of Magnetic Resonance, Series A. 1995; 113:196.
254. Di Bari L, Pintacuda G, Salvadori P. Eur. J. Inorg. Chem. 2000; 2000:75.

255. Aime S, Botta M, Ermondi G, Terreno E, Anelli PL, Fedeli F, Uggeri F. Inorg. Chem. 1996; 35:2726.
256. Ranganathan RS, Pillai RK, Raju N, Fan H, Nguyen H, Tweedle MF, Desreux JF, Jacques V. Inorg. Chem. 2002; 41:6846. [PubMed: 12470083]
257. Avecilla F, Peters JA, Geraldes CF. Eur. J. Inorg. Chem. 2003; 2003:4179.
258. Vojtísek P, Cígler P, Kotek J, Rudovský J, Hermann P, Lukeš I. Inorg. Chem. 2005; 44:5591. [PubMed: 16060608]
259. Rudovsky J, Cígler P, Kotek J, Hermann P, Vojtísek P, Lukeš I, Peters JA, vander Elst L, Muller RN. Chem. Eur. J. 2005; 11:2373. [PubMed: 15685711]
260. Kálmán FK, Baranyai Z, Tóth I, Bányai I, Kiraly R, Brücher E, Aime S, Sun X, Sherry AD, Kovacs Z. Inorg. Chem. 2008; 47:3851. [PubMed: 18380456]
261. Pollet R, Nair NN, Marx D. Inorg. Chem. 2011; 50:4791. [PubMed: 21520891]
262. Dolg M, Stoll H, Savin A, Preuss H. Theor. Chim. Acta. 1989; 75:173.
263. Moats RA, Fraser SE, Meade TJ. Angew. Chem. Int. Ed. 1997; 36:726.
264. Louie AY, Hüber MM, Ahrens ET, Rothbächer U, Moats R, Jacobs RE, Fraser SE, Meade TJ. Nat. Biotechnol. 2000; 18:321. [PubMed: 10700150]
265. Urbanczyk-Pearson LM, Femia FJ, Smith J, Parigi G, Duimstra JA, Eckermann AL, Luchinat C, Meade TJ. Inorg. Chem. 2008; 47:56. [PubMed: 18072754]
266. Urbanczyk-Pearson LM, Meade TJ. Nat Protoc. 2008; 3:341. [PubMed: 18323804]
267. Ali MM, Liu G, Shah T, Flask CA, Pagel MD. Acc. Chem. Res. 2009; 42:915. [PubMed: 19514717]
268. Song B, Wu Y, Yu M, Zhao P, Zhou C, Kiefer GE, Sherry AD. Dalton Trans. 2013; 42:8066. [PubMed: 23575743]
269. Li AX, Wojciechowski F, Suchy M, Jones CK, Hudson RHE, Menon RS, Bartha R. Magn. Reson. Med. 2008; 59:374. [PubMed: 18228602]
270. Delli Castelli D, Terreno E, Aime S. Angew. Chem. Int. Ed. 2011; 50:1798.
271. Zhang S, Malloy CR, Sherry AD. J. Am. Chem. Soc. 2005; 127:17572. [PubMed: 16351064]
272. Rojas-Quijano FA, Tircsó G, Tircsóné Benyó E, Baranyai Z, Tran Hoang H, Kálmán FK, Gulaka PK, Kodibagkar VD, Aime S, Kovacs Z, Sherry AD. Chem. Eur. J. 2012; 18:9669. [PubMed: 22740186]
273. Zhang S, Trokowski R, Sherry AD. J. Am. Chem. Soc. 2003; 125:15288. [PubMed: 14664562]
274. Matosziuk LM, Leibowitz JH, Heffern MC, Macrenaris KW, Ratner MA, Meade TJ. Inorg. Chem. 2013
275. Li W-H, Fraser SE, Meade TJ. J. Am. Chem. Soc. 1999; 121:1413.
276. Woods M, Woessner DE, Sherry AD. Chem. Soc. Rev. 2006; 35:500. [PubMed: 16729144]
277. Vinogradov E, Sherry AD, Lenkinski RE. J. Magn. Reson. 2013; 229:155. [PubMed: 23273841]
278. Aime S, Carrera C, Delli Castelli D, Geninatti Crich S, Terreno E. Angew. Chem. Int. Ed. 2005; 44:1813.
279. Hingorani DV, Randtke EA, Pagel MD. J. Am. Chem. Soc. 2013; 135:6396. [PubMed: 23601132]
280. Que EL, Chang CJ. Chem. Soc. Rev. 2010; 39:51. [PubMed: 20023836]
281. Que EL, Domaille DW, Chang CJ. Chem. Rev. 2008; 108:1517. [PubMed: 18426241]
282. Haas KL, Franz KJ. Chem. Rev. 2009; 109:4921. [PubMed: 19715312]
283. Li W-H, Parigi G, Fragai M, Luchinat C, Meade TJ. Inorg. Chem. 2002; 41:4018. [PubMed: 12132928]
284. Kubíček V, Vitha T, Kotek J, Hermann P, vander Elst L, Muller RN, Lukeš I, Peters JA. Contrast Media Mol. Imaging. 2010; 5:294. [PubMed: 20973114]
285. Dhingra K, Fouskova P, Angelovski G, Maier ME, Logothetis NK, Tóth É. J. Biol. Inorg. Chem. 2007; 13:35. [PubMed: 17874148]
286. Mishra A, Logothetis NK, Parker D. Chem. Eur. J. 2011; 17:1529. [PubMed: 21268155]
287. Esqueda AC, López JA, Andreu-de-Riquer G, Alvarado-Monzón JC, Ratnakar J, Lubag AJM, Sherry AD, de León-Rodríguez LM. J. Am. Chem. Soc. 2009; 131:11387. [PubMed: 19630391]

288. de León-Rodríguez LM, Lubag AJM, López JA, Andreu-de-Riquer G, Alvarado-Monzón JC, Sherry AD. Med. Chem. Commun. 2012; 3:480.
289. Major JL, Parigi G, Luchinat C, Meade TJ. Proc. Natl. Acad. Sci. USA. 2007; 104:13881. [PubMed: 17724345]
290. Major JL, Boiteau RM, Meade TJ. Inorg. Chem. 2008; 47:10788. [PubMed: 18928280]
291. Que EL, Gianolio E, Baker SL, Wong AP, Aime S, Chang CJ. J. Am. Chem. Soc. 2009; 131:8527. [PubMed: 19489557]
292. De Leon-Rodriguez L, Verwilst P, Lubag AJM Jr, Eliseeva SV, Sherry AD, vander Elst L, Burtea C, Laurent S, Petoud S, Muller RN, Parac-Vogt TN, de Borggraeve WM. Inorg. Chim. Acta. 2012; 393:12.
293. Huang C-H, Morrow JR. J. Am. Chem. Soc. 2009; 131:4206. [PubMed: 19317496]
294. Huang C-H, Hammell J, Ratnakar SJ, Sherry AD, Morrow JR. Inorg. Chem. 2010; 49:5963. [PubMed: 20509631]
295. Hammell J, Buttarazzi L, Huang C-H, Morrow JR. Inorg. Chem. 2011; 50:4857. [PubMed: 21548563]
296. Surman AJ, Bonnet CS, Lowe MP, Kenny GD, Bell JD, Tóth É, Vilar R. Chem. Eur. J. 2011; 17:223. [PubMed: 21207619]
297. Duimstra JA, Femia FJ, Meade TJ. J. Am. Chem. Soc. 2005; 127:12847. [PubMed: 16159278]
298. Hanaoka K, Kikuchi K, Terai T, Komatsu T, Nagano T. Chem. Eur. J. 2008; 14:987. [PubMed: 17992679]
299. Chang Y-T, Cheng C-M, Su Y-Z, Lee W-T, Hsu J-S, Liu G-C, Cheng T-L, Wang Y-M. Bioconjugate Chem. 2007; 18:1716.
300. Arena F, Singh JB, Gianolio E, Stefanìa R, Aime S. Bioconjugate Chem. 2011; 22:2625.
301. Chauvin T, Durand P, Bernier M, Meudal H, Doan B-T, Noury F, Badet B, Beloeil J-C, Tóth É. Angew. Chem. Int. Ed. 2008; 47:4370.
302. Que EL, Gianolio E, Baker SL, Aime S, Chang CJ. Dalton Trans. 2010:469. [PubMed: 20023983]
303. Que EL, Chang CJ. J. Am. Chem. Soc. 2006; 128:15942. [PubMed: 17165700]
304. Mizukami S, Takikawa R, Sugihara F, Hori Y, Tochio H, Wälchli M, Shirakawa M, Kikuchi K. J. Am. Chem. Soc. 2008; 130:794. [PubMed: 18154336]
305. Jastrzębska B, Lebel R, Therriault H, McIntyre JO, Escher E, Guérin B, Paquette B, Neugebauer WA, Lepage M. J. Med. Chem. 2009; 52:1576. [PubMed: 19228016]
306. Querol M, Chen JW, Weissleder R, Bogdanov A. Org. Lett. 2005; 7:1719. [PubMed: 15844889]
307. Chen JW, Pham W, Weissleder R, Bogdanov A. Magn. Reson. Med. 2004; 52:1021. [PubMed: 15508166]
308. Chen JW, Querol Sans M, Bogdanov A, Weissleder R. Radiology. 2006; 240:473. [PubMed: 16864673]
309. Breckwoldt MO, Chen JW, Stangenberg L, Aikawa E, Rodriguez E, Qiu S, Moskowitz MA, Weissleder R. Proc. Natl. Acad. Sci. USA. 2008; 105:18584. [PubMed: 19011099]
310. Louie AY, Meade TJ. Proc. Natl. Acad. Sci. USA. 1998; 95:6663. [PubMed: 9618469]
311. Karttunen J, Shastri N. Proc. Natl. Acad. Sci. USA. 1991; 88:3972. [PubMed: 1902576]
312. Crich S. Chem. Commun. 1999:1577.
313. Lowe MP, Parker D, Reany O, Aime S, Botta M, Castellano G, Gianolio E, Pagliarin R. J. Am. Chem. Soc. 2001; 123:7601. [PubMed: 11480981]
314. Woods M, Kiefer GE, Bott S, Castillo-Muzquiz A, Eshelbrenner C, Michaudet L, McMillan K, Mudigunda SDK, Ogrin D, Tircsó G, Zhang S, Zhao P, Sherry AD. J. Am. Chem. Soc. 2004; 126:9248. [PubMed: 15281814]
315. Giovenzana GB, Negri R, Rolla GA, Tei L. Eur. J. Inorg. Chem. 2012; 2012:2035.
316. Zhang S, Wu K, Sherry AD. Angew. Chem. Int. Ed. 1999; 38:3192.
317. Kálmán FK, Woods M, Caravan P, Jurek P, Spiller M, Tircsó G, Kiraly R, Brücher E, Sherry AD. Inorg. Chem. 2007; 46:5260. [PubMed: 17539632]

318. Wu Y, Soesbe TC, Kiefer GE, Zhao P, Sherry AD. J. Am. Chem. Soc. 2010; 132:14002. [PubMed: 20853833]
319. Aime S, Delli Castelli D, Terreno E. Angew. Chem. Int. Ed. 2002; 114:4510.
320. Aime S, Barge A, Delli Castelli D, Fedeli F, Mortillaro A, Nielsen FU, Terreno E. Magn. Reson. Med. 2002; 47:639. [PubMed: 11948724]

Biographies

Marie C. Heffern

Marie Heffern was born in Quezon City, Philippines and grew up in Hawaii, California, and Nevada. She attended the University of Southern California where she was performed undergraduate research under the guidance of Professor Richard Brutchey. She entered the chemistry Ph.D. program at Northwestern University in 2009 and joined the laboratory of Professor Thomas J. Meade. She is currently a National Science Foundation Graduate Research Program Fellow. Her graduate studies focus on metal complexes as inhibitors of proteins involved in disease progression. Her general research interests lie in interdisciplinary approaches within the field of bioinorganic chemistry.

Lauren M. Matosziuk

Lauren Matosziuk was born in Altoona, Pennsylvania. She attended Duquesne University, where she received a B.S. in Chemistry in 2008. In 2013 she earned her PhD from Northwestern University under the direction of Profs. Thomas Meade and Mark Ratner. Currently, Lauren is a postdoctoral researcher in the laboratory of Prof. Laura Kiessling at the University of Wisconsin, where she is exploring how the physical properties of antigens affect B cell signaling.

Thomas J. Meade

Thomas J. Meade, PhD is the Eileen M. Foell Professor of Cancer Research and Professor of Chemistry, Molecular Biosciences, Neurobiology, Biomedical Engineering and Radiology at Northwestern University. He received his masters in Biochemistry and PhD in inorganic chemistry and after completing a NIH fellowship and fellow in Radiology at Harvard Medical School he joined the laboratory of Professor Harry B. Gray as a postdoctoral fellow at the California Institute of Technology. In 1991 he joined the Division of Biology and the Beckman Institute at Caltech. In 2002 he moved to Northwestern University, where he is the Director of the Center for Advanced Molecular Imaging (CAMI). Professor Meade's research focuses on coordination chemistry and its application in bioinorganic problems that include biological molecular imaging, transcription factor inhibitors and the development of electronic biosensors for the detection of DNA and proteins. Professor Meade holds more then 100 patents and has founded three companies, Clinical Micro Sensors, PreDx and Ohmx that are developing hand-held detection devices for protein and DNA detection and bioactivated MR contrast agents for clinical imaging.

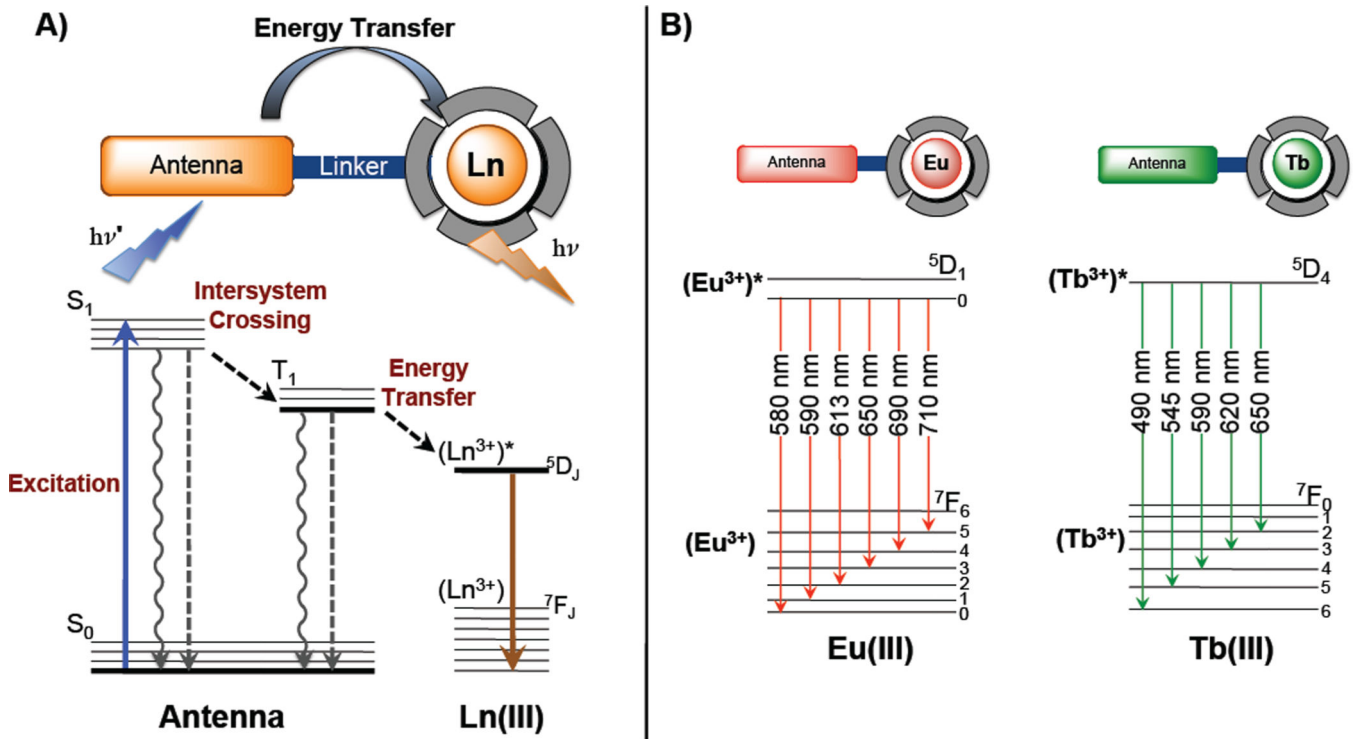

Figure 1.

(A) The antenna effect.[13,17,19,22] The general architecture of emissive lanthanide complexes consists of the metal center surrounded by a chelate and equipped with a sensitizer or antenna. The chelate serves to prevent the release of free lanthanides into the biological systems and to protect the lanthanide from quenching from vibrational energy dissipation by oscillators like O-H of water. The antenna harvests energy through high molar absorption to the singlet excited state. After undergoing intersystem crossing to the triplet state, the antenna transfers energy to the excited state ^5D_J state of the lanthanide. The radiative transition of electrons from the excited ^5D_J state to the ^7F_J states results in luminescent emission from the lanthanide ion. (B) Luminescent 4f-4f transitions of europium and terbium complexes and commonly observed emission wavelengths to emit red and green light, respectively.[1,13]

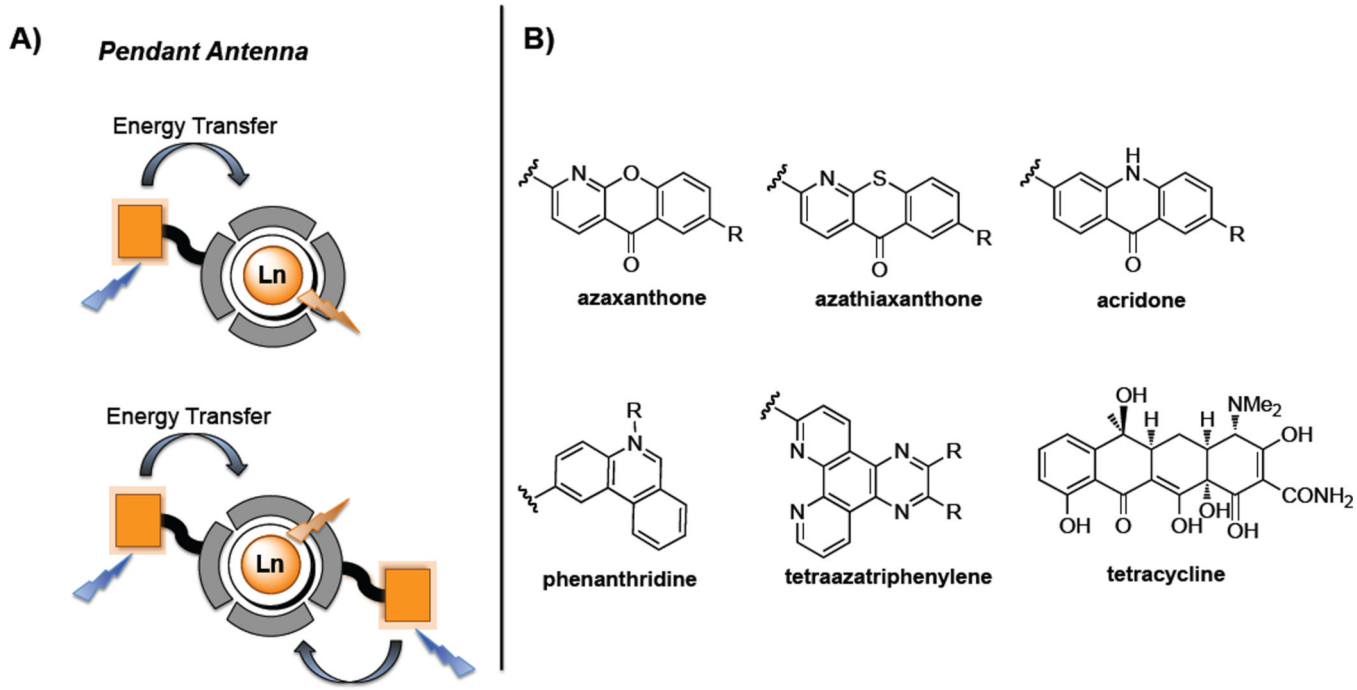

Figure 2.

Pendant antennae used to sensitize lanthanide complexes. (A) Schematic of lanthanide chelates that utilize pendant antennae. The pendant antenna is attached to the chelate (e.g. DO3A or DTPA) with a linker (top), and multiple pendant antennae can be incorporated (bottom).[1,19] (B) Examples of common sensitizers used as pendant antennae. Pendant antennae are derived from organic fluorophores based on favorable photophysical properties for sensitization.

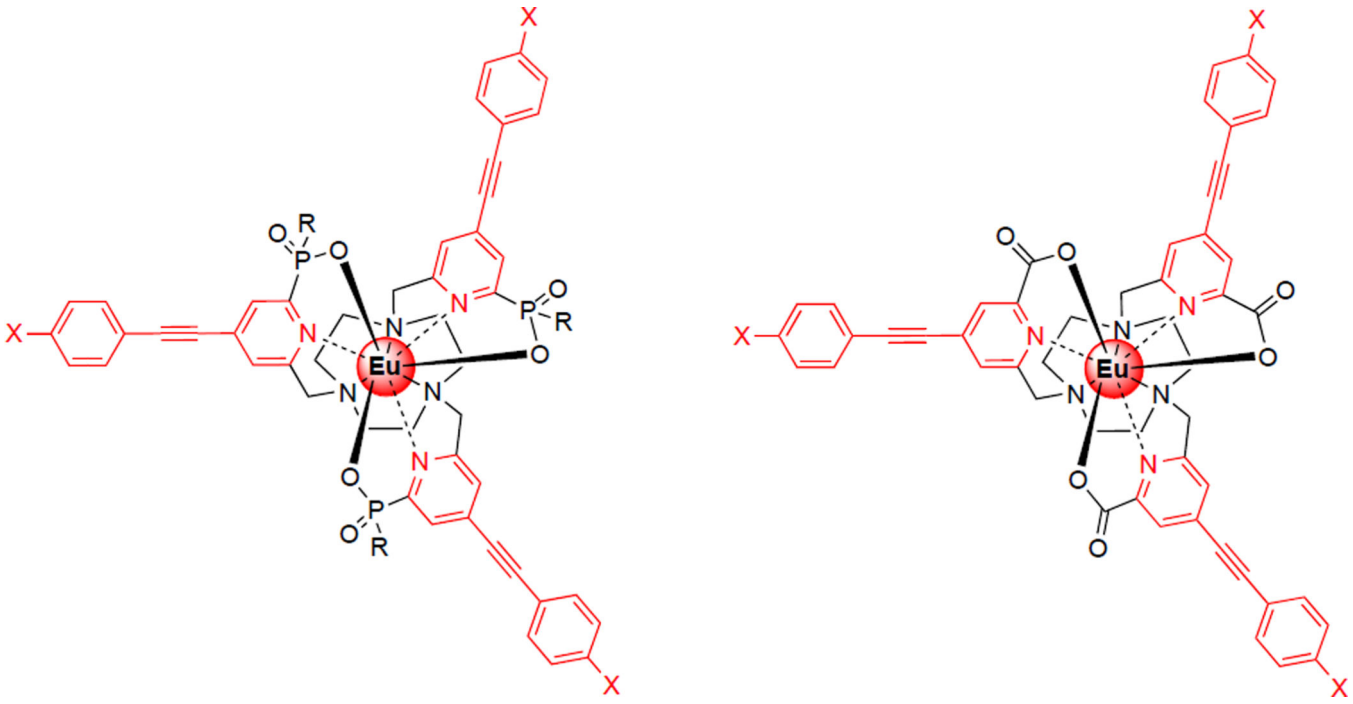

Figure 3.

Bright Eu(III) luminescence probes that incorporate multiple pendant antennae into a triazacyclononane chelate.[54] Alkynylpyridyl units are used as antennae that coordinate to the Eu(III) center through the pyridine nitrogen to decrease metal-antenna distance and increase electron transfer efficiency (η_{ET}). Further, Eu(III)-coordinating carboxylate or phosphinate units are *p*-substituted on the pyridine moiety to achieve coordinative saturation and prevent solvent quenching.

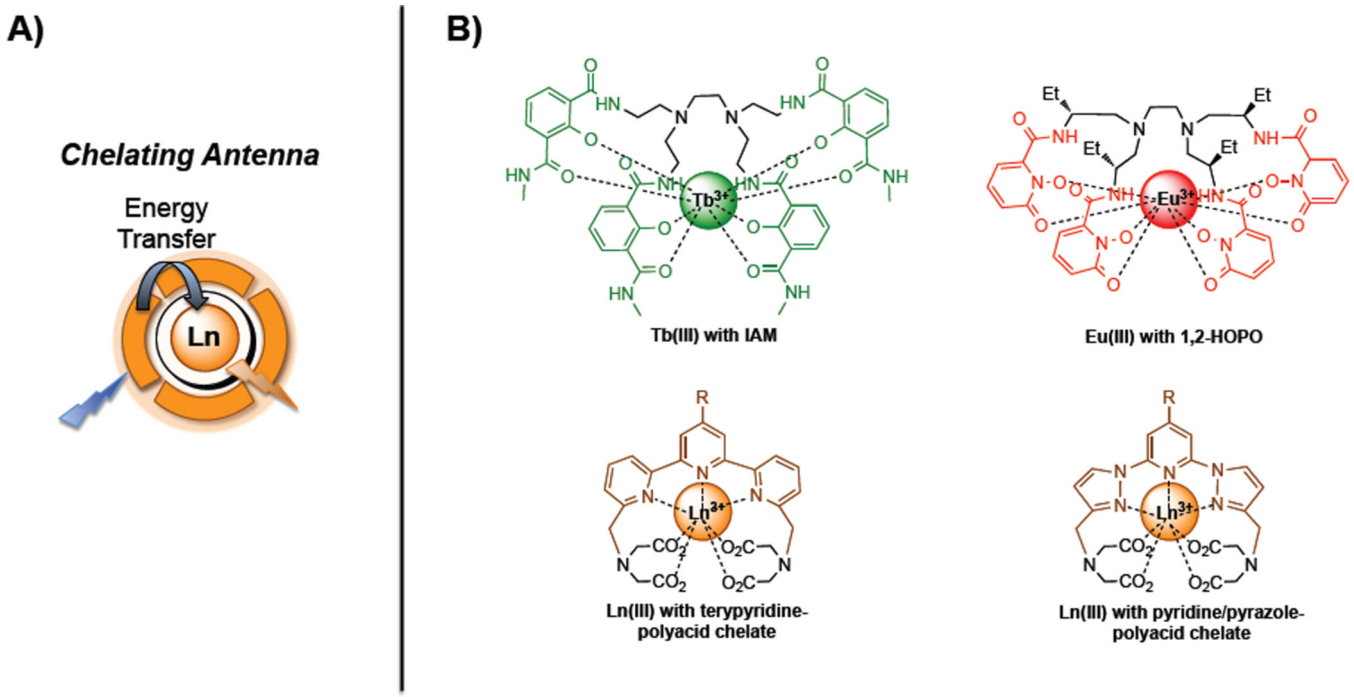

Figure 4.

Chelating antennae used to sensitize lanthanide complexes. (A) Schematic of a chelating antennae that serves dual function as both the protective lanthanide chelate and the sensitizing antenna. The decreased metal-antenna distance affords efficient energy transfer. (B) Examples of recently reported lanthanide complexes with chelating antennae. The chelating antennae based on the IAM and 1,2-HOPO binding units (top, in green and red, respectively) coordinate to the metal centers through the through salicylate- and catecholate-type coordination, respectively.[19,67,68] The poly-acid based chelates (bottom) by Yuan and coworkers coordinate to the lanthanide center through the pyridine/pyrazole moieties and the carboxylates.[69]

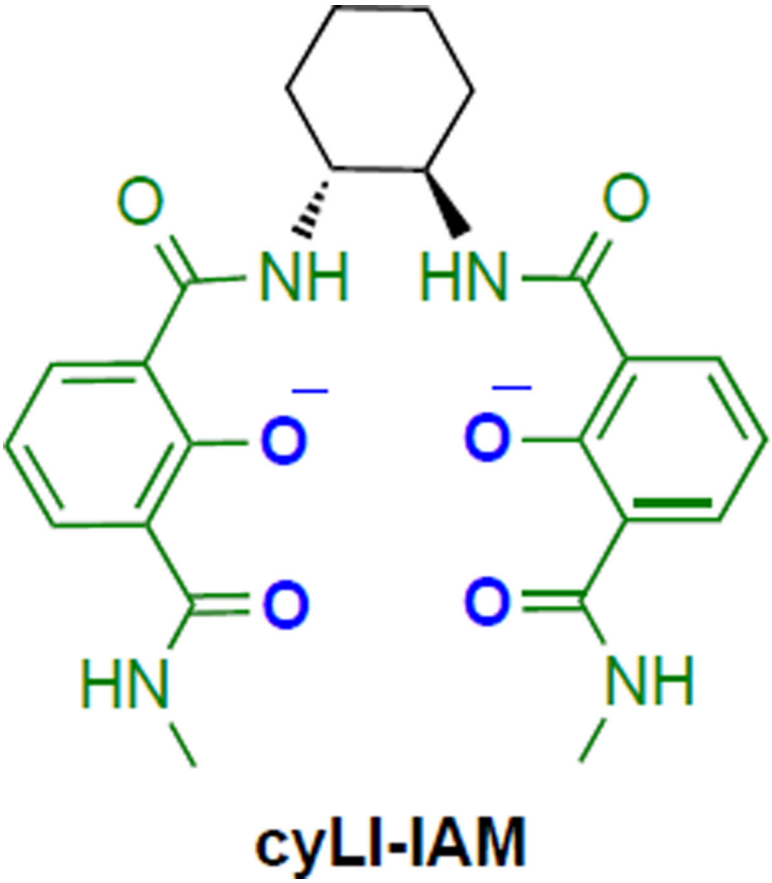

Figure 5.

Chiral IAM tetradentate chelates with strong CPL signal.[70] The CPL signal is highly influenced by the rigidity of the ethylenediamine backbone (black). The oxygens labeled in blue coordinate to the metal center in a salicylate-type manner.

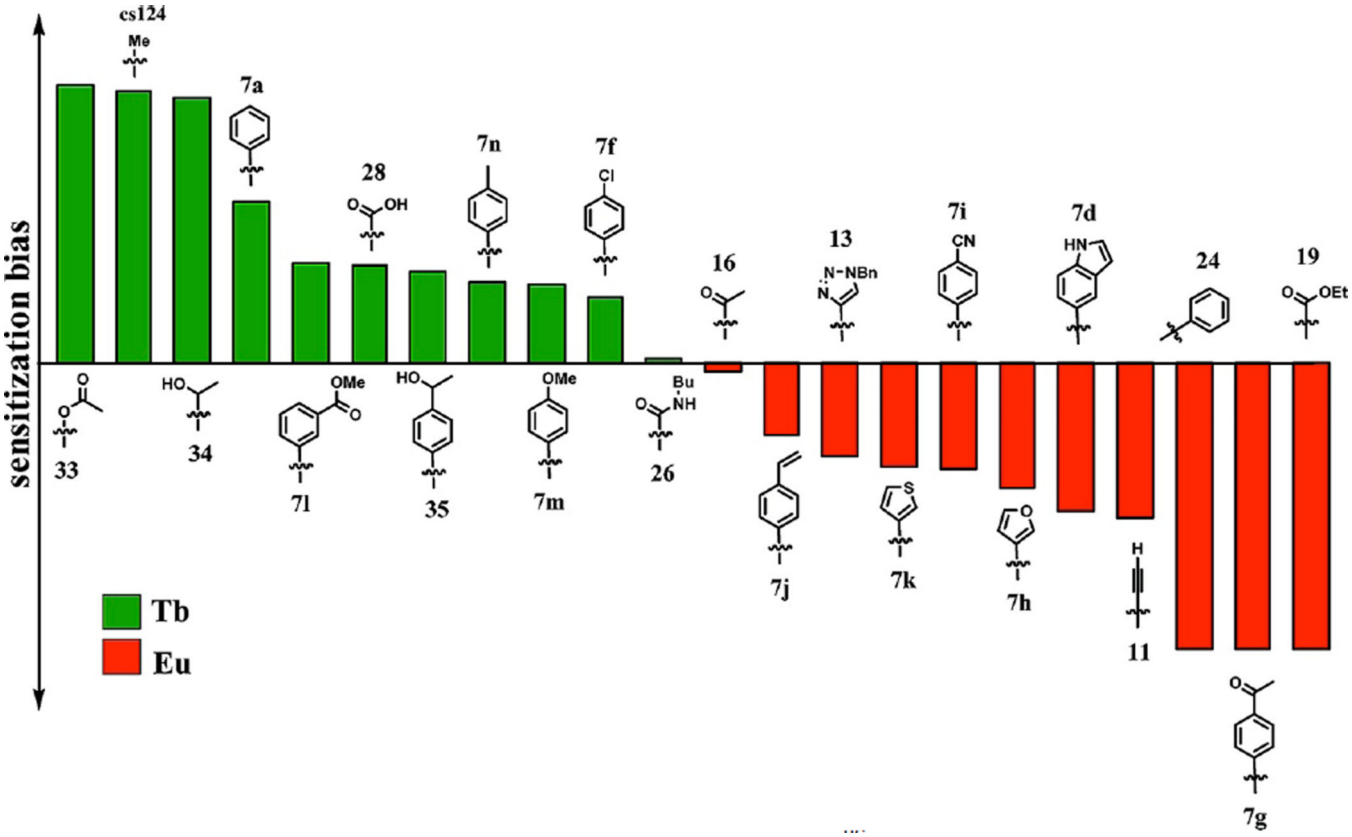

Figure 6.

Sensitization bias of varying carbostyril derivatives.[86] Tremblay et al. demonstrated the principle of ratiometric detection by antenna modification. Altered functionalities on the antenna exhibit differential sensitization of Tb(III) and Eu(III) luminescence. This can be harnessed for ratiometric switches. (Reprinted with permission from reference 86. Copyright 2007 American Chemical Society.)

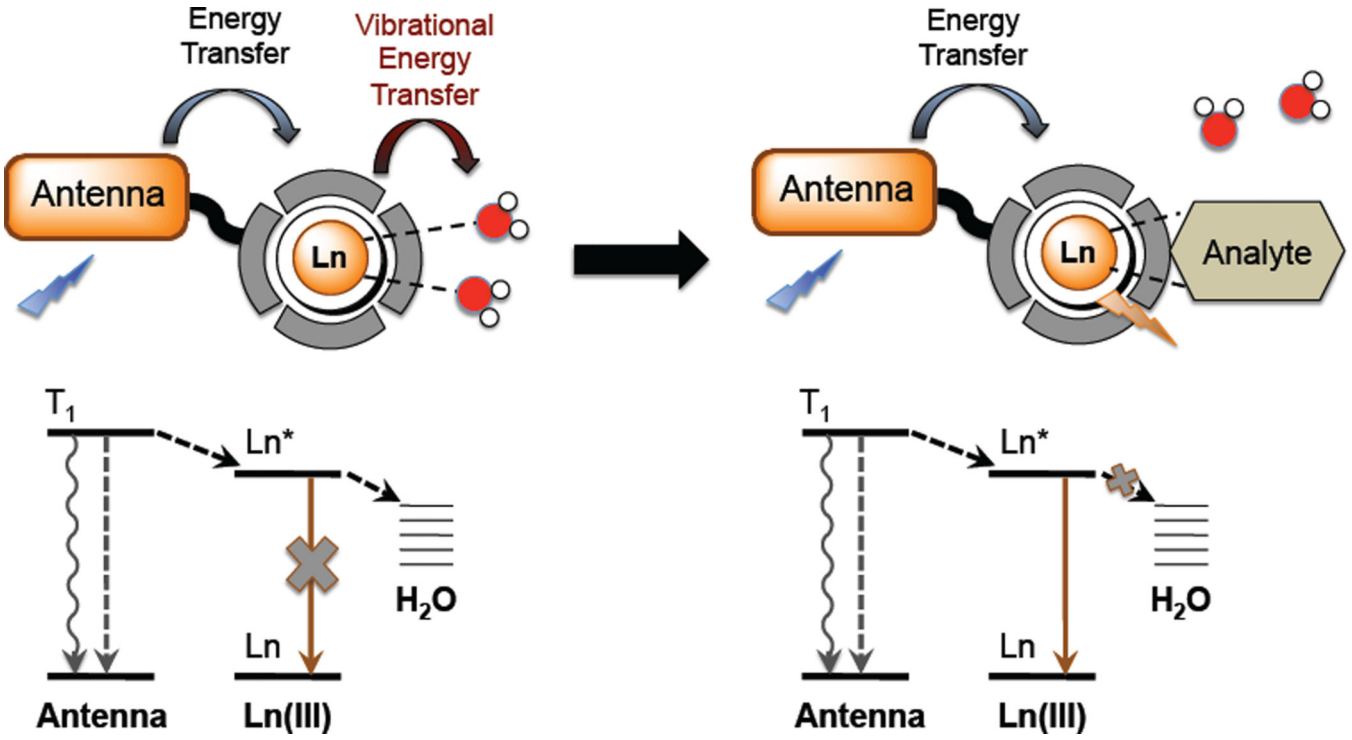

Figure 7.

General scheme for luminescent lanthanides that respond to an analyte by modulation of *q*, the number of waters bound.[33] Water can quench luminescence through promoting energy dissipation by vibrational transfer to the O-H oscillator. Replacement of water with an anionic analyte of interest can increase emission intensity through relieving quenching by this process. Furthermore, ligand exchange of water leads to change in ligand polarization and thus, emission bands corresponding to electric dipole transitions.

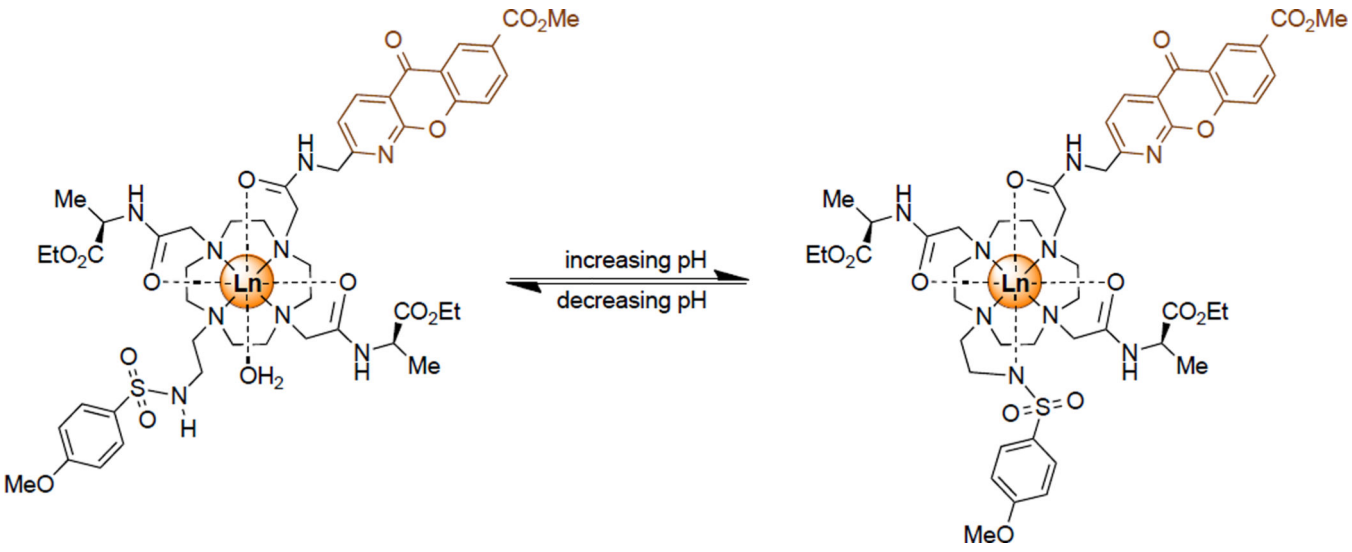

Figure 8.

A pH-responsive lanthanide luminescent probe that localizes in the lysosomes.[95] The amide-linked azaxanthone sensitizer promotes cell uptake through macropinocytosis, resulting in trafficking through the mitochondria and finishing in the lysosomes. The sulfonamide moiety confers pH-sensitivity to the probe: in acidic conditions, the sulfonamide is protonated, precluding coordination to the lanthanide ion and opening a coordination site for one water molecule. As the probe encounters a higher pH environment, the sulfonamide is deprotonated, permitting coordination through the nitrogen and displacement of the bound water.[95]

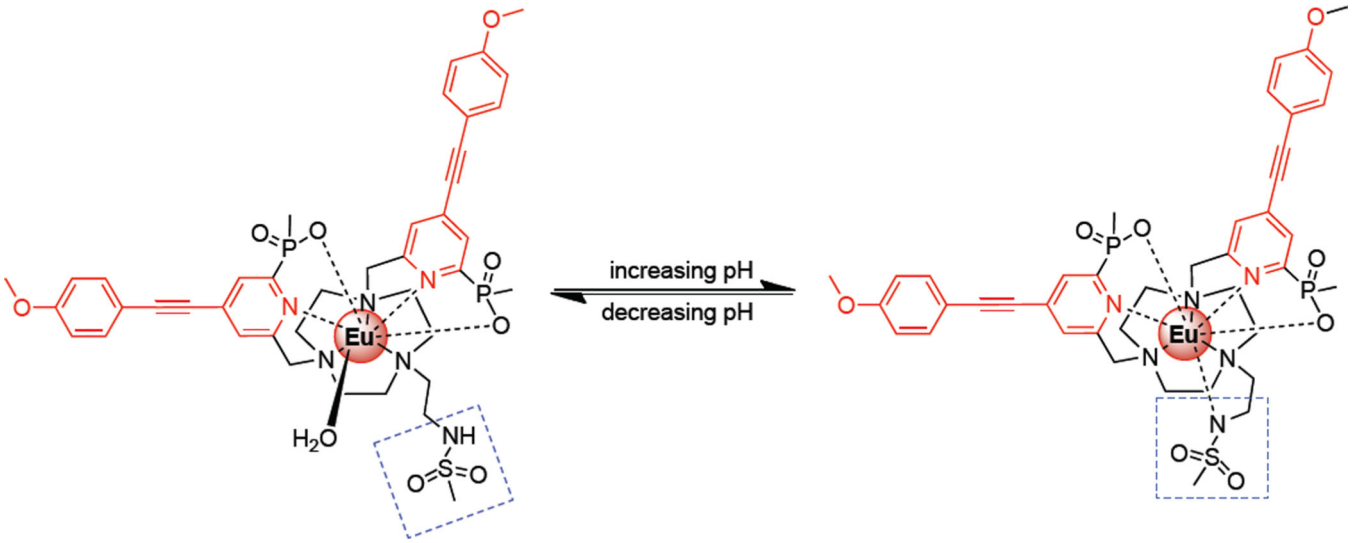

Figure 9.

A bright pH-responsive europium luminescent probe that localizes in the endoplasmic reticulum.[96] High quantum yields were achieved by incorporating mutiple aryl-alkynyl groups as sensitizers (quantum yield = 50% compared to the azaxanthone at 6% or less). In combination with the pyridyl groups, the aryl-alkynyl groups localize the probes in the endoplasmic reticulum. The sulfonamide moiety confers pH-sensitivity to the probe similar to the azaxanthone-containing pH probe.

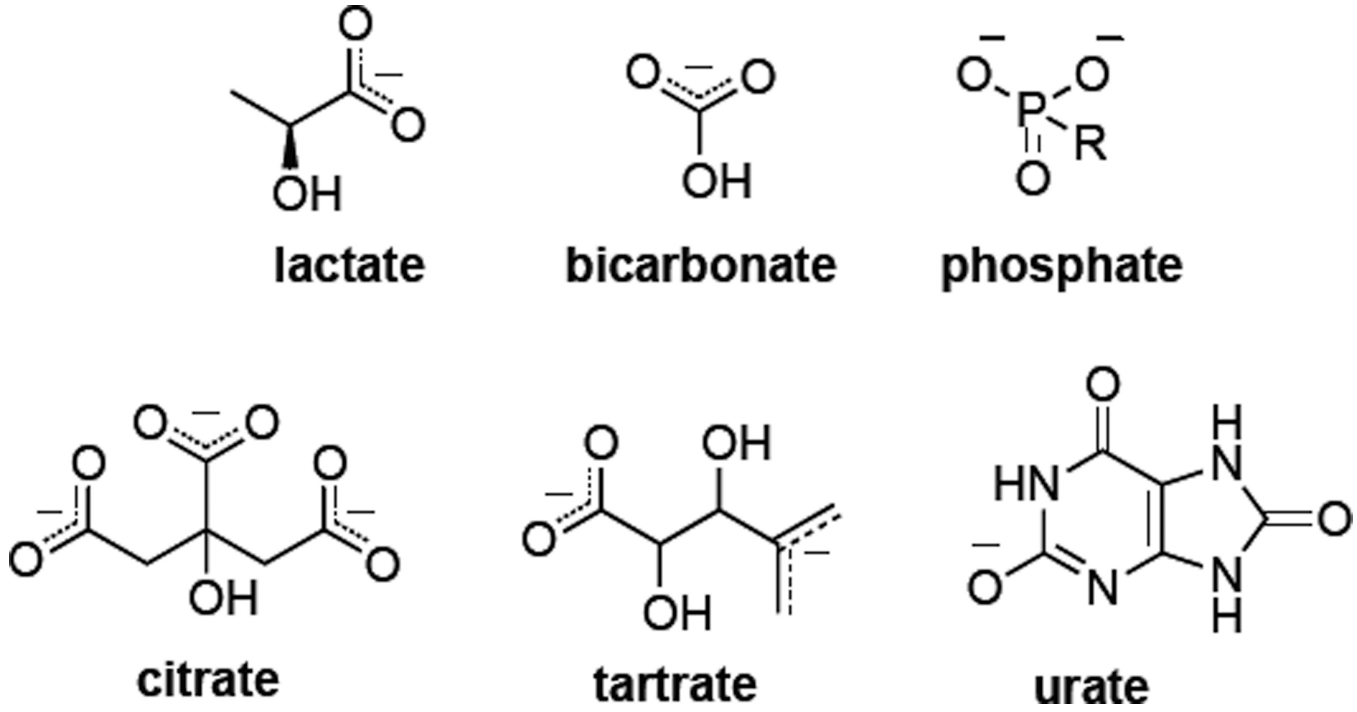

Figure 10.

Examples of oxyanions that have been detected with luminescent lanthanide probes through *q*-modulation.[33] Sterics and charge of the lanthanide complex govern selectivity for the target anion.

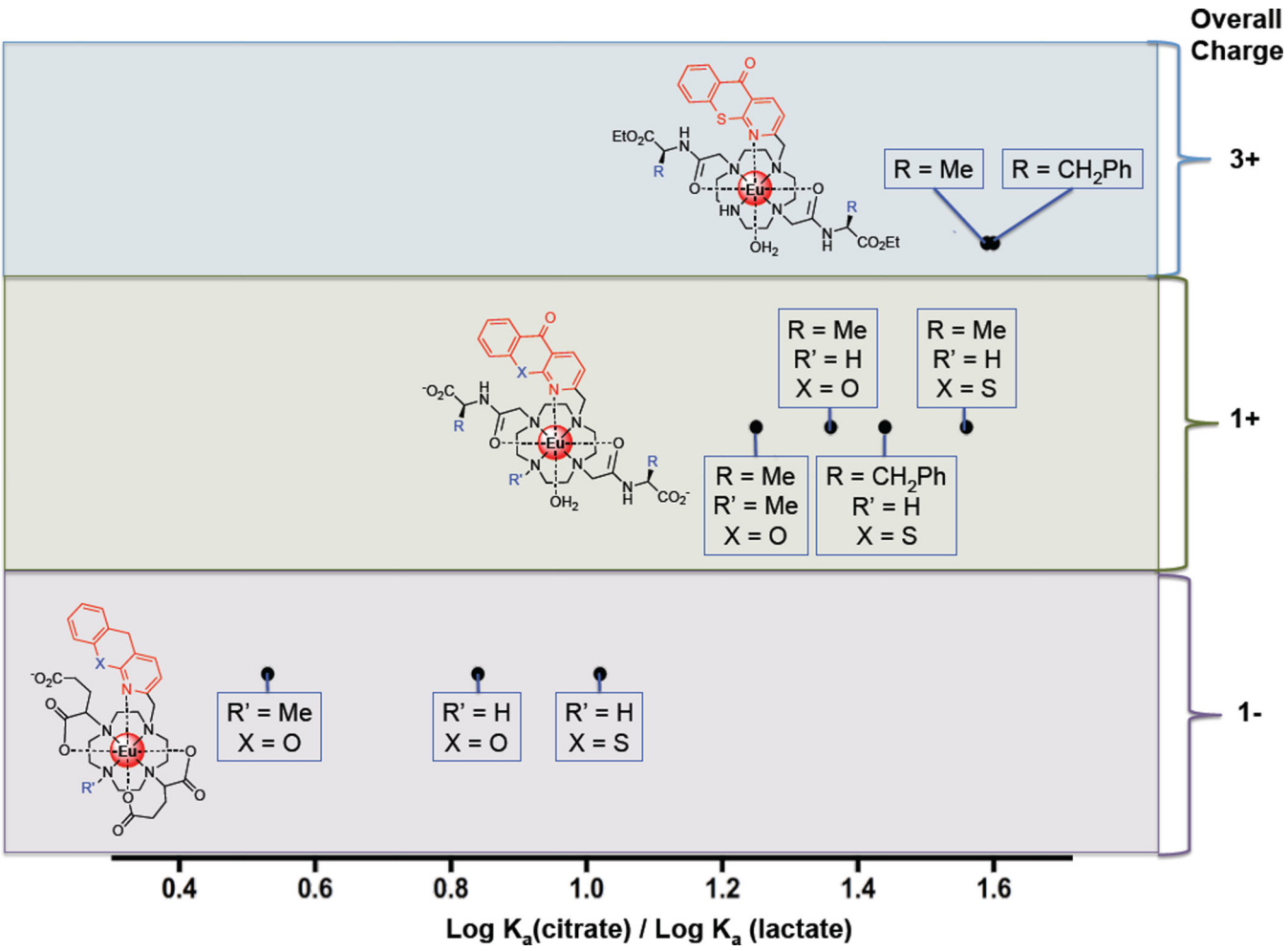

Figure 11.

Comparison of binding affinities of citrate and lactate for a series of oxy-anion binding Eu(III) complexes.[99] Ratios of citrate to lactate binding affinities are calculated from log K_a reported in reference 9 and represented in terms of ligand modifications and overall charge.

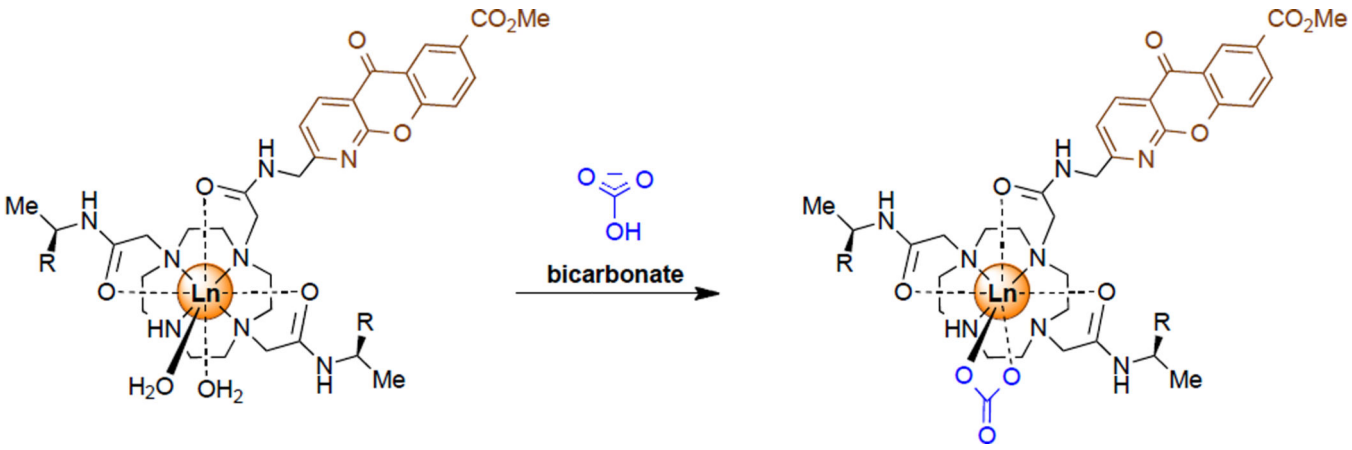

Figure 12.

Bicarbonate-selective complexes that localize in the mitochondria.[102] Bicarbonate serves as an anionic analyte that can displace the bound water molecules and change spectra form and emission intensity. The amide-linked azaxanthone encourages macropinocytosis and consequential localization in the mitochondria. Steady-state concentrations of bicarbonate could be ratiometrically measured ΔJ=2/ΔJ=1 emission intensities of the Eu(III) complex.

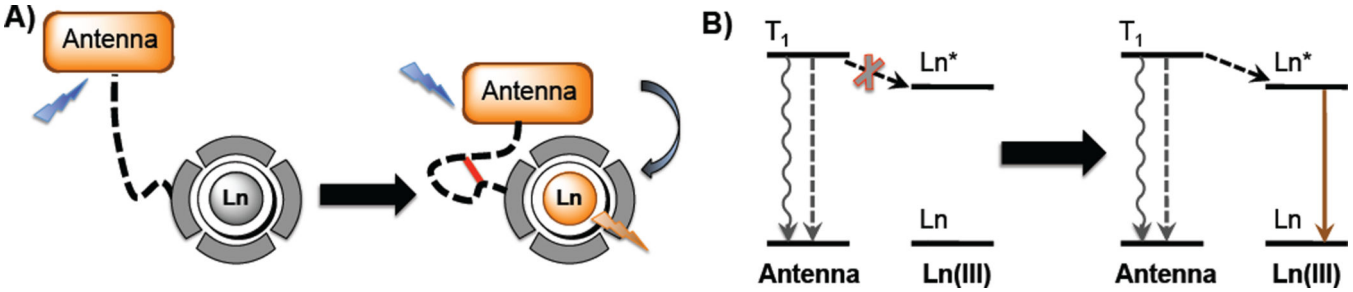

Figure 13.

Luminescent lanthanides that respond to an analyte by decreasing the distance between the metal center and the antenna. In the absence of the analyte, the antenna is either not attached to the lanthanide chelate or separated by a flexible linker, resulting in low efficiency in energy transfer (and sensitization). The analyte brings the antenna in close proximity to the lanthanide, increasing the efficiency of energy transfer and emission intensity.

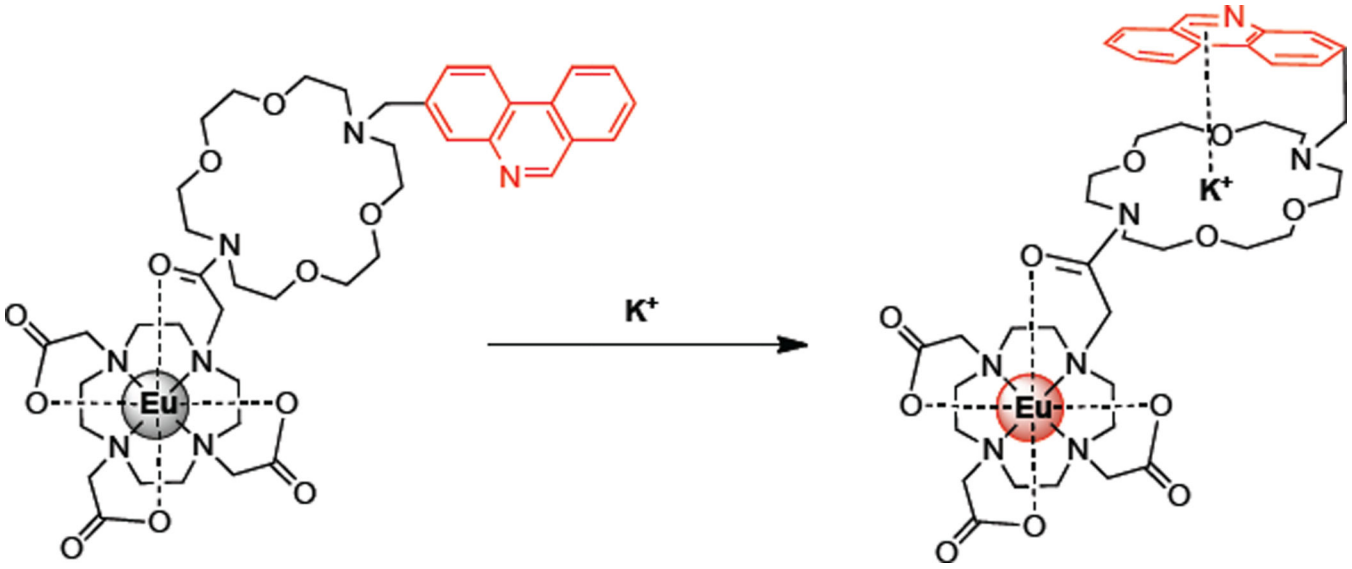

Figure 14.

Structure and mode of action of the distance-deEu-KPhen.[105] In the presence of potassium, concomitant complexation of the ion by the crown ether and the phenanthridine (through a cation-π interaction) decreases the distance between the antenna and the Eu(III) center, increasing luminescence intensity.

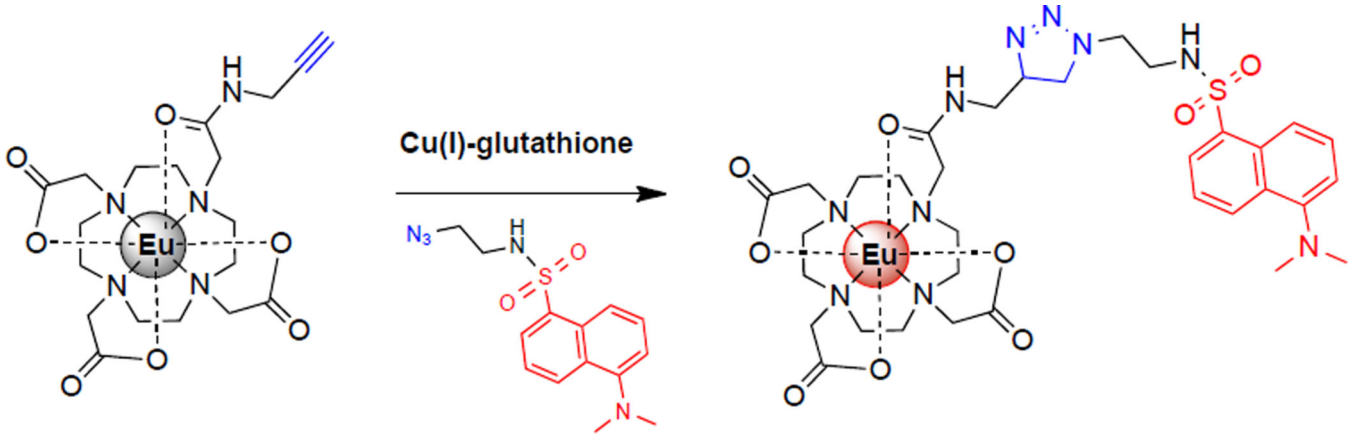

Figure 15.

Copper(I)-sensitive luminescent lanthanide that responds by decreasing the distance between the antenna and the metal center.[107] A drastic “switch-on” response is observed through a copper-dependent “click” reaction that attaches the dansyl azide antenna to the Eu(III) chelate and permits energy transfer.

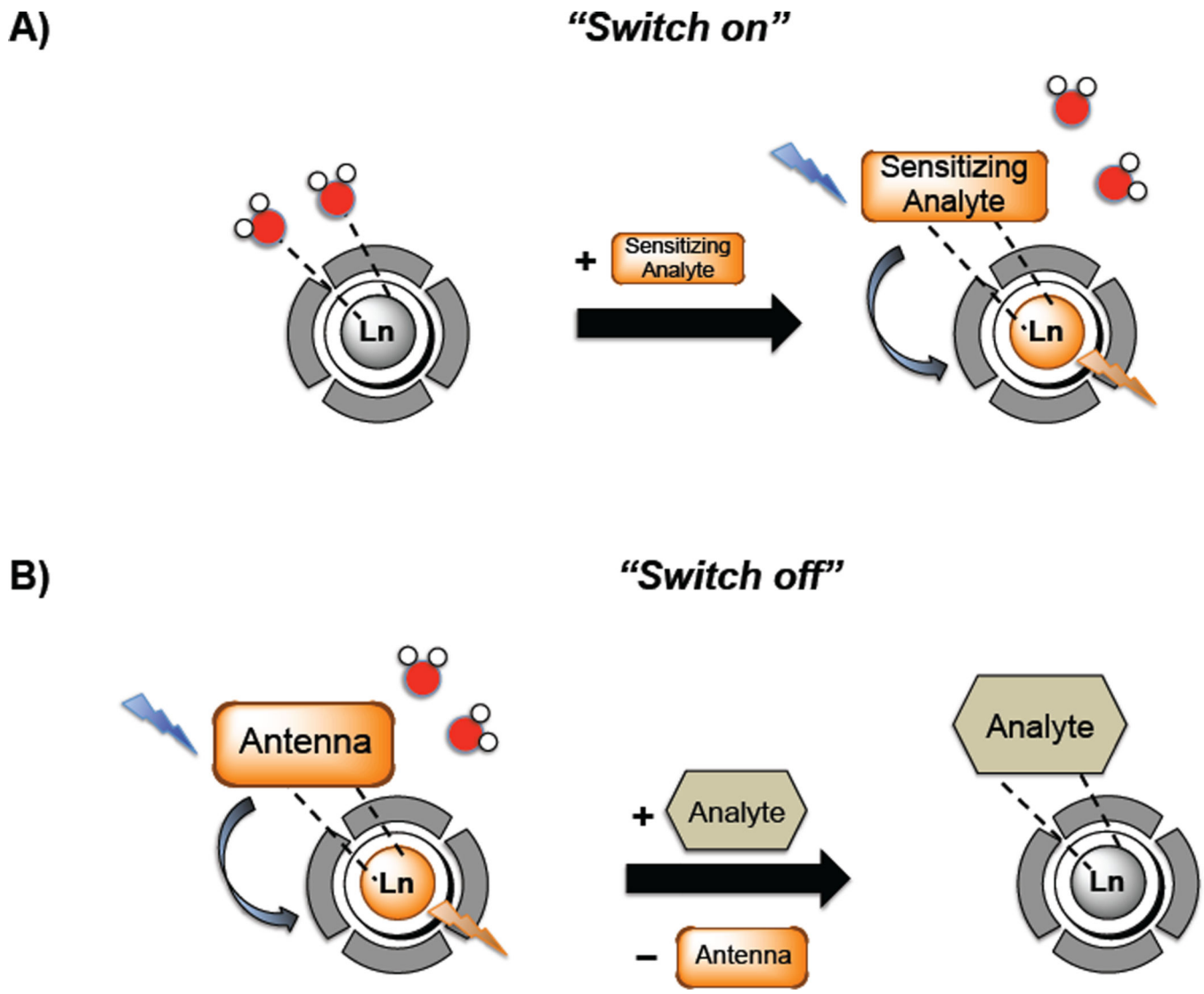

Figure 16.

Modulation of antenna-Ln(III) distance by reversible coordination of the antenna. (A) "Switch on" designs involve the coordination of a sensitizing analyte such as aromatic carboxylates whereas (B) "switch off" probes rely on the displacement of the antenna by an anionic analyte.

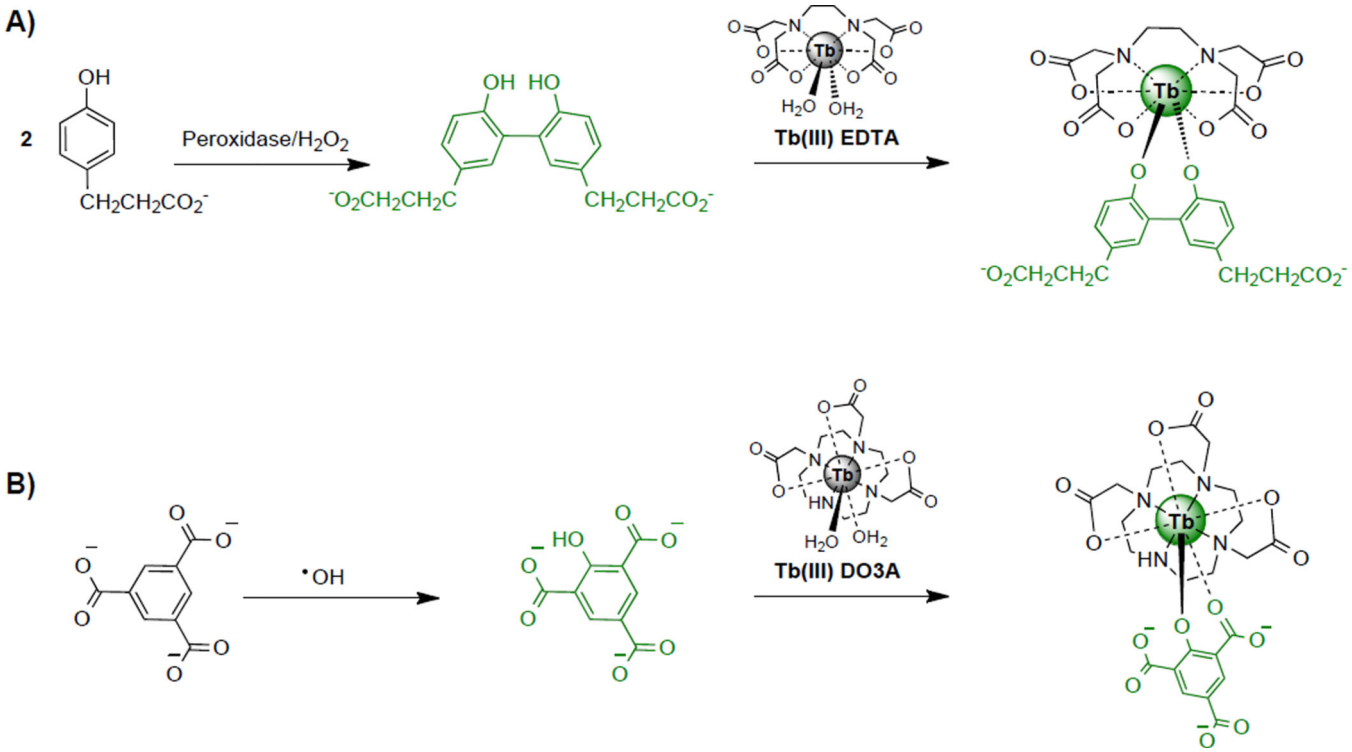

Figure 17.

Modified reaction-based approach for the detection of non-sensitizing analytes by reversible antenna coordination. (A) Meyer and Karst detected peroxidase activity using a pro-antenna, *p*-hydroxyphenylpropionic acid as a substrate.[111] In the presence of the enzyme, the pro-antenna dimerizes to the biphenol that can coordinate and sensitize Tb(III) EDTA. (B) Page et al. detected hydroxyl radicals through reaction with the trimesate pro-antenna to form the 2-hydroxytrimesic acid antenna that can coordinate to Tb(III) DO3A.[112]

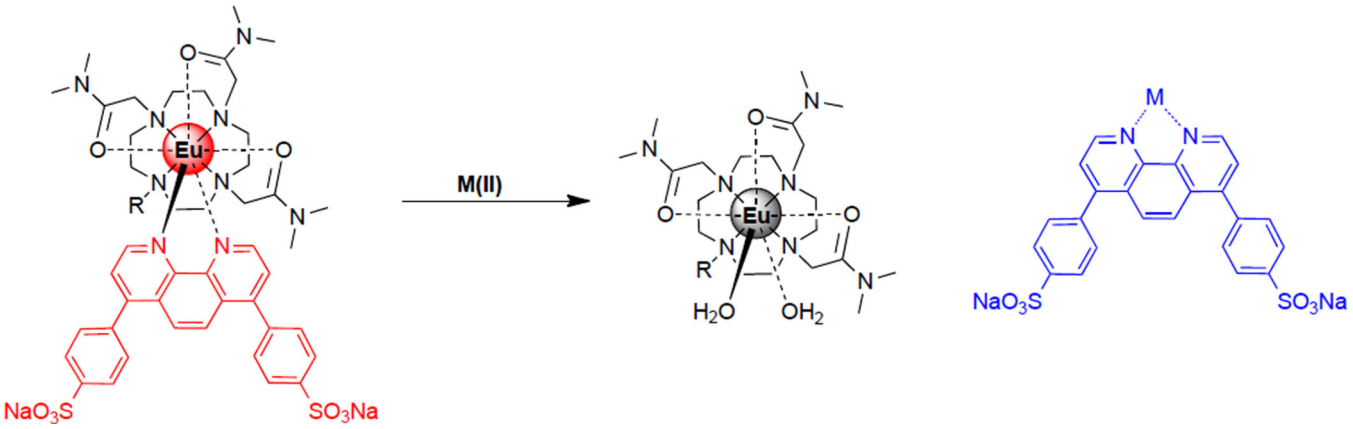

Figure 18.

Gunnlaugsson and coworkers have used coordinating antennae to detect dicationic transition metals [M(II)].[116,117] Selectivity is influenced by affinity of the ligand for the transition metal ion. In the absence of M(II), the antenna coordinates the Eu(III) center and sensitizes luminescence. Preferred M(II) can compete for coordination of the antenna to switch off the Eu(III) luminescence, and in some cases, produce a luminescent d-metal complex.

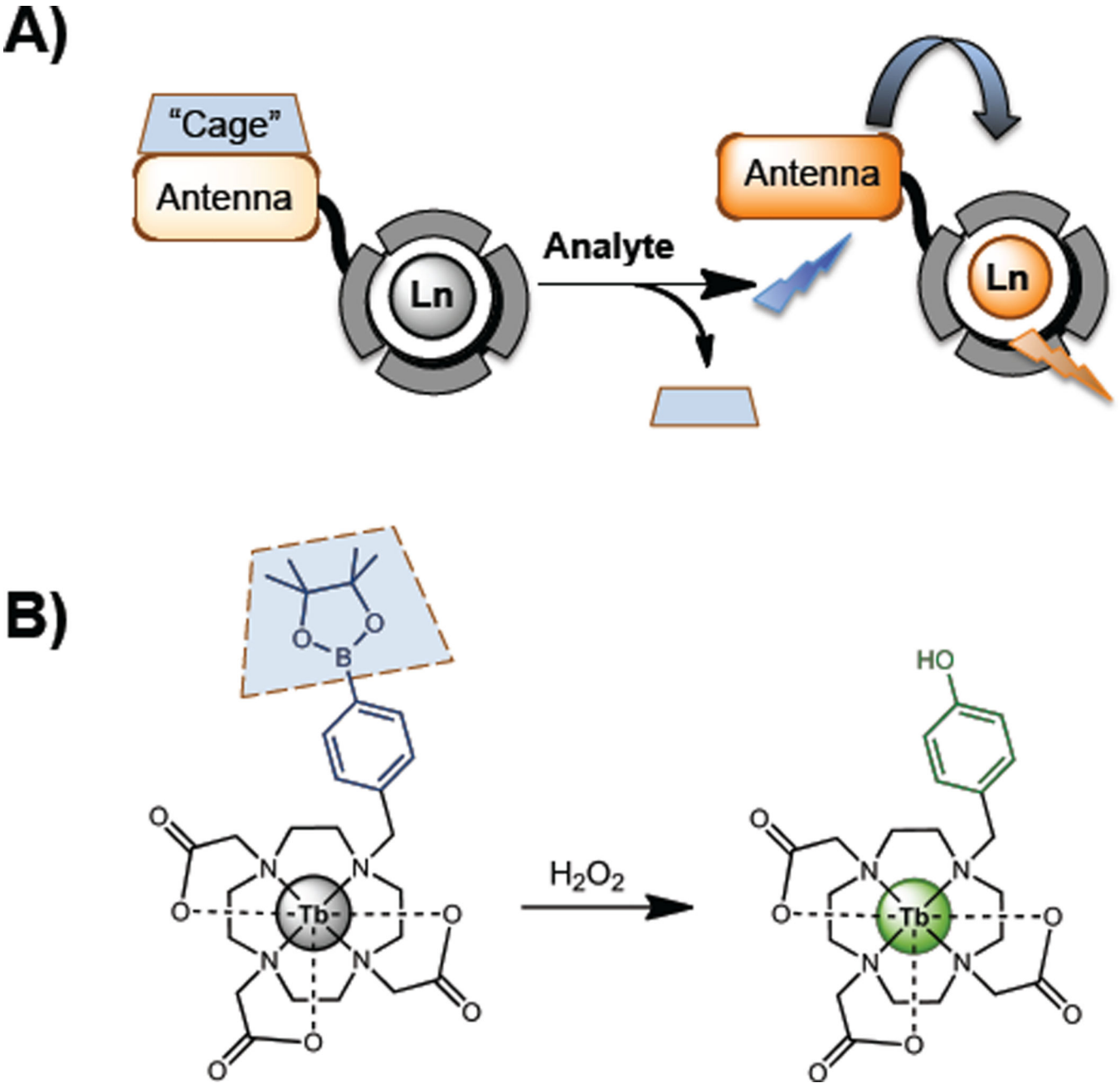

Figure 19.

(A) Bioresponsive lanthanides that employ caged antennae.[128,129] In the absence of an analyte, the antenna precursor is not an efficient sensitizer. The analyte reacts with the cage to trigger formation of a sensitizing chromophore, producing Ln(III) luminescence. (B) The caged antenna approach for the detection of hydrogen peroxide.[129] The boronate ester mask is chemoselective for hydrogen peroxide. Analyte reaction results in an aniline or phenol that can efficiently sensitize Tb(III) luminescence.

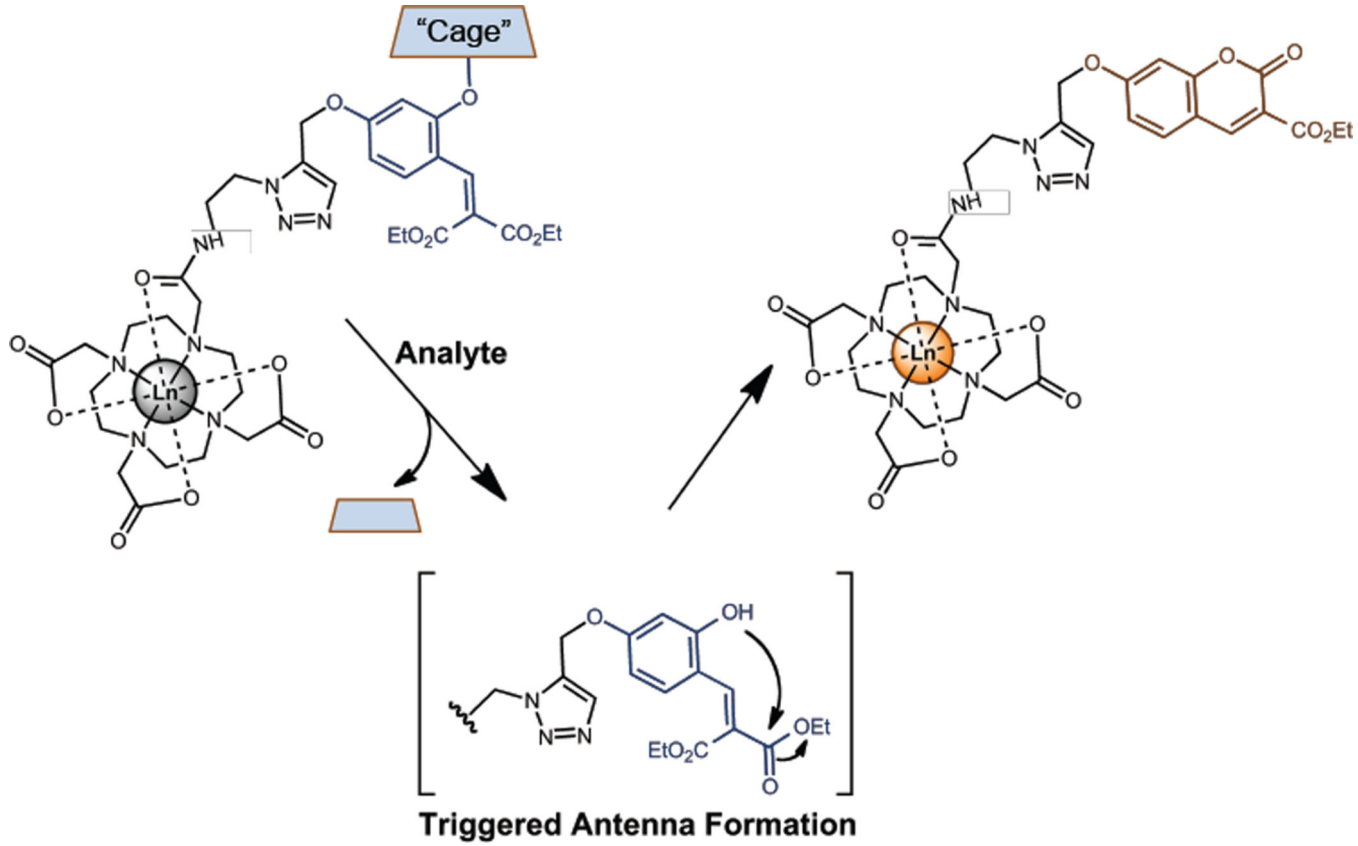

Figure 20.

Antenna-triggered formation of coumarin sensitizer for the detection of a series of analytes.[128] Synthetic procedures were simplified by using an azide-modified chelate that could be attached to an alkyne-modified antenna building block. The antenna building block (blue) was derivatized with either phenylboronic acid, triisopropylsilane, allyl, or galactose cages for the detection of hydrogen peroxide, fluoride, palladium, or β-galactosidase, respectively. In the presence of the analyte, the cage is removed driving formation of the coumarin antenna (orange) for sensitized Ln(III) luminescence.

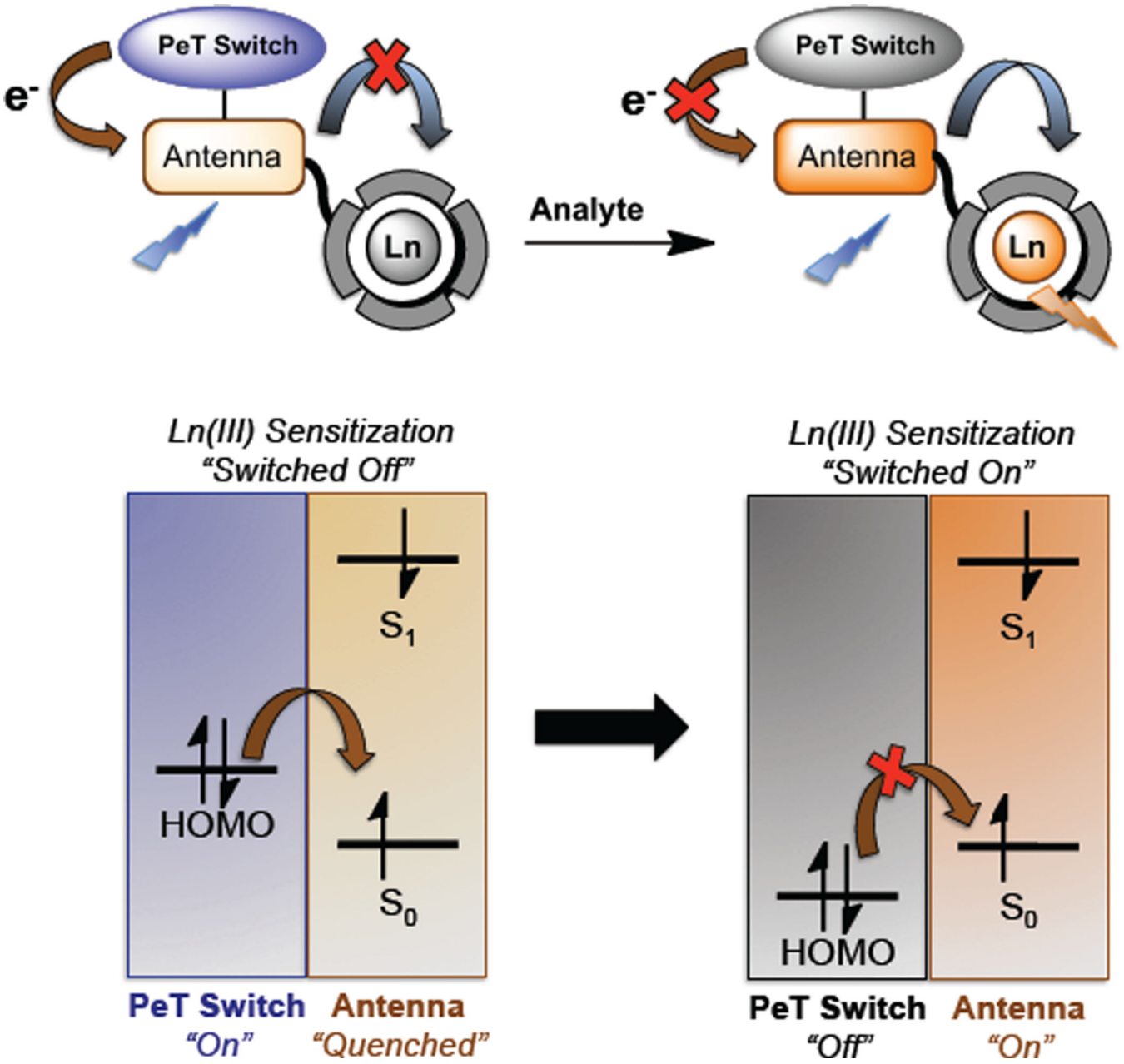

Figure 21.

PeT-switchable luminescent lanthanides.[97,127] In the "switched-off" state of a PeT-switchable emissive lanthanide system, the HOMO of the PeT switch is higher in energy than the S_0 ground state of the antenna (left). The PeT switch donates an electron to pair to the S_0 ground state of the antenna, quenching its fluorescence. The PeT process competes with radiative decay and reduces the sensitizing efficiency of the antenna and, consequently, lanthanide luminescence. When an analyte chemically alters the PeT switch to decrease its HOMO energy, it can no longer serve as an electron donor to the antenna (right). In turn, the antenna's sensitizing capacity is restored and the lanthanide luminescence is "switched on".

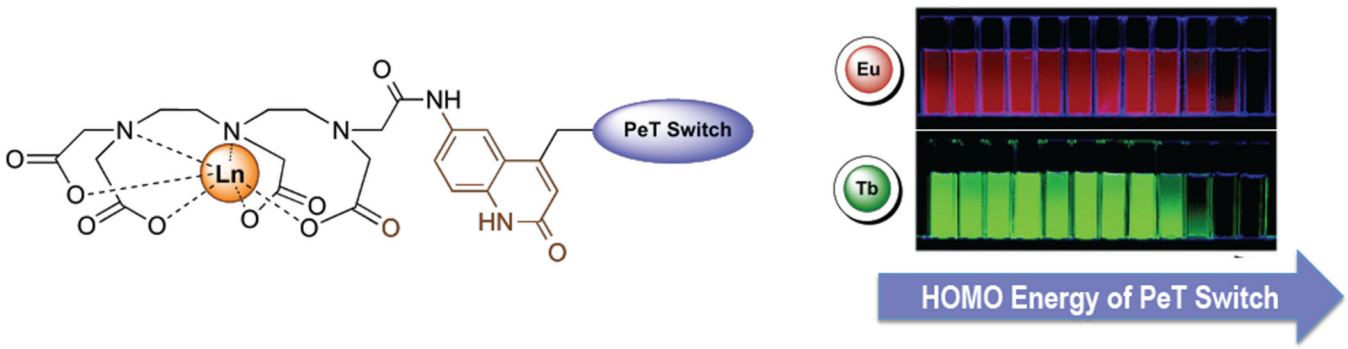

Figure 22.

Investigating the PeT switch mechanism for modulating Ln(III) luminescence. In a systematic investigation, Terai et al. evaluated the PeT quenching of a quinolinone antenna by a series of organic moieties with varying HOMO energies. The PeT switch approach was validated in this study, as decreasing HOMO energies (which is expected to correspond to decreased donor capacity and decreased quinolone quenching) increased the observed luminescence.[127] (Adapted with permission from reference 127. Copyright 2006 American Chemical Society.)

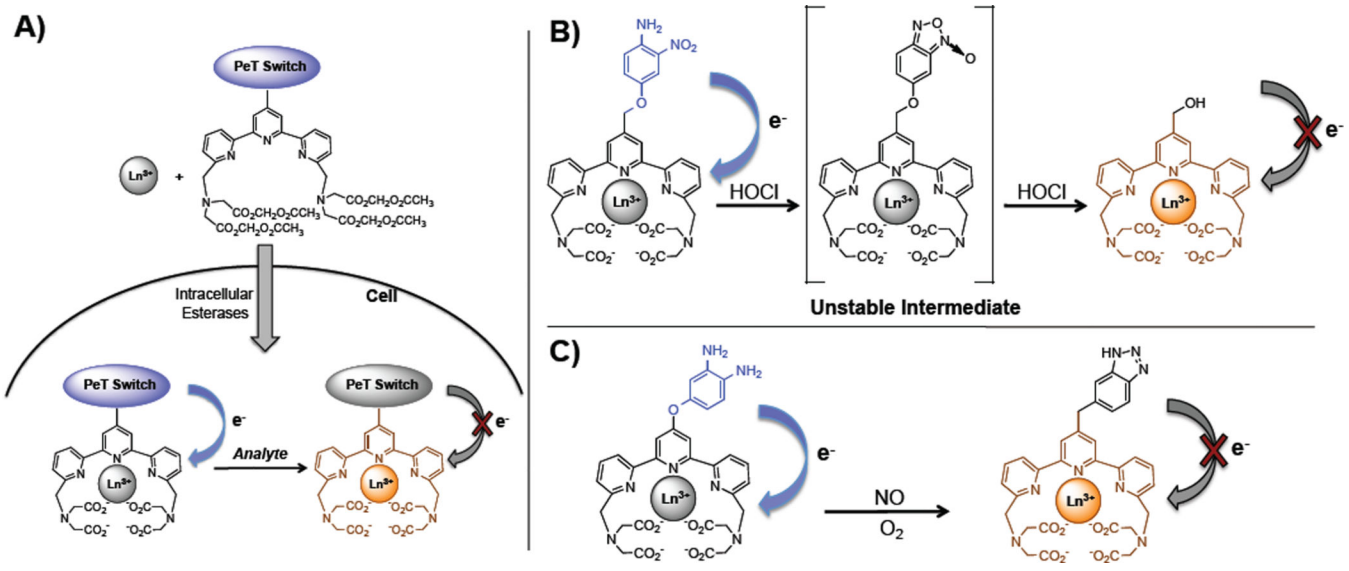

Figure 23.

PeT switchable Ln(III) complexes with chelating polyacid antennae. In the general design, a PeT switch is conjugated to the central pyridine of the chelate.[75,76,118,133–140] Analyte interaction with the PeT decreases electron transfer to the antenna and increases luminescence intensity. (A) The chelated complex is cell-impermeable so a method of administration was devised wherein the cells are simultaneously treated with the free Ln(III) salt and an ester-protected form of the chelate.[127] Upon cell internalization, intracellular esterases cleave the ester protecting groups to expose the polyacids, permitting self-assembling of the chelate in the cell. This strategy has been used for the detection of several reactive small molecules, such as (B) HOCl[137] and (C) NO[76].

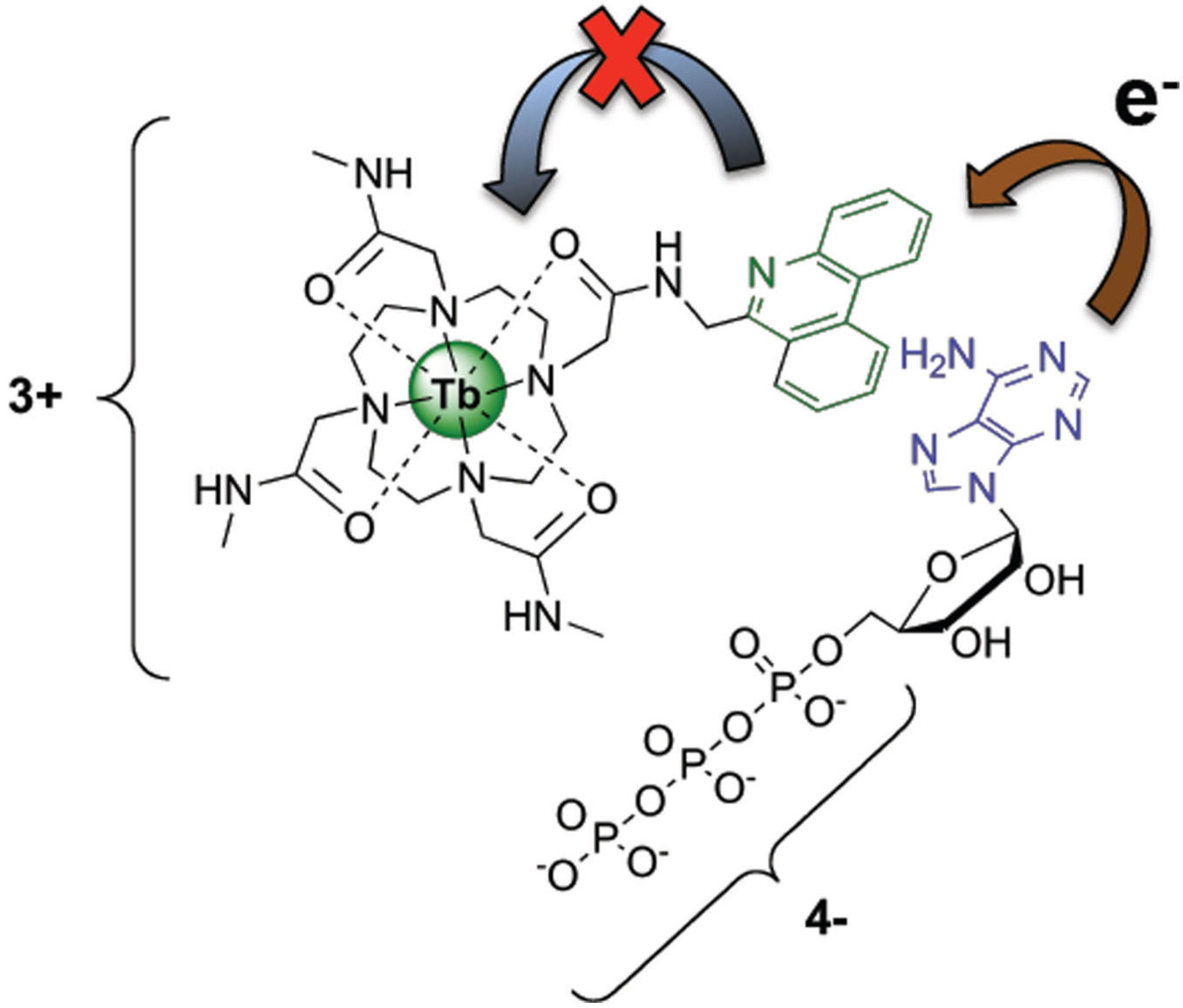

Figure 24.

ATP-selective probe driven by PeT from the adenosine of ATP to the phenanthridine antenna.[145] Nucleoside phosphate selectivity over other anionic phosphates is partially driven by π-π stacking interactions between the adenosine and the phenanthridine antenna. Further, this antenna-nucleoside interaction alters luminescence by PeT from the analyte to the antenna (decreasing luminescence). The tricationic charge of the Tb(III) complex confers selectivity for the 4- charge of ATP (over the 3- and 2- charge of ADP and AMP, respectively).

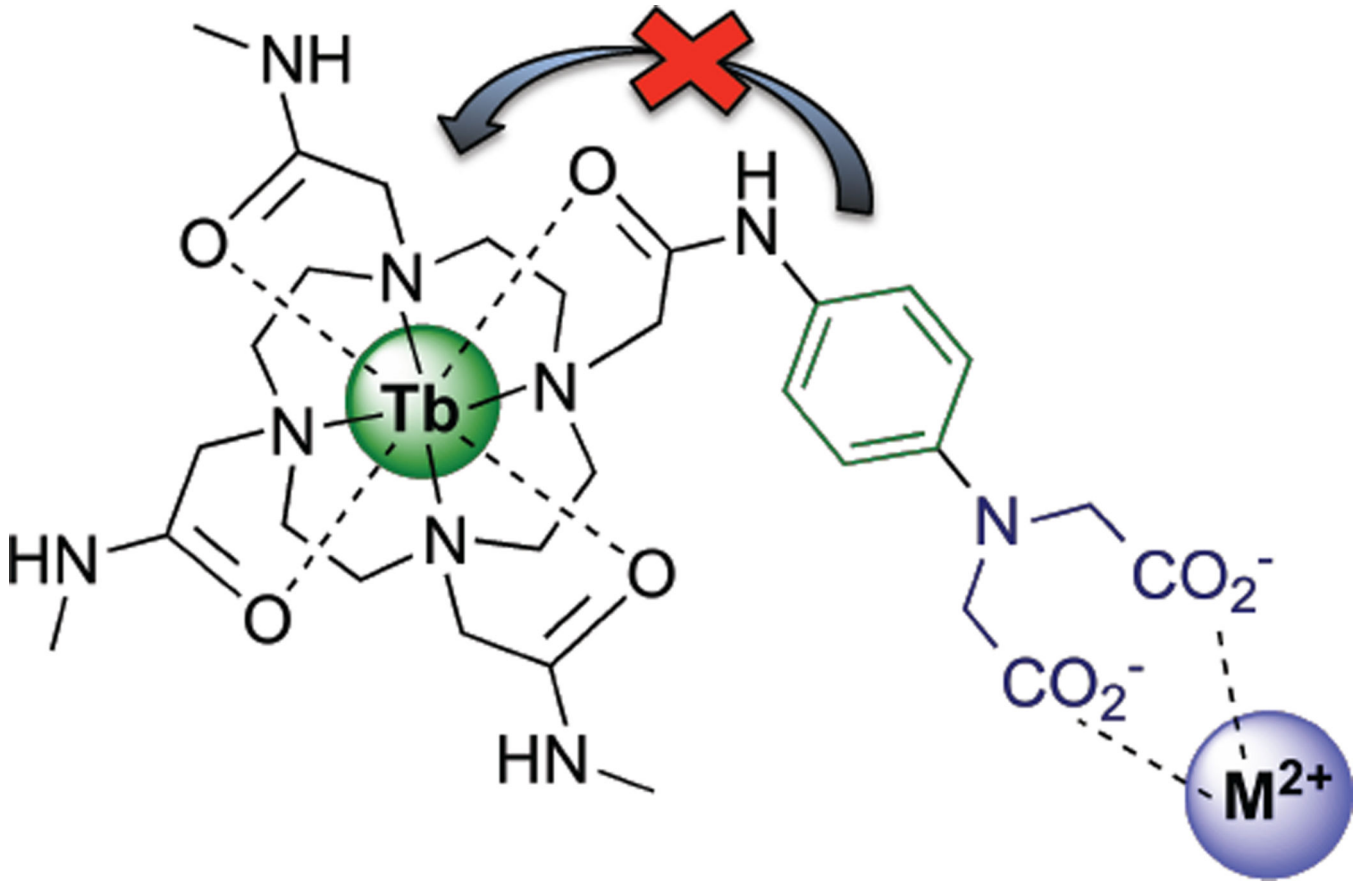

Figure 25.

Modulation of antenna sensitization with an analyte receptor unit for the detection of Cu(II) or Hg(II).[146] The iminodiacetate receptor unit can coordinate to d-metal ions. Coordination of Cu(II) or Hg(II) alters the excited state of the phenyl antenna and quenches Tb(III) luminescence.

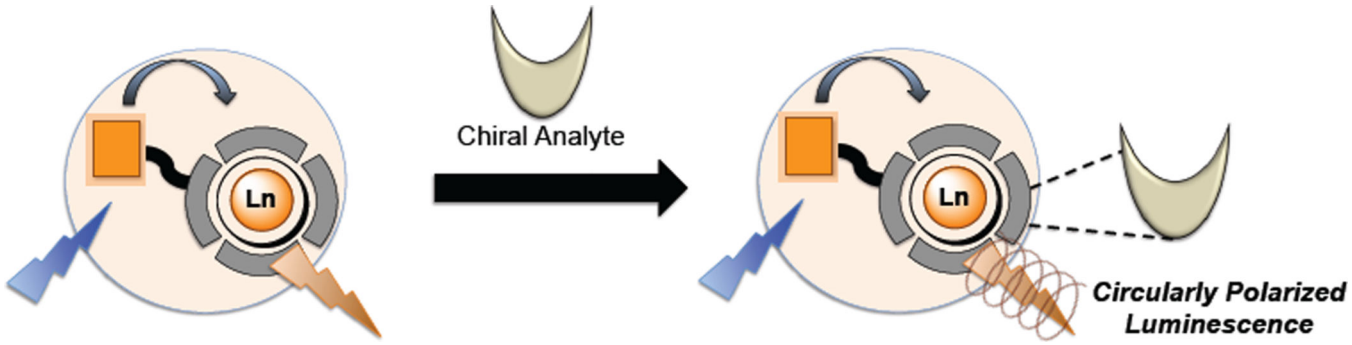

Figure 26.

Schematic for analyte detection by CPL "fingerprints." Binding of a chiral analyte (through either direct metal coordination or non-covalent interactions) to a luminescent lanthanide can introduce detectable chirality to or alter the chiroptical properties of the lanthanide complex. As a result, the analyte-bound complex produces detectable circularly polarized luminescence.

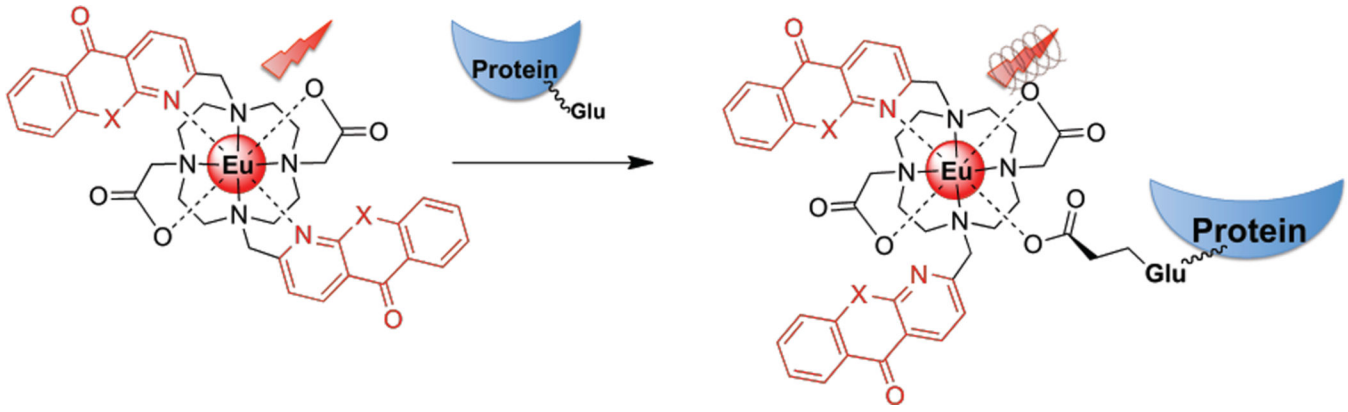

Figure 27.

Chiral Eu(III) probe for the detection of “acute-phase” proteins by CPL.[147] Protein binding occurs through hydrophobic interactions with the azaxanthone or azathioxanthone antenna units and coordinative interactions between the Eu(III) center and a glutamate side chain. The protein alters the chirality of the chelate, inducing a change in CPL signal profile and intensity.

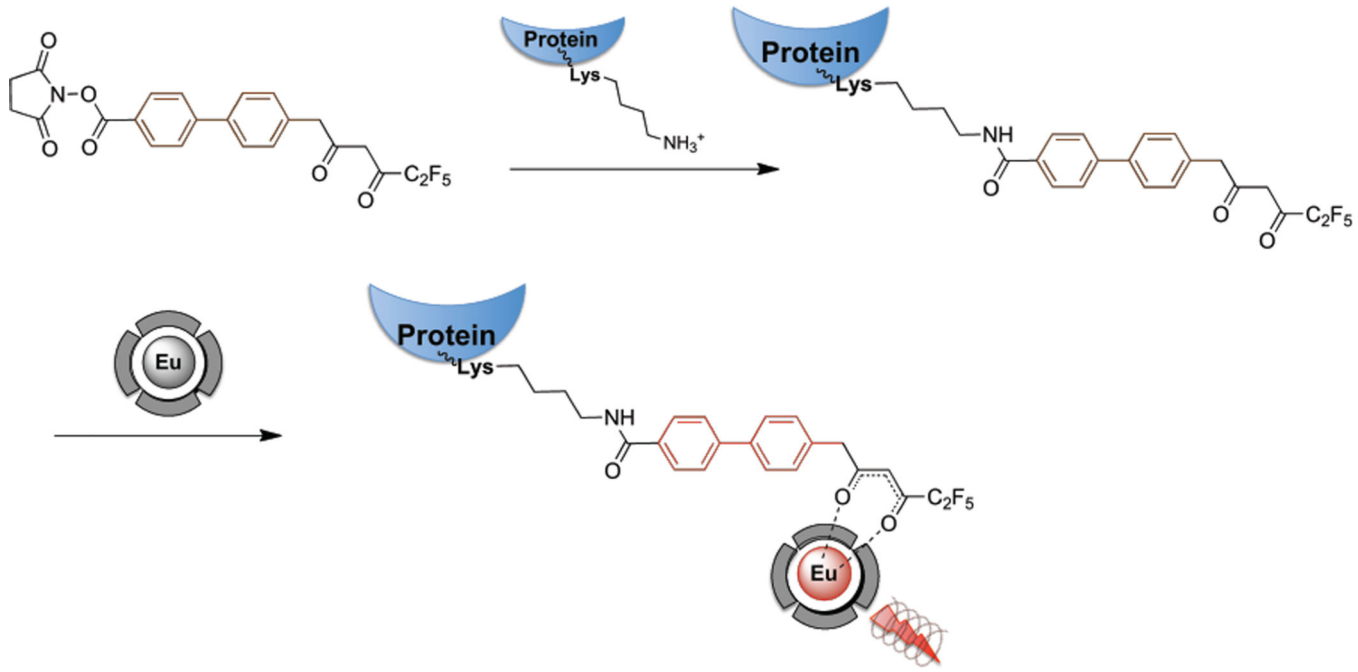

Figure 28.

CPL-active Eu(III) probes for protein labeling.[78] The approach utilizes the CPL fingerprints of different proteins to identify the analytes. The antenna is first labeled with the protein of interest through a peptide bond. The addition of the antenna to a Eu(III) chelate leads to self-assembly of the luminescent lanthanide with well-defined CPL signal.

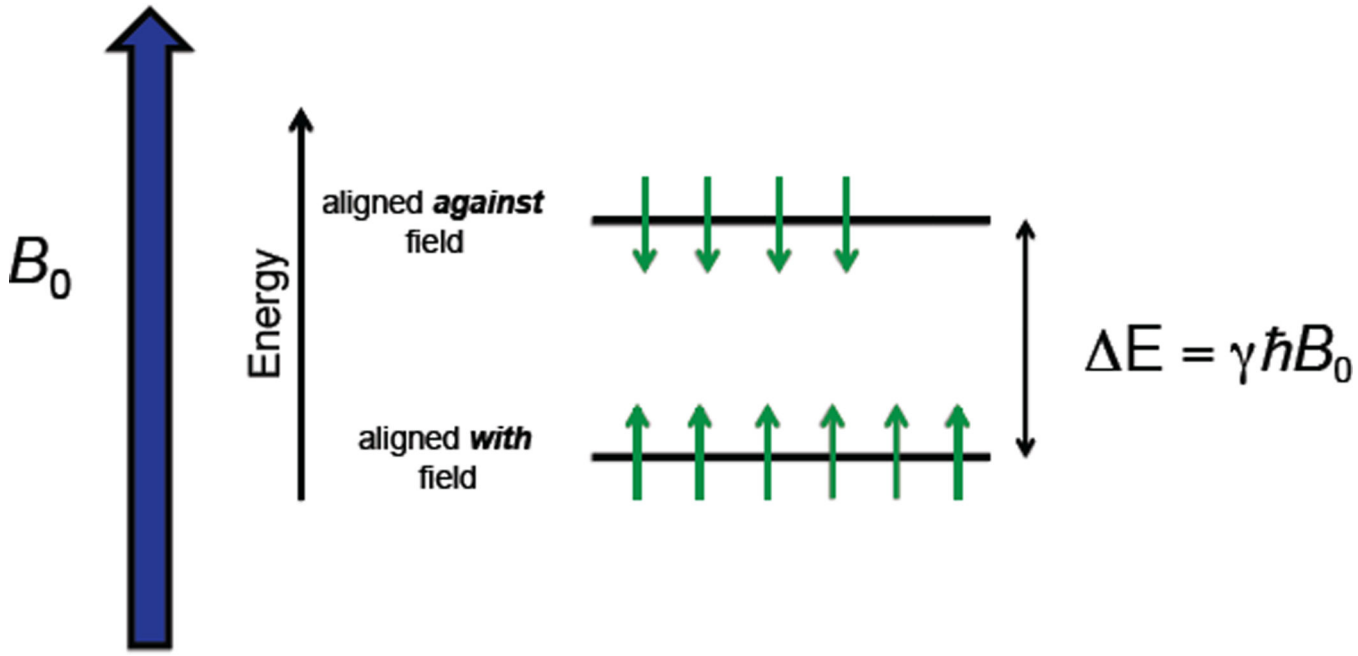

Figure 29.

When placed in a magnetic field $I = ½$ nuclei will either align with or against the field. The population of the two states is determined by the Boltzmann distribution; consequently, slightly more nuclei will occupy the lower energy state, i.e., the state aligned with the magnetic field.

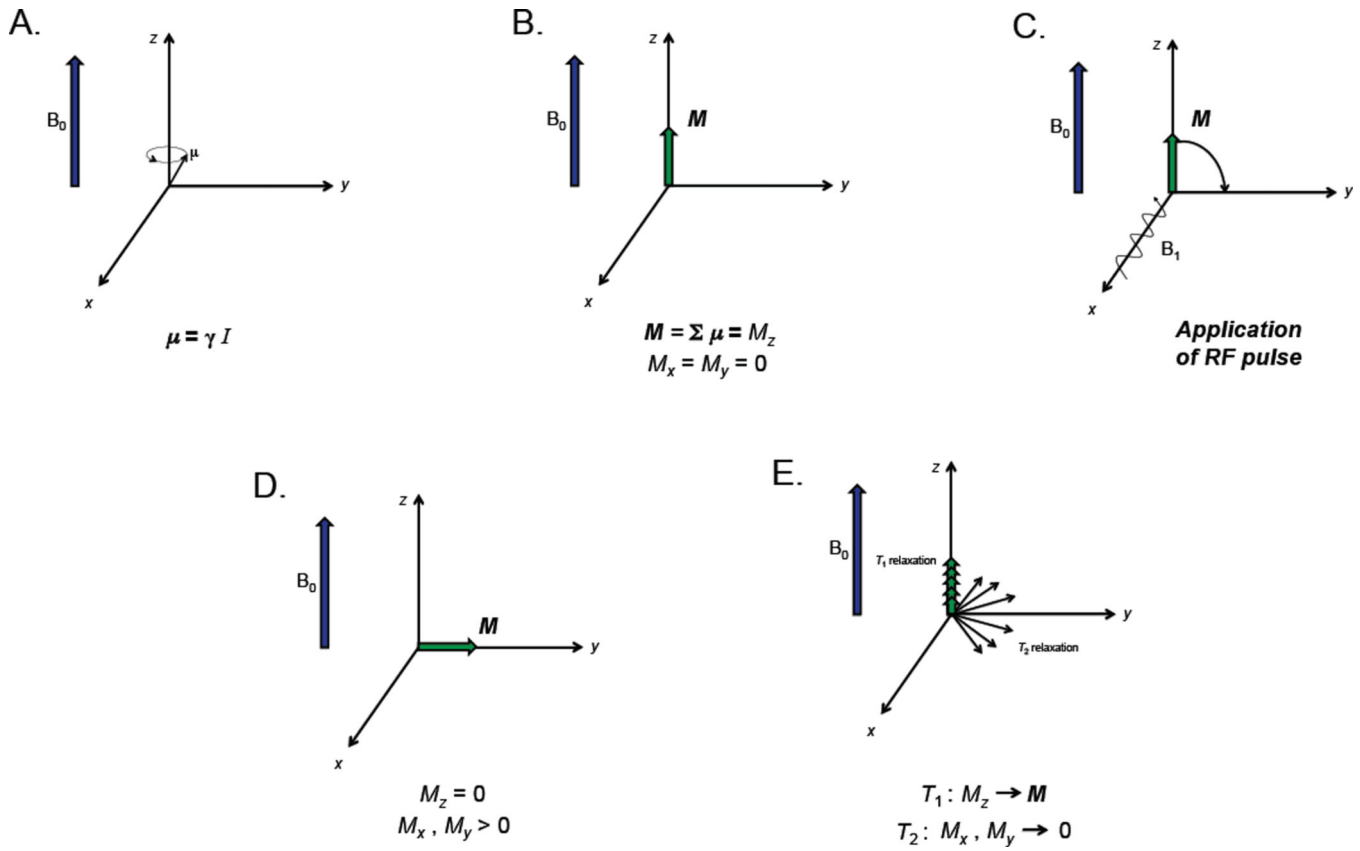

Figure 30.

A.) The spin angular momentum of each proton nucleus creates a magnetic moment (μ) which, in the presence of an external magnetic field ($\boldsymbol{B}_0$), precesses about the *z*-axis with a characteristic frequency (ω_0). B.) In a macroscopic sample, the magnetic moment of the individual nuclei can be summed into a single magnetization vector which lies along the *z*-axis. C.) The application of an RF pulse creates a secondary magnetic field ($\boldsymbol{B}_1$) which rotates the magnetization vector away from the *z*-axis, tipping it toward the *xy* plane. D.) Assuming the application of a 90° pulse, immediately after the RF field is removed, the magnetization vector will lie in the *xy* plane. E.) Over time, various relaxation processes return M_x, M_y, and M_z to their equilibrium values. Spin-lattice, or T_1, relaxation processes are responsible for the recovery of the M_z component of the magnetization vector. Spin-spin, or T_2, relaxation processes are responsible for returning M_x and M_y to zero.

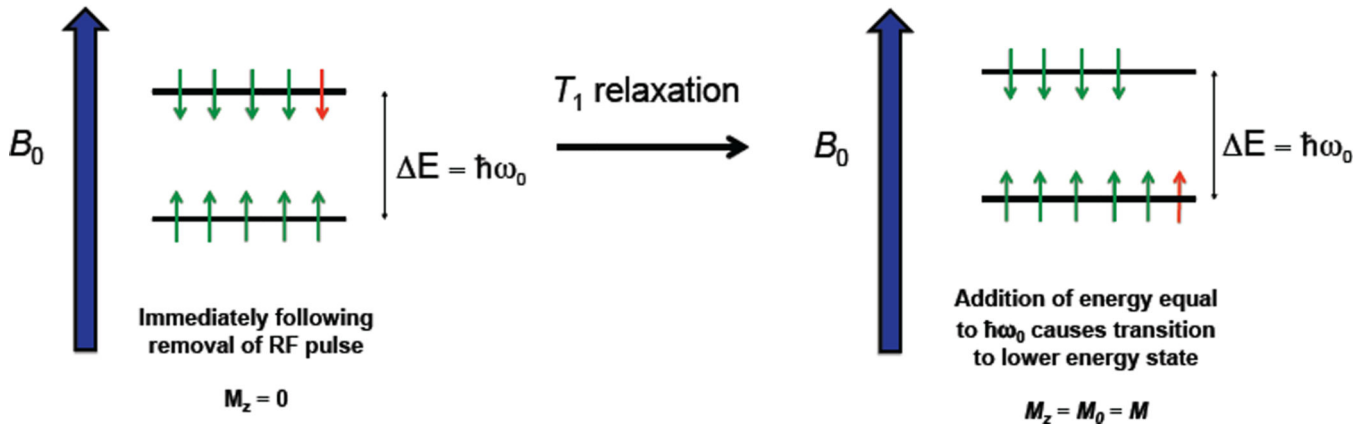

Figure 31.

Immediately following the removal of the RF field, there is an equal distribution of spins in the high and low energy state, resulting in a net M_z of 0. A number of nuclei must transition back to the low energy state to restore the initial Boltzmann distribution and return M_z to its equilibrium value. These transitions occur when the nuclei undergo stimulated emission, mediated by surrounding magnetic fields fluctuating at the Larmor frequency (ω_0).

Figure 32.

Gd(III)-DOTA is a clinically approved contrast agent where the Gd(III) ion is chelated by a macrocyclic polyaminocarboxylate ligand, leaving a single coordination site open on the lanthanide for water access.

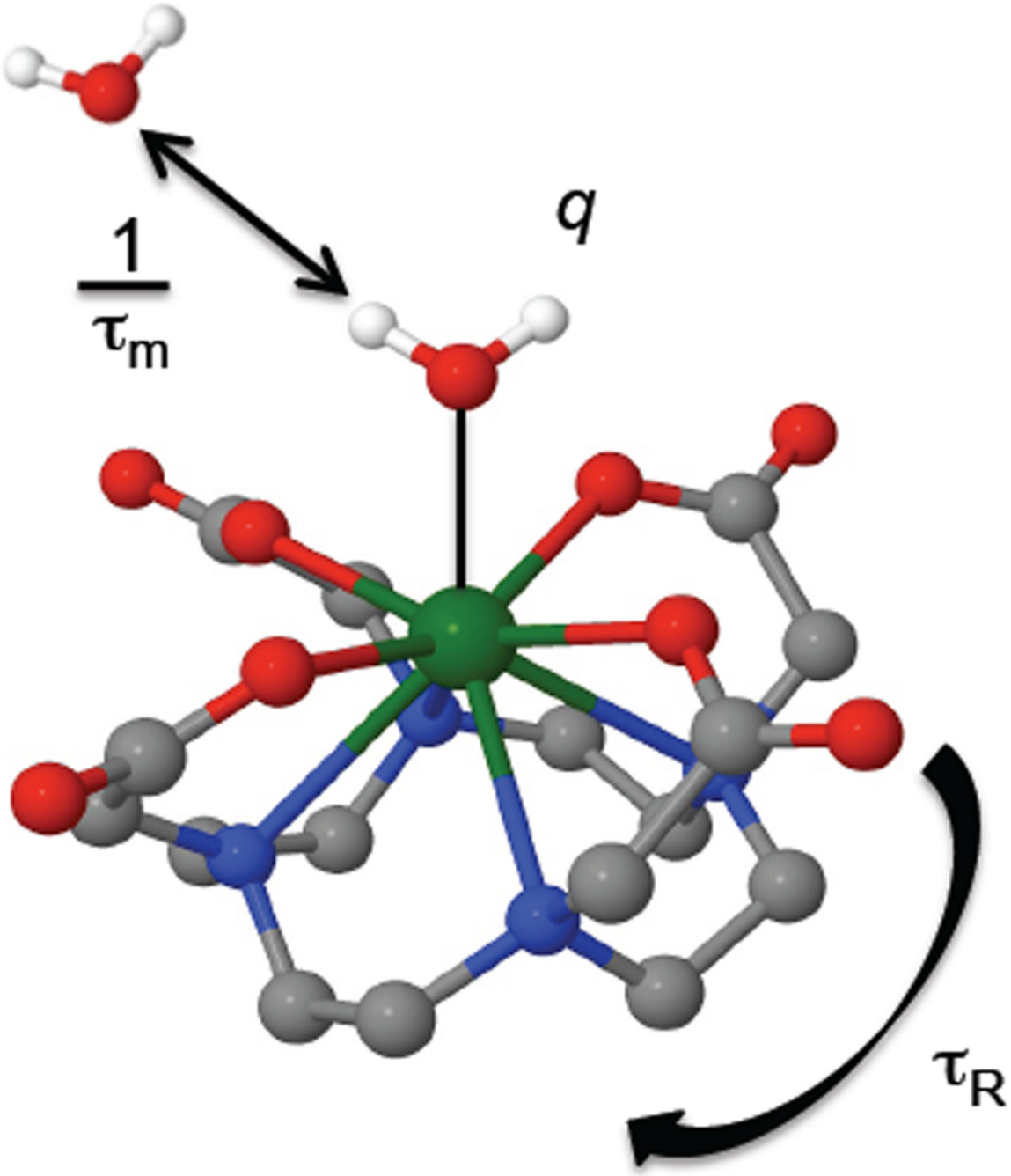

Figure 33.

There are three parameters that influence r_1 that can be modified by structural changes to the chelate structure: q, the number of water molecules directly bound to the Gd(III) center; τ_m, the inverse of the rate of exchange of the bound water with the bulk solvent; and τ_R, the rotational correlation time of the complex, or how rapidly it tumbles in solution.

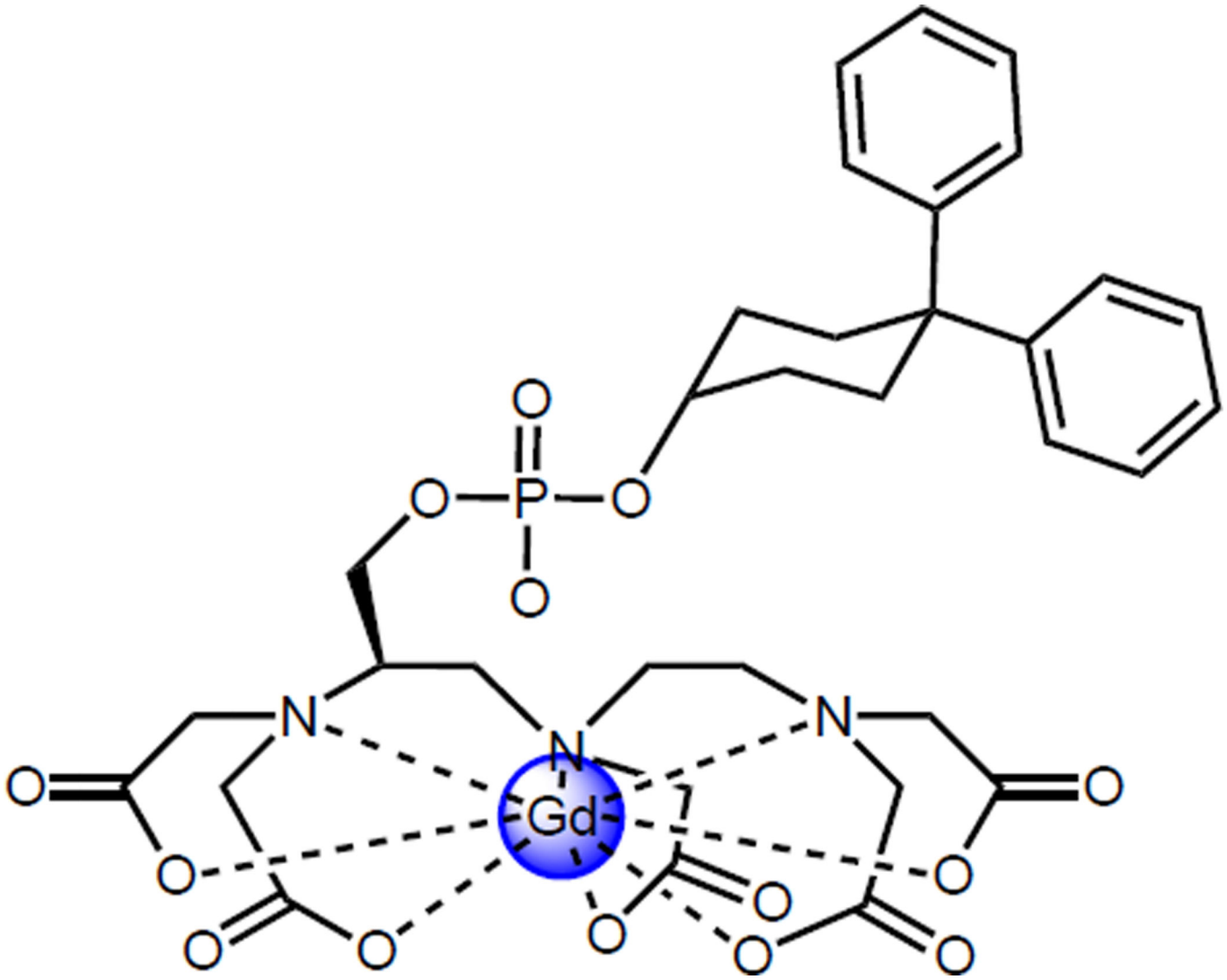

Figure 34.

The biphenylcyclohexyl moiety of MS-325 binds to HSA, a 67 kDa protein.[186,187]

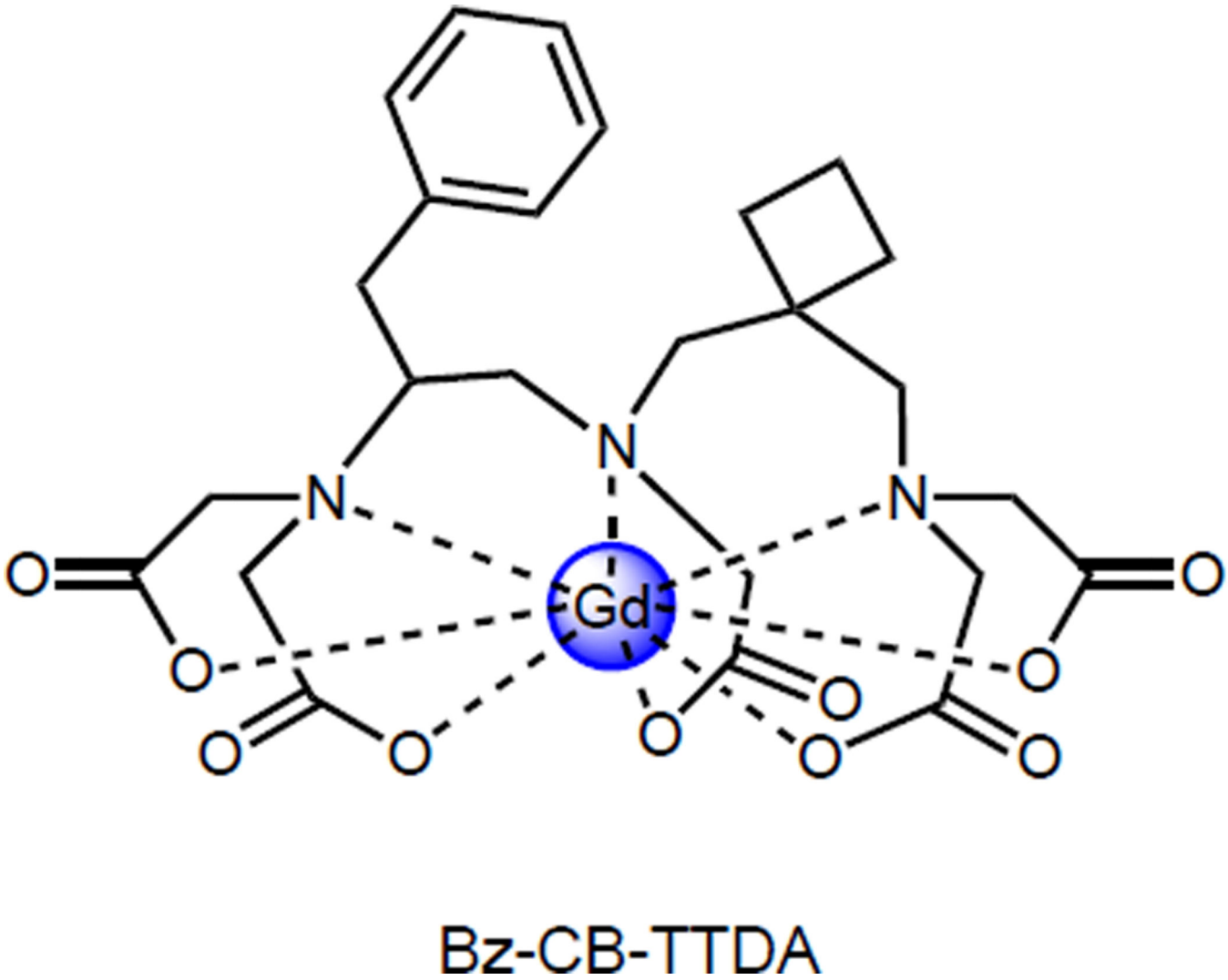

Figure 35.
Bz-CB-TTDA, an HSA-binding derivative of TTDA.[189]

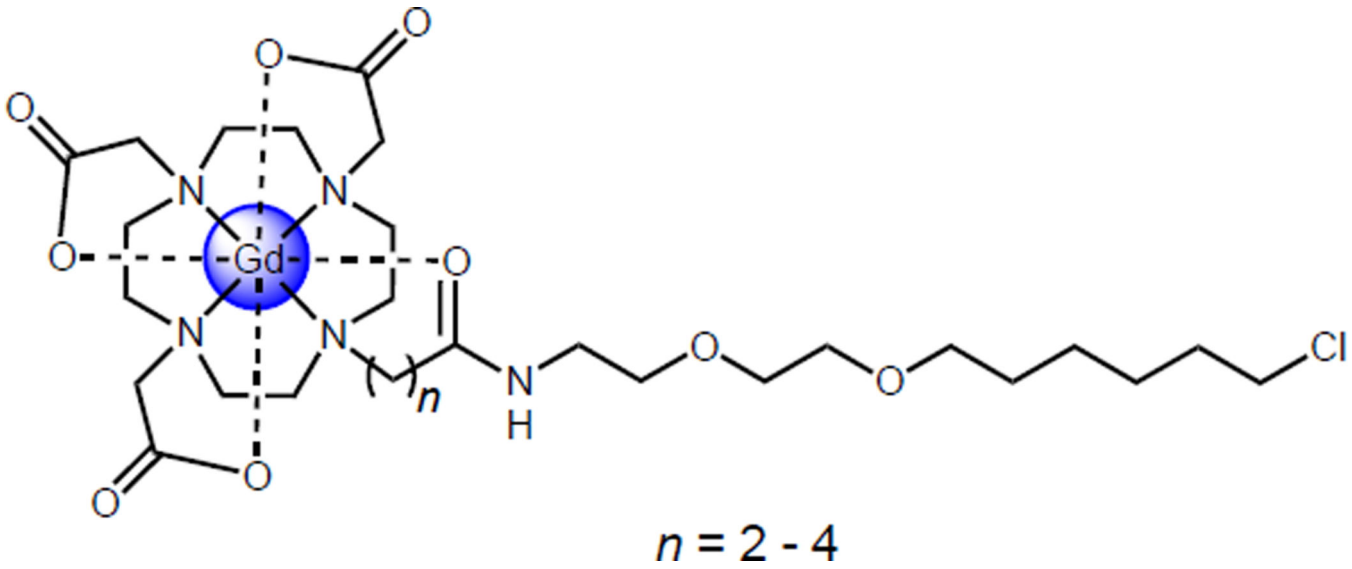

Figure 36.

The *n*-CHTGd series of probes forms a covalent bond with the reporter protein HaloTag, undergoing a 6-fold increase in relaxivity upon protein binding.[39]

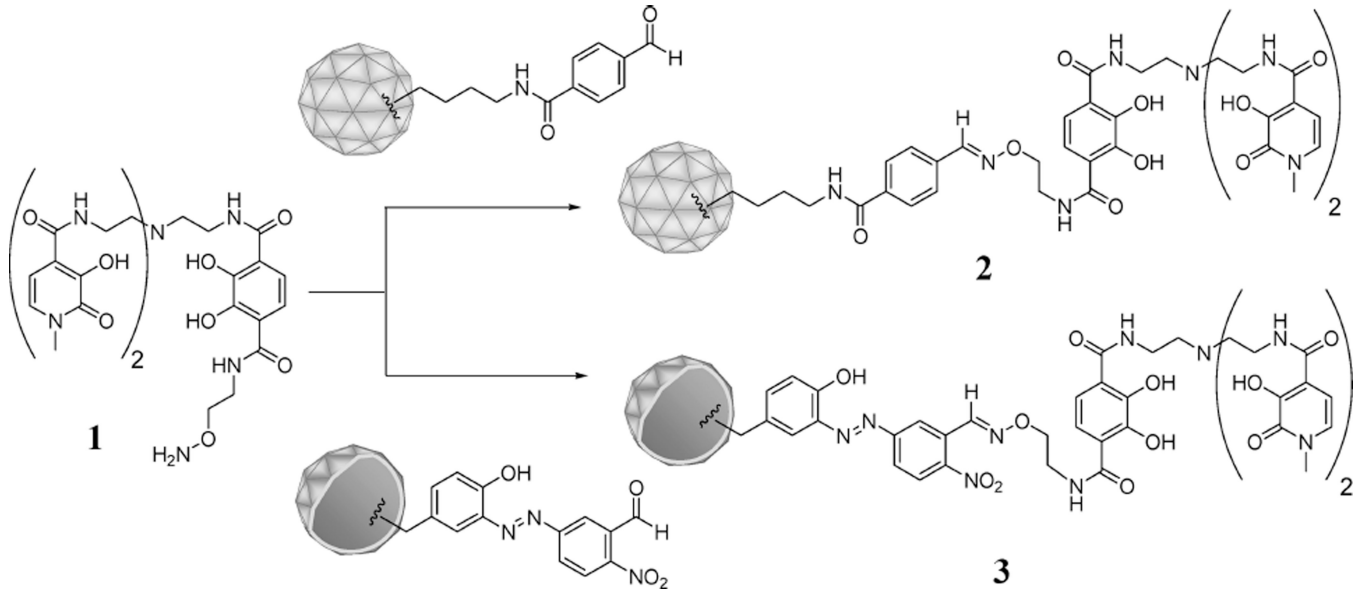

Figure 37.

Strategies for selective conjugation of the HOPO ligand to the interior or exterior surface of MS2 viral capsids.[195] (Figure reproduced with permission from reference 195. Copyright 2008 American Chemical Society.)

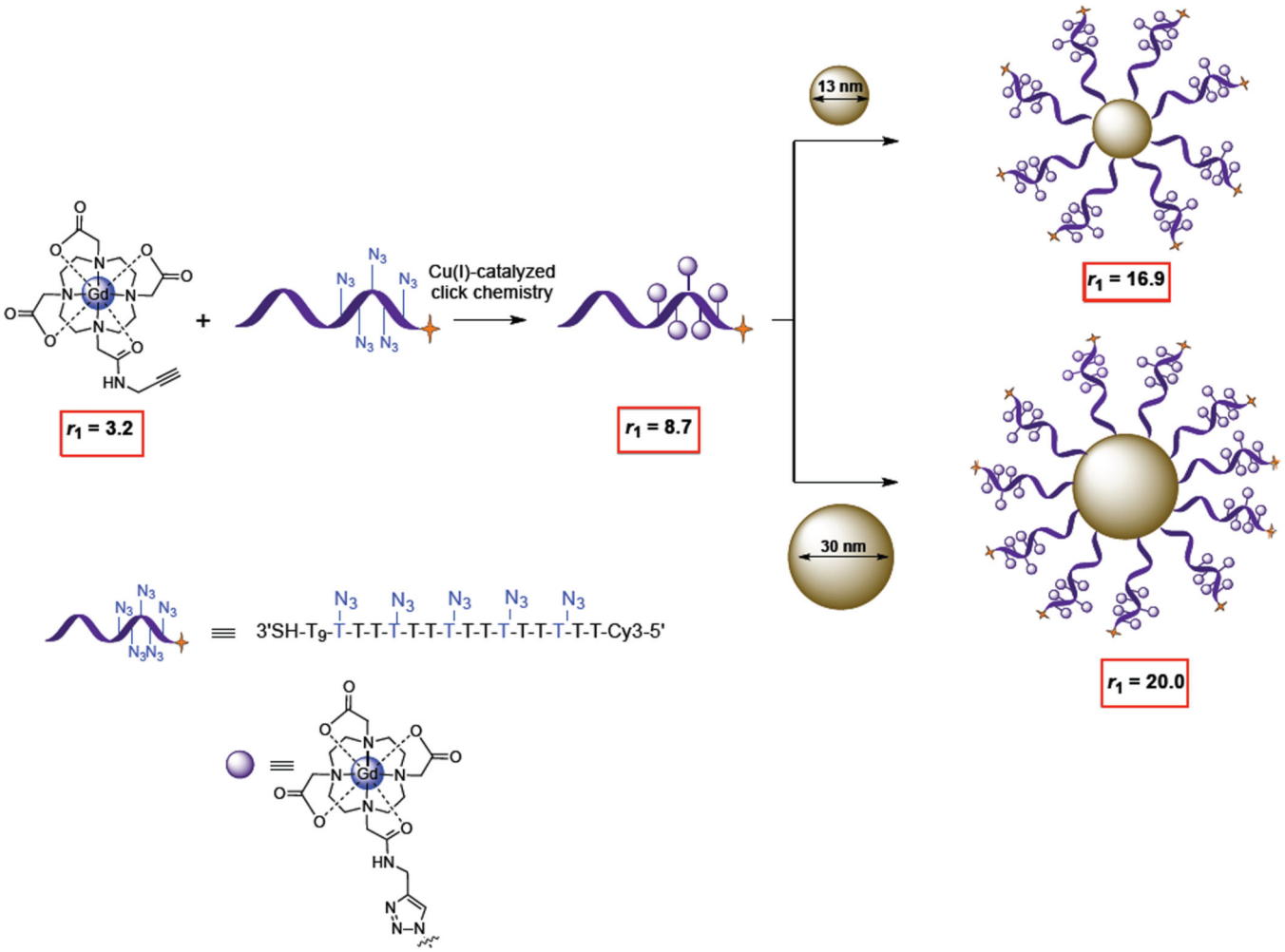

Figure 38.

Alkyne modified Gd-DO3A chelates were conjugated to azide-functionalized DNA strands using copper-catalyzed click chemistry. The Gd(III)-modified DNA was then immobilized on 30 or 13 nm AuNPs.[198] All relaxivity values are in $mM^{-1}s^{-1}$, were acquired at 60 MHz and are reported per Gd(III) ion.

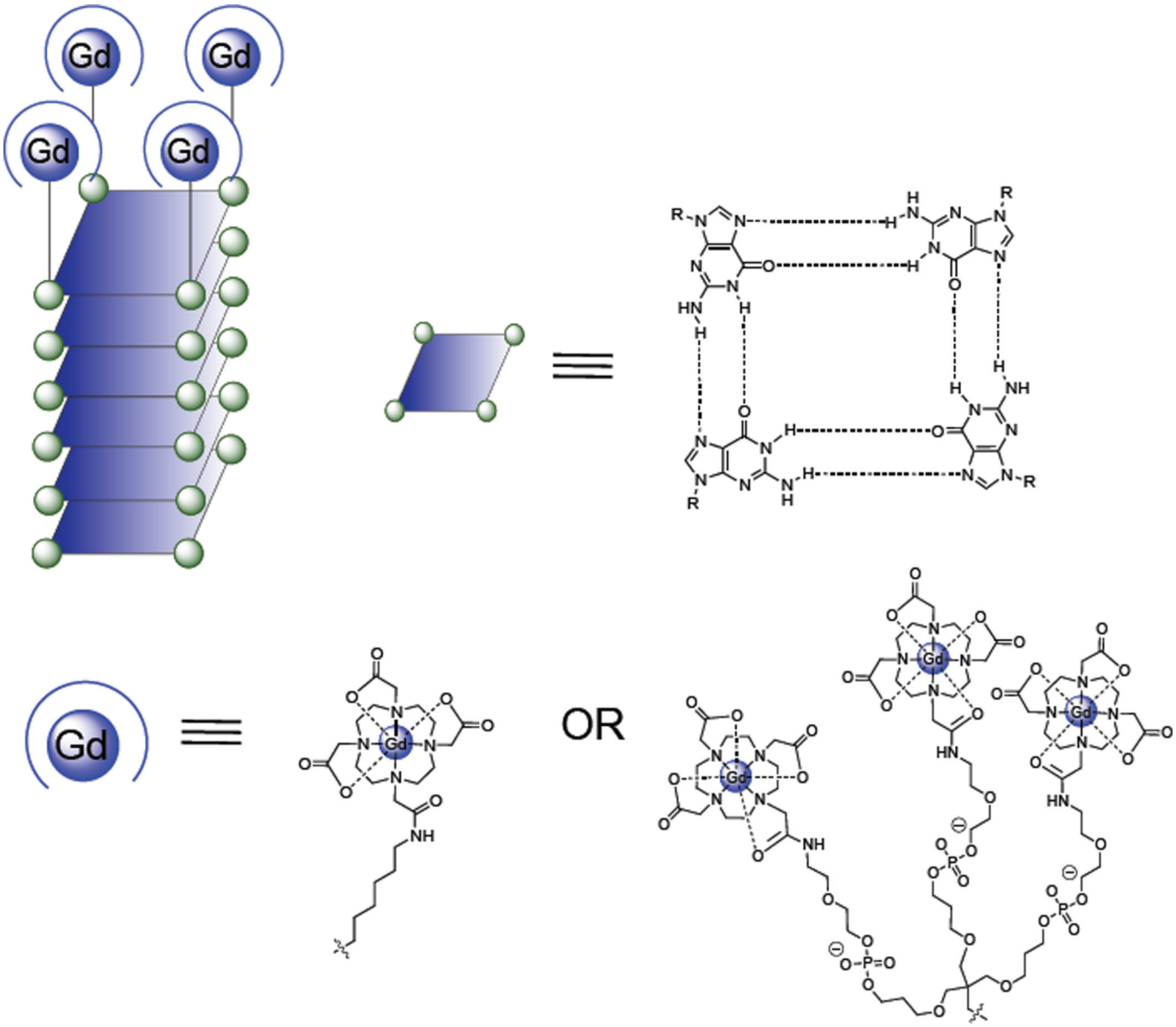

Figure 39.

By peptide coupling Gd(III) chelates to quadruplex-forming oligonucleotides, Hamilton et al. developed macromolecular structures with high relaxivity, biocompatibility and modularity.[48]

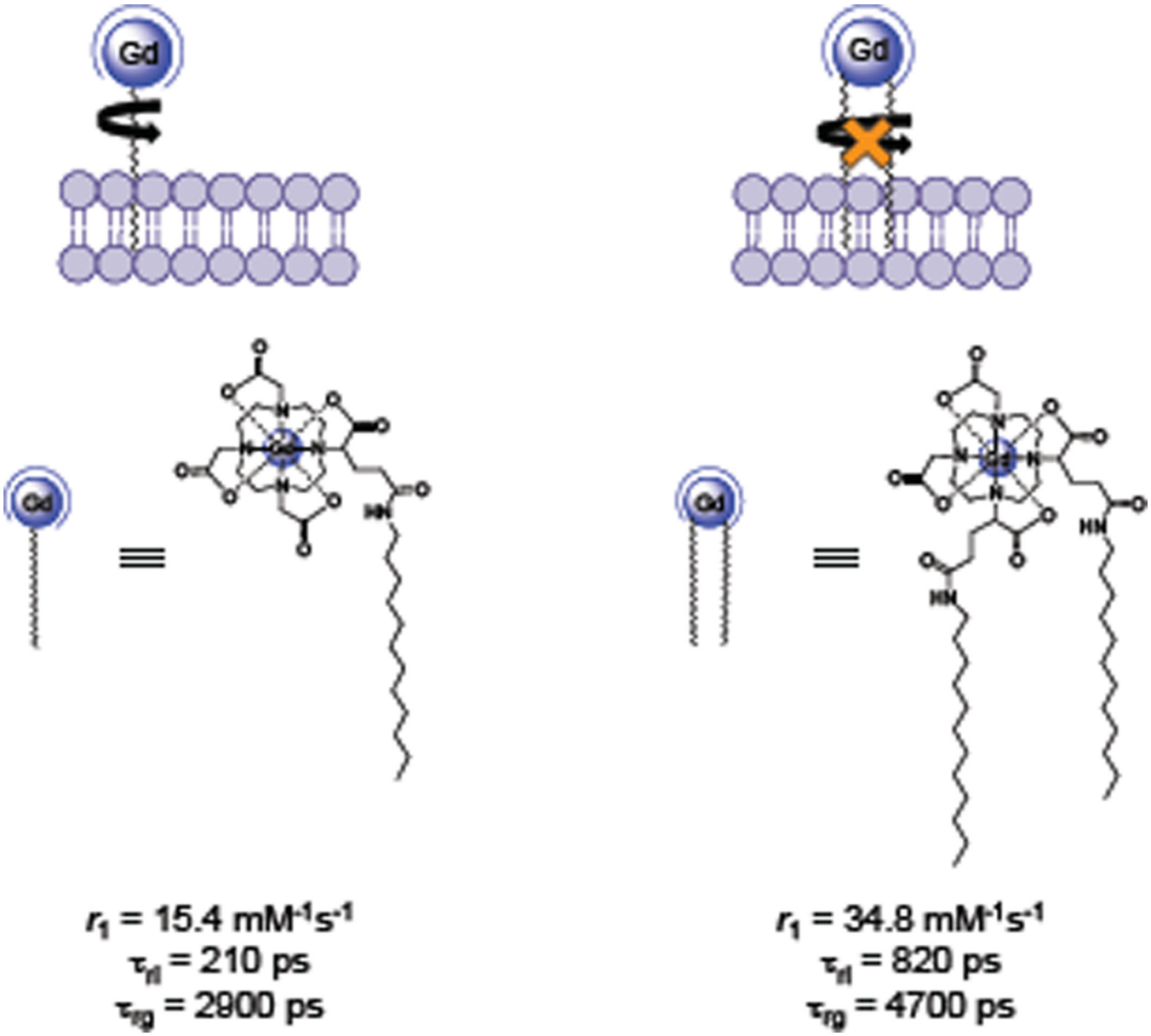

Figure 40.

Lipophillic complexes developed by Botta et al. The introduction of two aliphatic chains restricts rotation of the chelate once it has been incorporated into a liposome or micelle.[55]

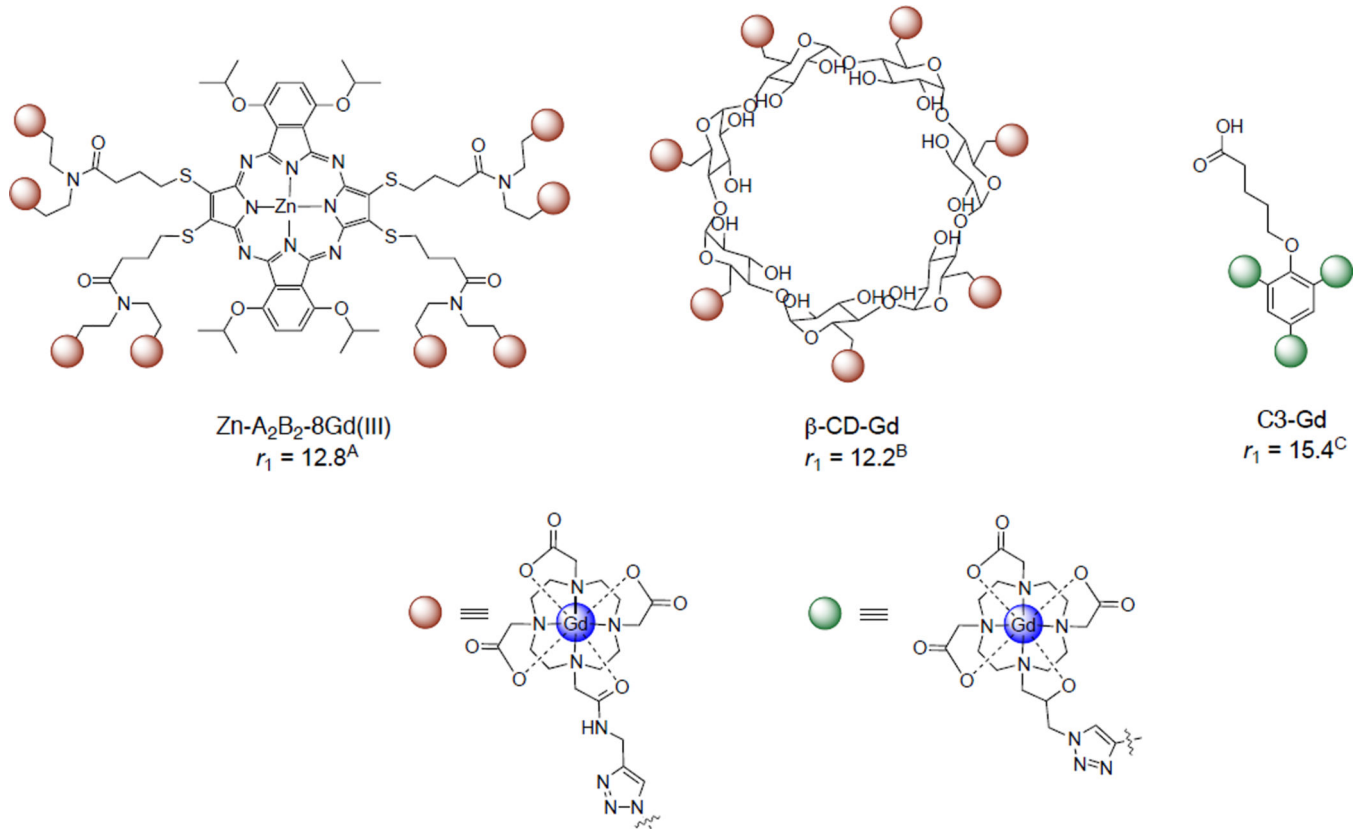

Figure 41.

Multimeric Gd(III) complexes conjugated to organic scaffolds via copper-catalyzed click chemistry. The relaxivity values were measured at 60 MHz and are reported per Gd(III) ion.[57–59]

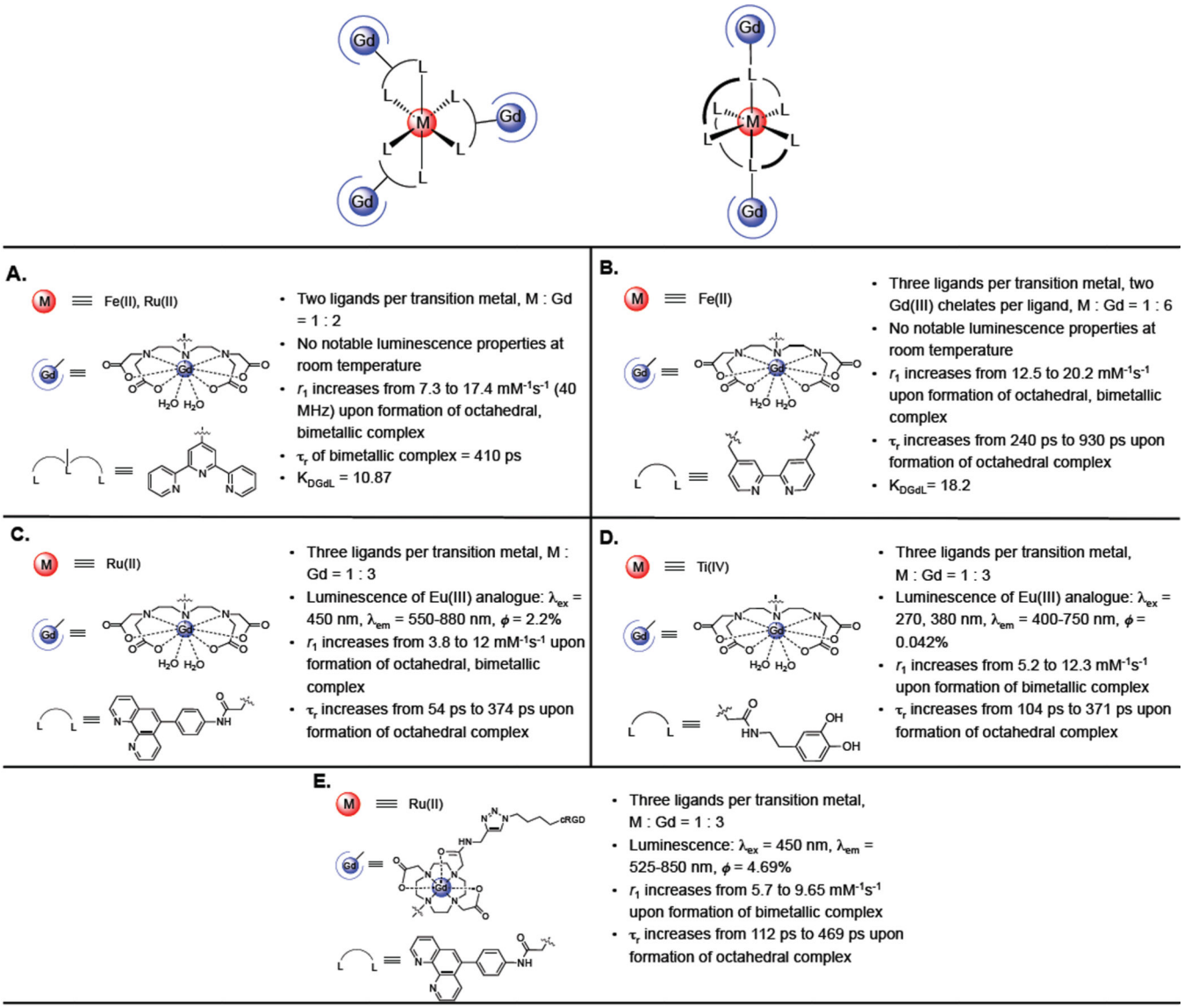

Figure 42.

Metallostar structures that have been developed and the parameters of interest. All relaxivity values were measured at 20 MHz unless otherwise noted, and are given on a per Gd(III) basis. **A** and **B** utilize a DTTA chelate with a q = 2,[219,220] leading to high r_1 values; however, by changing the ligand from a terpyridine (tpy) to bpy and extending the linker between the Gd(III) chelate and the ligand, Tóth and Ruloff were able to increase the log K_{DGdL} from 10.87 to 18.2.[212–214]

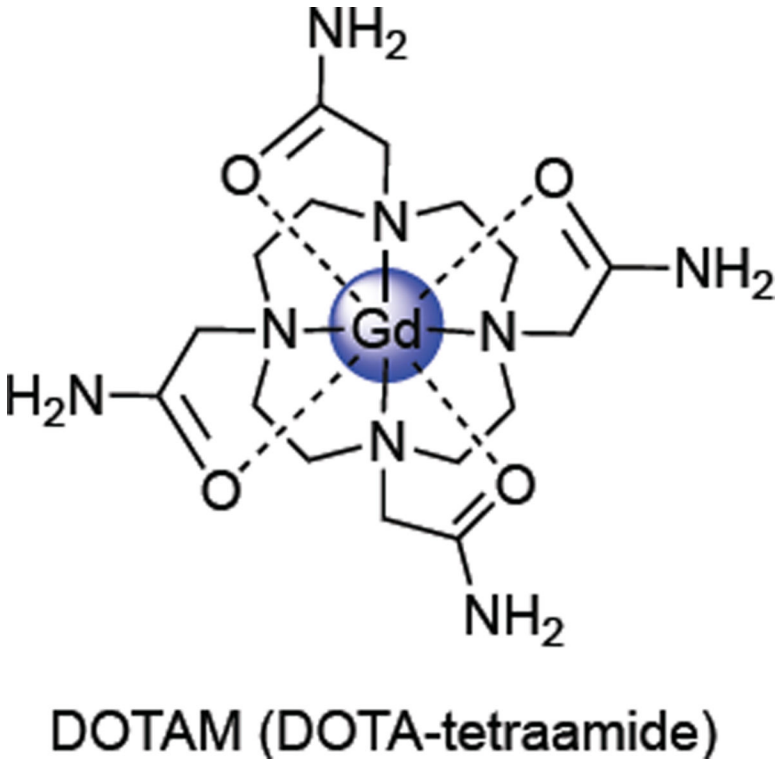

Figure 43.

The tetraamide derivative of Gd(III)-DOTA displays dramatically slower water exchange than the anionic Gd(III)-DOTA.[223]

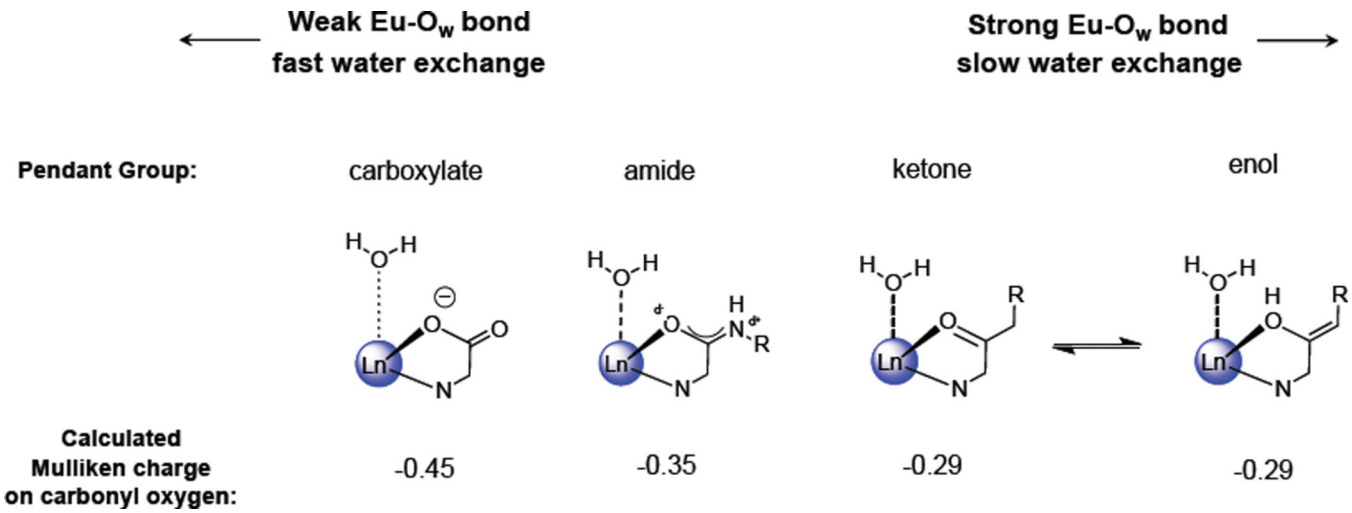

Figure 44.

Sherry et al. computed the Mulliken charge of the chelating oxygen atom for Eu(III) chelates with pendant carboxylate, amide and ketone arms.[229] The carboxylate oxygen had the largest partial negative charge, the ketone oxygen (or the enol tautomer) had the smallest negative charge, and the amide oxygen was intermediate between the two. A systematic investigation of a series of chelates with pendant amide and ketone arms confirmed that incorporation of less negatively charged ketone groups results in slower water exchange, likely due to a stronger Gd-O_w resulting from a more electropositive metal center.

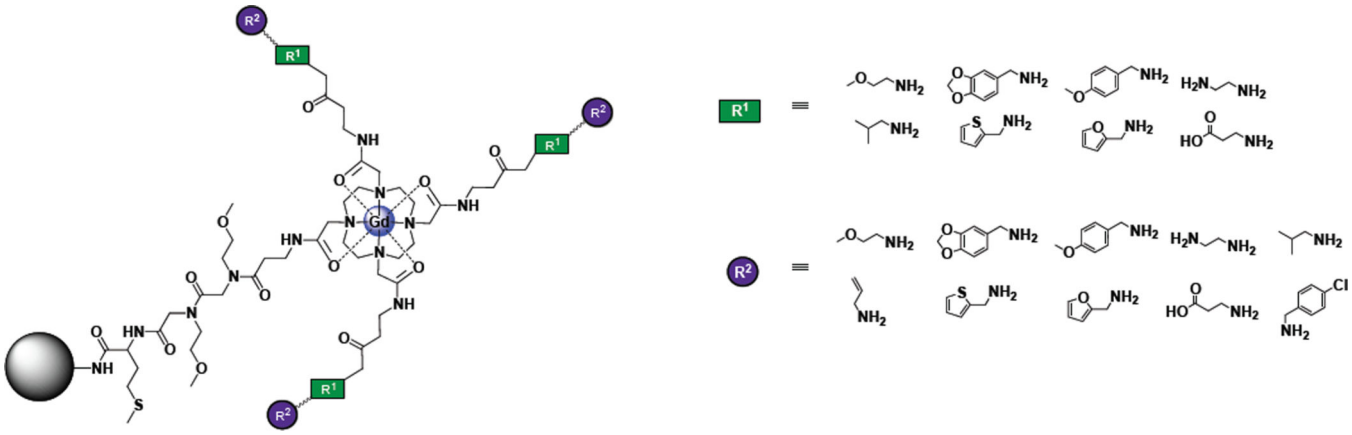

Figure 45.

Schematic of library of peptoid-modified Eu(III) DOTA – tetraamide derivatives.[230]

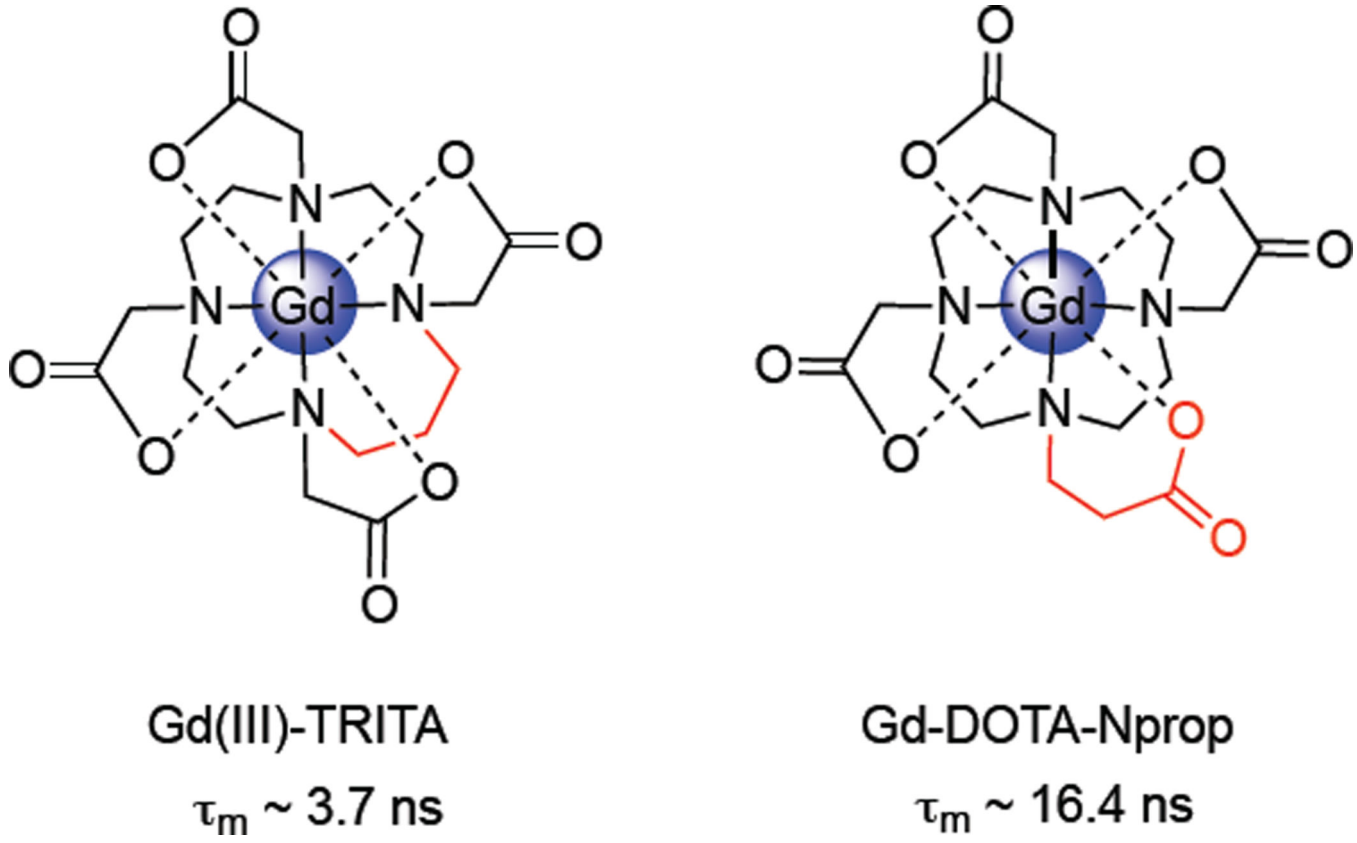

Figure 46.

Sterically crowded structures studied by Merbach et al. that exhibit optimal water exchange rates. Incorporation of an additional methylene group (shown in red).[231–233]

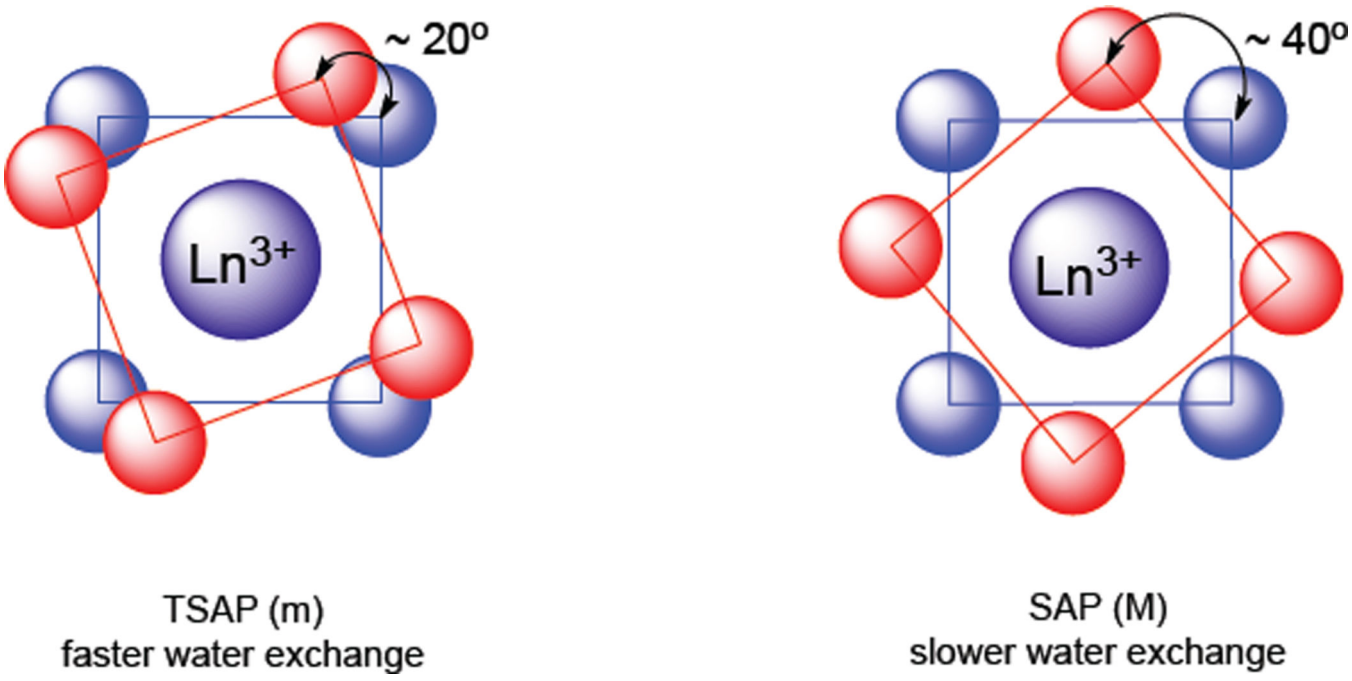

Figure 47.

The SAP (M) and TSAP (m) isomers of macrocyclic lanthanide chelates differ in the twist angle between the planes defined by the chelating nitrogen and oxygen atoms. It is proposed that the TSAP isomer is more sterically crowded about the water binding site, weakening the Gd-O_w bond and leading to faster water exchange.

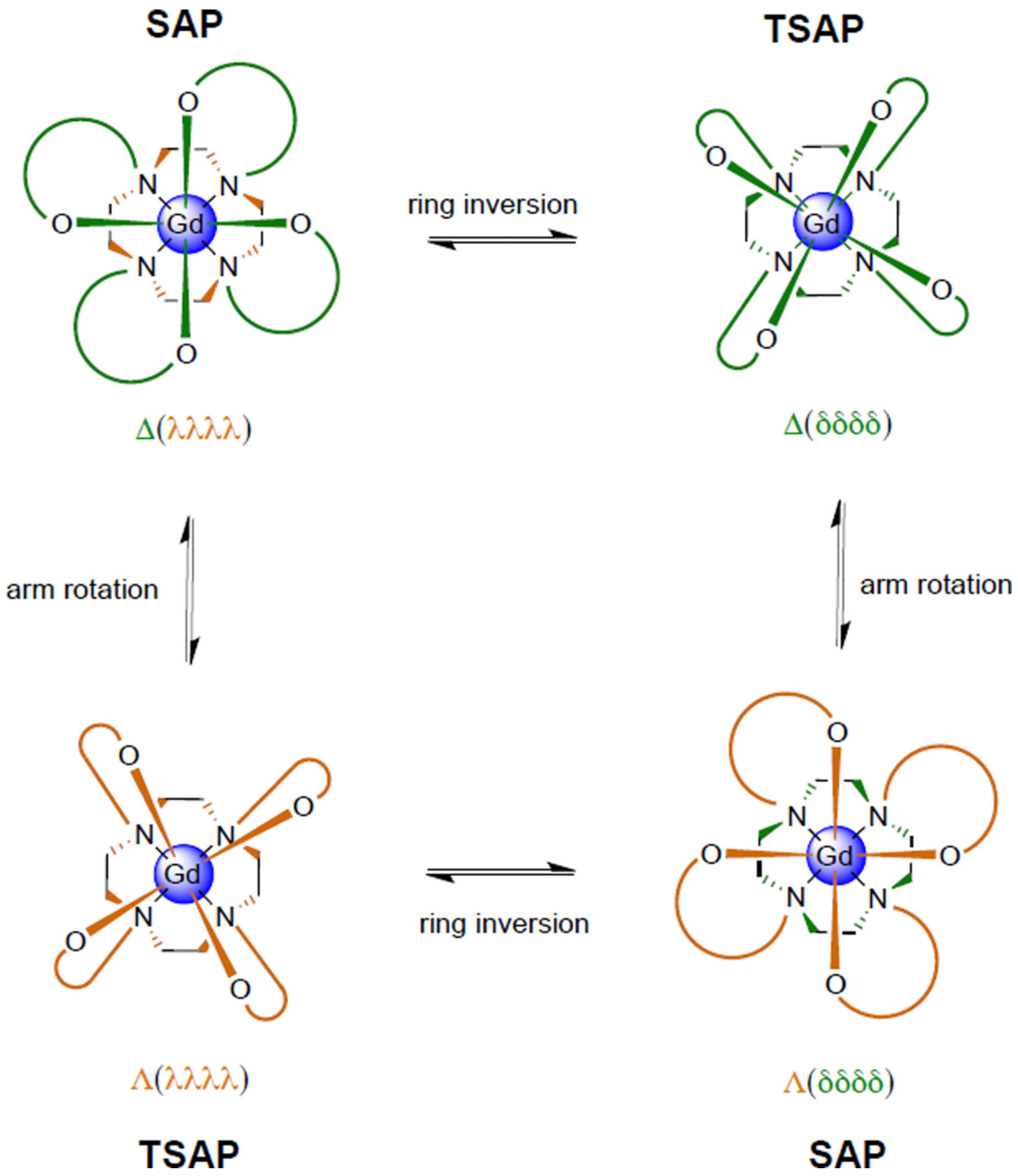

Figure 48.

SAP/TSAP interconversion occurs by either arm rotation or ring inversion. Sequential application of both processes leads to enantiomerization.[235] (Figure adapted with permission from reference 235. Copyright 2012 American Chemical Society.)

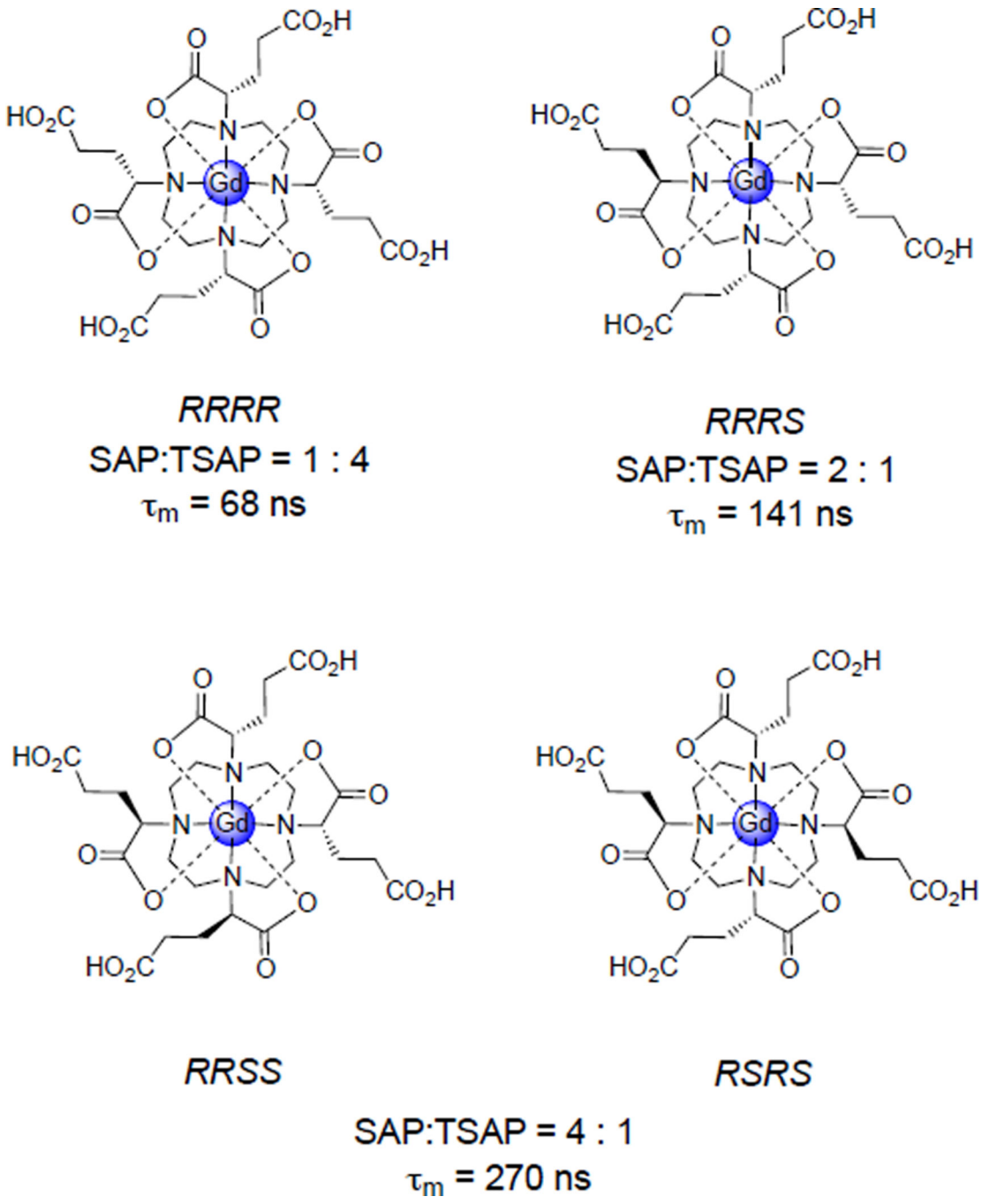

Figure 49.

Woods et al. examined the SAP : TSAP ratio and water exchange kinetics of three derivatives of Gd(III)-DOTA that incorporate a carboxyethyl substituent α to the macrocycle and determined that the complexes with lower SAP : TSAP ratios exhibit significantly faster water exchange.[150]

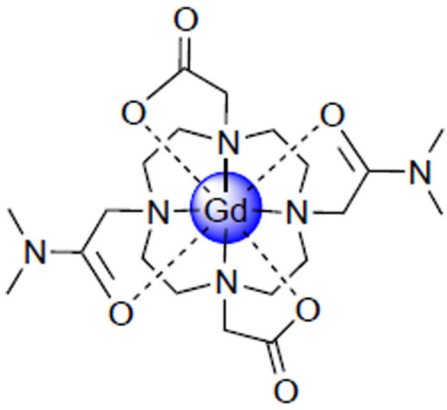

Gd(III)-DOTA-2DMA
TSAP: τ_m = 14.2 ns
SAP: τ_m = 1350 ns

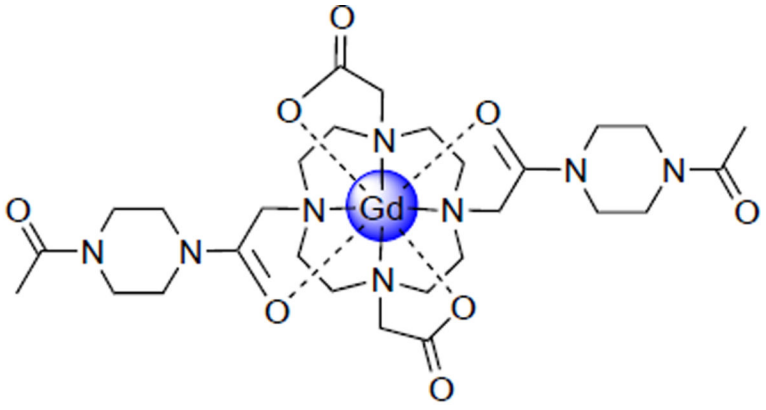

Gd(III)-DOTA-2APA
TSAP: τ_m = 3 ns
SAP: τ_m = 2350 ns

Figure 50.

Substitution of carboxylate groups for two of the amide back-binding groups of DOTAM magnifies the difference in water exchange rate of the SAP and TSAP isomers.[226]

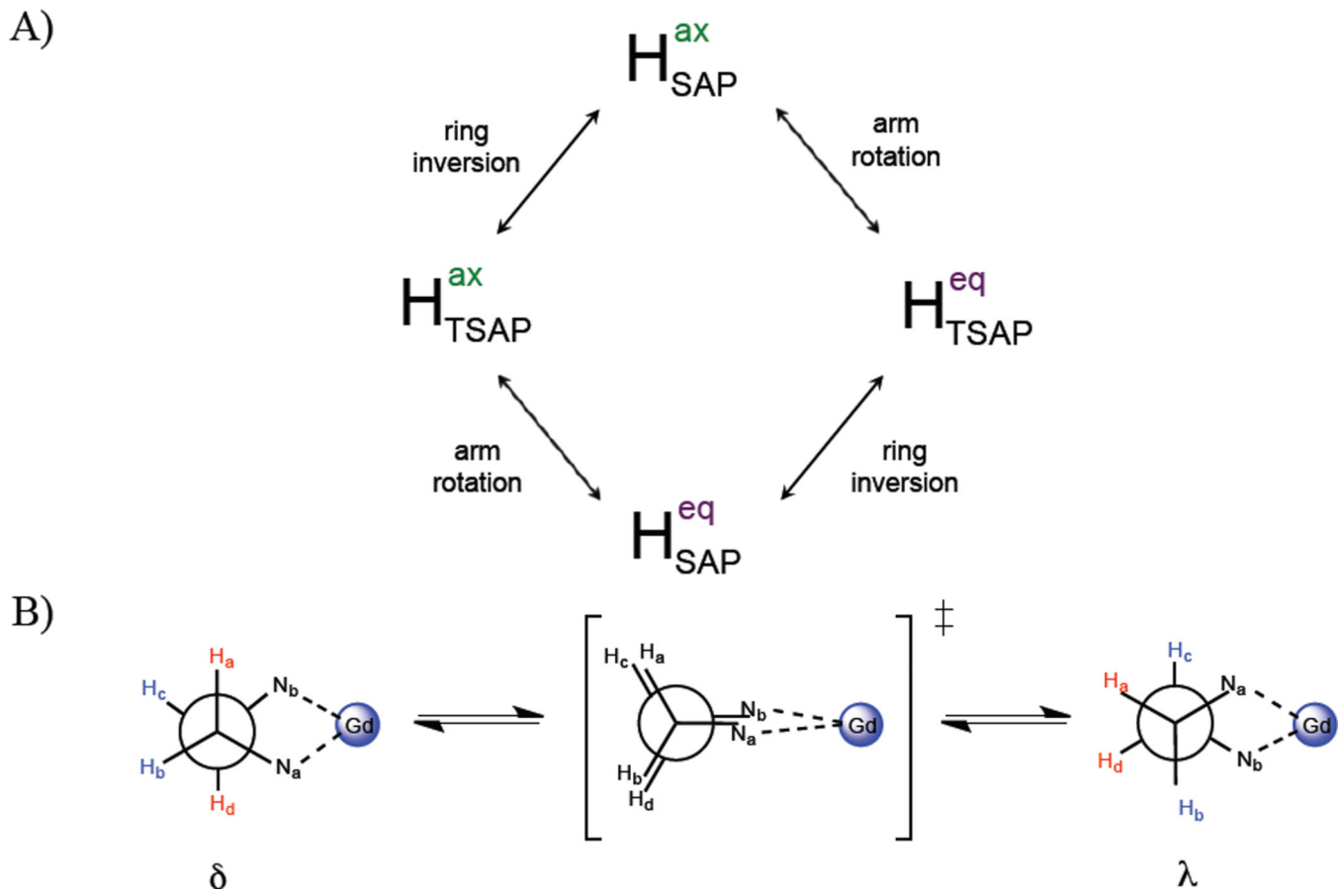

Figure 51.

(A) The process of ring inversion exchanges axial protons (H_a and H_d, shown in red) with equatorial protons (H_c and H_b, shown in blue) and vice versa. (Figure adapted with permission from reference 150. Copyright 2000 American Chemical Society.) (B) During the ring inversion process, the axial and equatorial protons of the two isomers exchange with one another; conversely, during the arm rotation process, the axial protons of one isomer exchange only with the axial protons of the other. (Figure reproduced with permission from reference 252. Copyright 2010 American Chemical Society.)

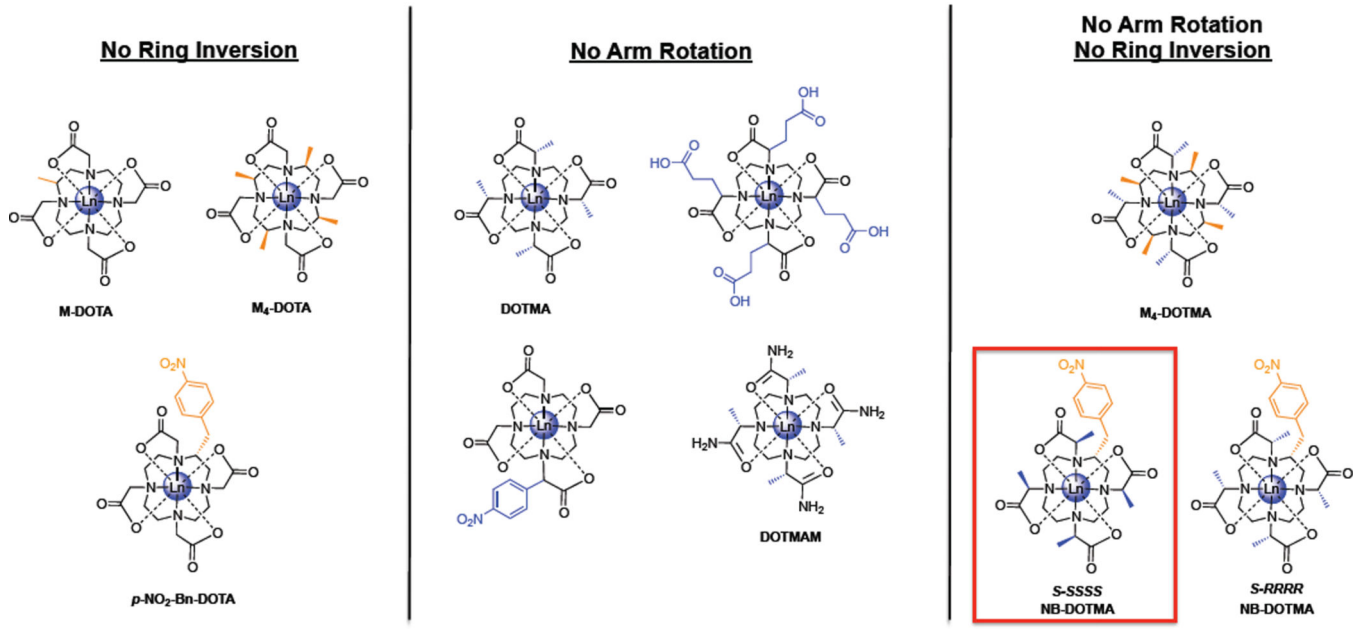

Figure 52.

Substituted DOTA derivatives that restrict isomerization processes. Substitution on the backbone of the macrocycle (shown in orange) restricts ring inversion, while substitution of the pendant carboxylates/amides of the chelate (shown in blue) prevents arm rotation. Substitution at both positions effectively locks the chelate in a single conformation, either SAP or TSAP, depending on the absolute stereochemistry at the substituted positions. *S-SSSS* *p*-NO_2-Bn-DOTMA (boxed in red) is effectively locked in the desired TSAP conformation.

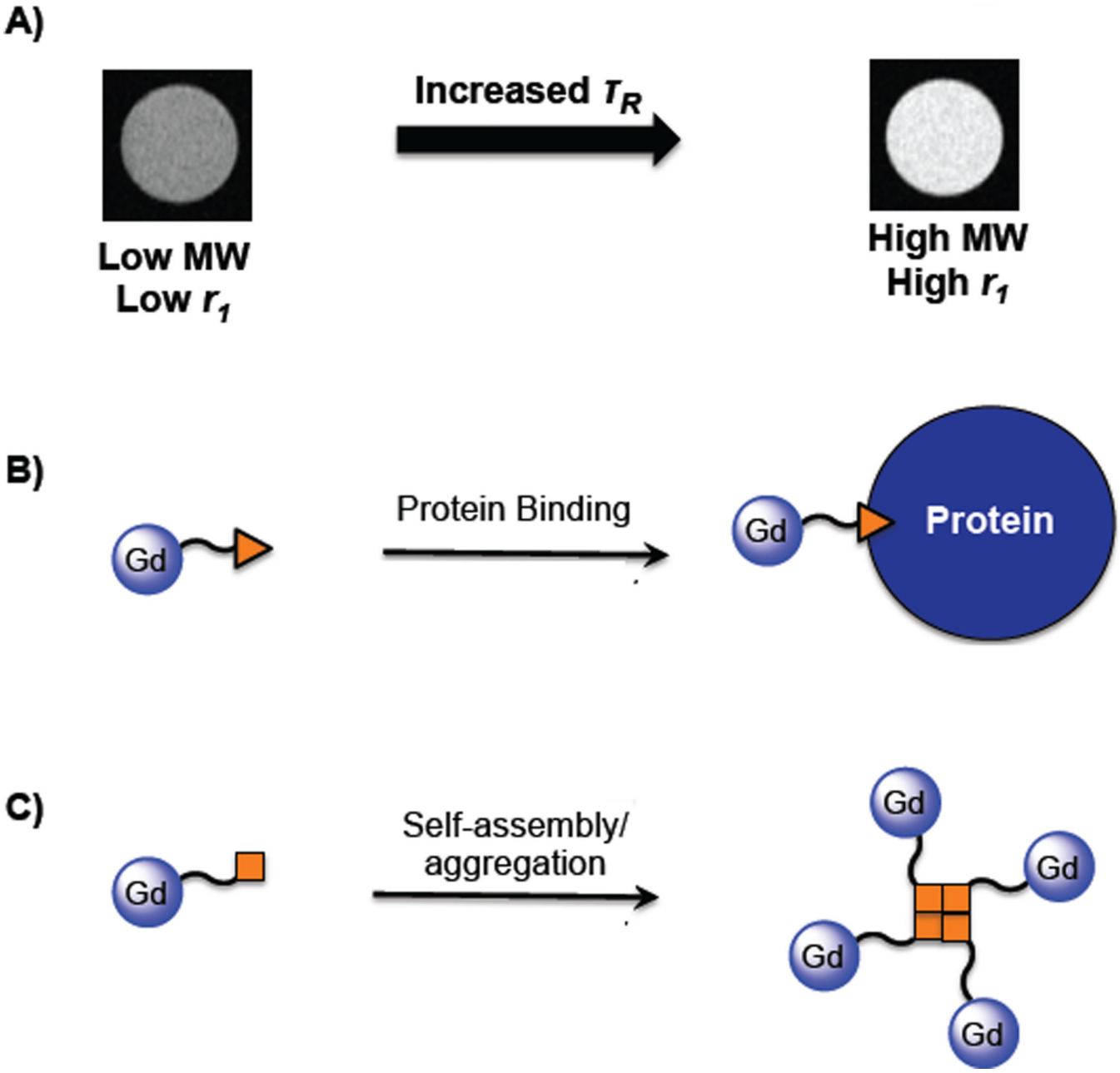

Figure 53.

(A) τ_r-modulated contrast agents undergo an increase in molecular weight upon activation by the event of interest, causing an increase in τ_r and consequently relaxivity. Increase in MW typically occurs through (B) protein binding or (C) self-assembly due to a biological event of interest.

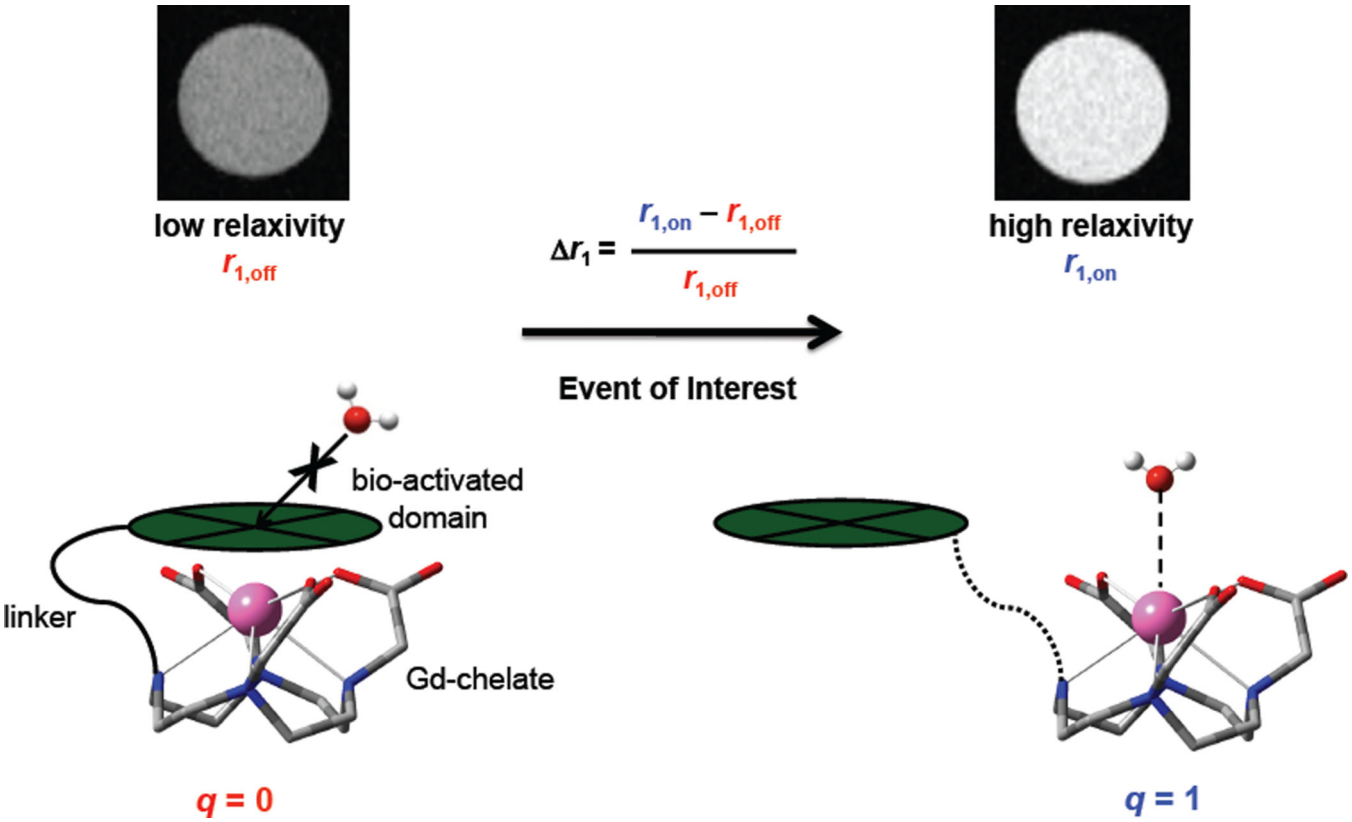

Figure 54.

In response to the biological event of interest, *q*-modulated contrast agents transform from a low-relaxivity $q = 0$ state to a high relaxivity $q = 1$ state.[6,274,276] (Figure reproduced with permission from reference 274. Copyright 2013 American Chemical Society.)

Figure 55.

Example of a system in which CEST can occur. Water protons and amine protons resonate at different NMR frequencies and can undergo chemical exchange with one another. If the water protons (H_B) are selectively saturated, chemical exchange will transfer some of the magnetization saturation to the amine protons (H_A), allowing for indirect saturation of the signal from H_A.[276,277]

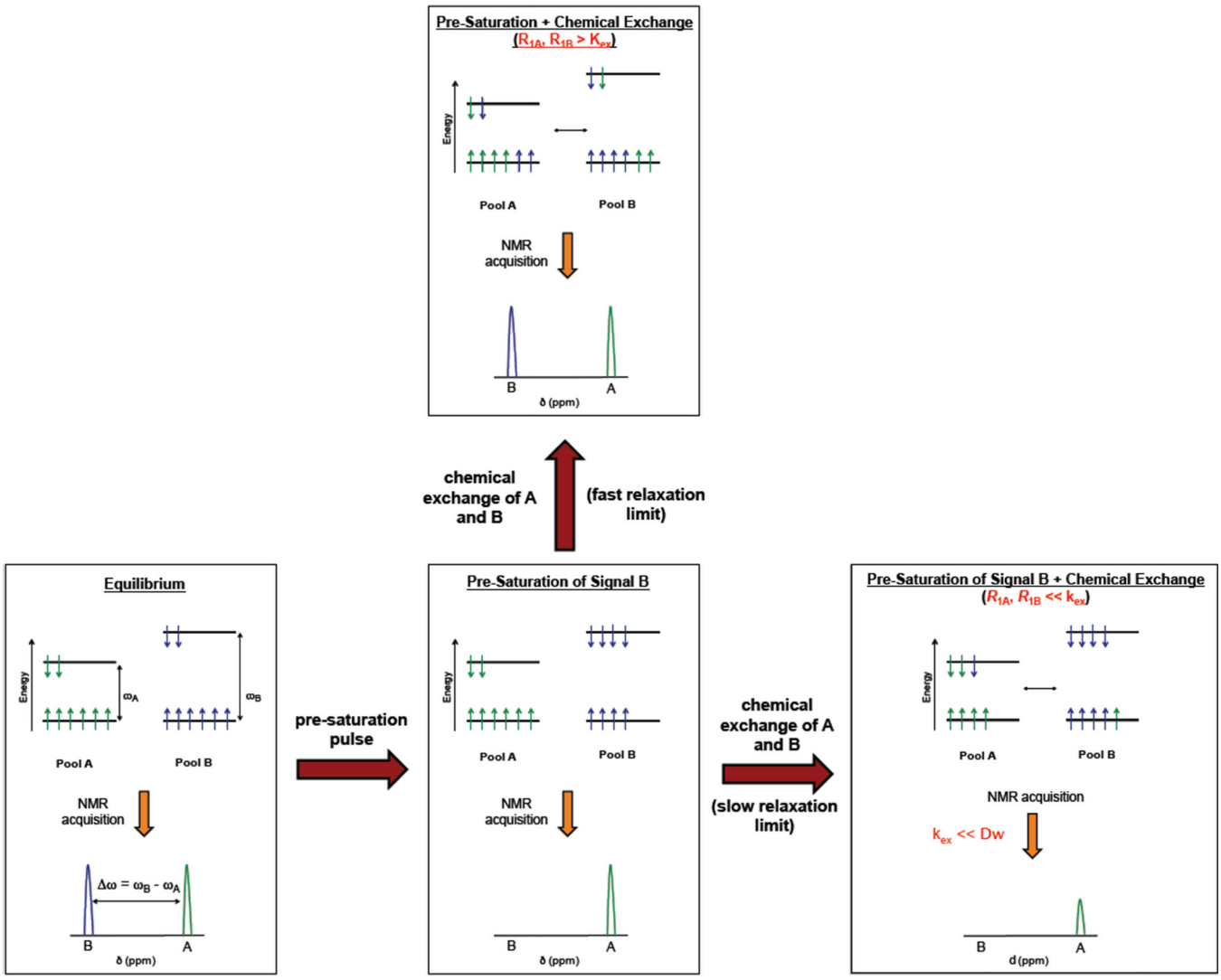

Figure 56.

A presaturation pulse applied to Pool B increases the number of spins aligned against the magnetic field in this pool (middle). The distribution of the spins in Pool A will depend upon the longitudinal relaxation rates of both Pool A and Pool B. If the relaxation rate of either pool is faster than the rate constant of exchange, then the system will relax back to the Boltzmann distribution before exchange can transfer the altered spin state to Pool A (top). The result will be a normal NMR spectrum. If relaxation is slow compared to chemical exchange, then the high energy level spins will equilibrate thus reducing the bulk magnetization in this pool (right). The result will be signal intensity reduction in both Pool A and Pool B.[276]

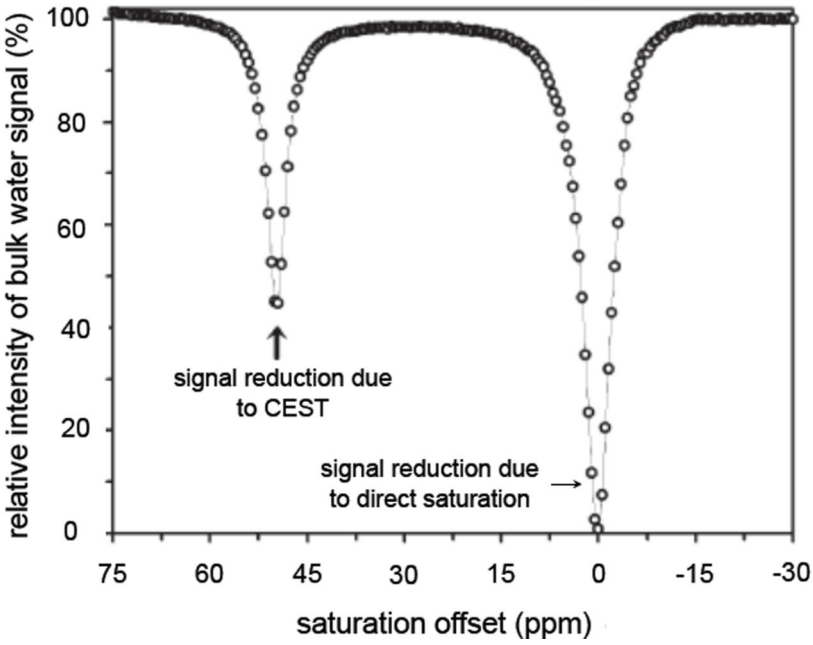

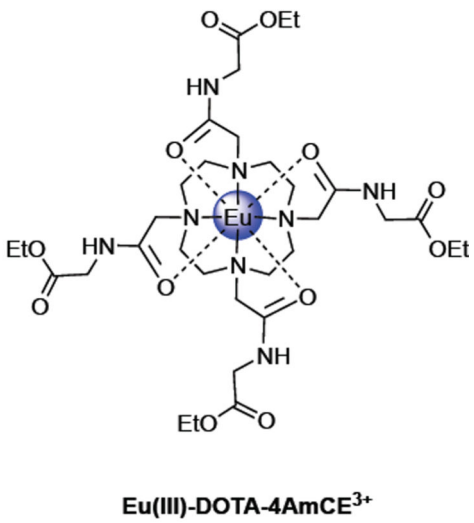

Eu(III)-DOTA-4AmCE^{3+}

Figure 57.

CEST spectrum of a 30 mM solution of a tetraamide Eu(III) analogue, Eu(III)-DOTA-4AmCE^{3+}, acquired at 270 MHz and 25 °C. The sharp signal reduction at 0 ppm is due to direct saturation of the bulk water signal, whereas the sharp reduction near +50 ppm is due to the PARACEST effect arising from saturation of water molecule coordinated to the lanthanide that is in exchange with the bulk solution.[276,278] Image adapted from reference 276 with permission. Copyright 2006 Royal Society of Chemistry).

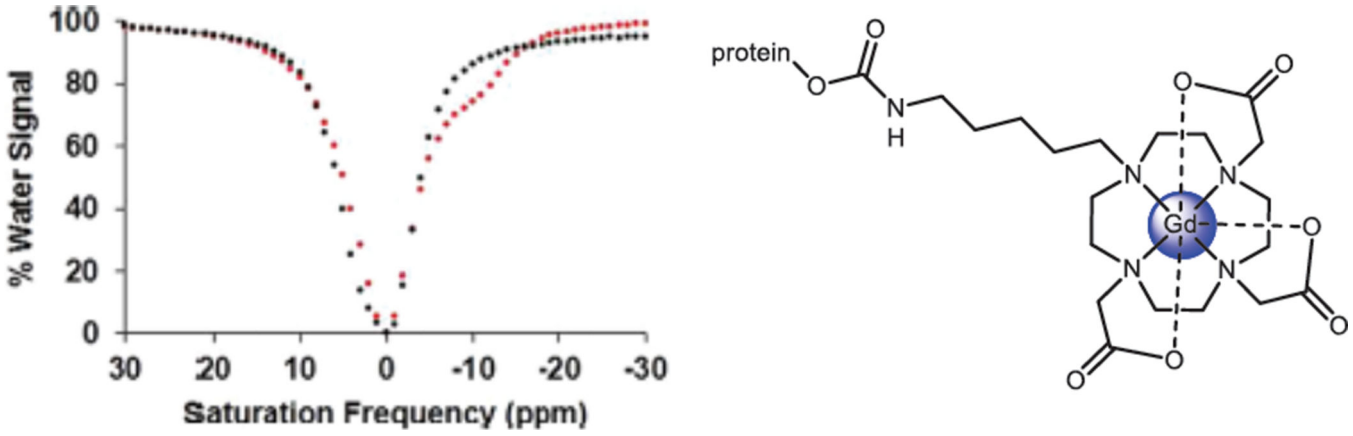

Figure 58.

Spectrum showing change in CEST before (black) and after (red) covalent binding of Tm-DO3A-cadaverine (right) to glutamine side chains of albumin by transglutaminase. Upon creation of the new bond by the enzyme, CEST decreased at +4.6 ppm and increased at −9.2 ppm.[275,279] (Figure reproduced with permission from reference 279. Copyright 2013 American Chemical Society.)

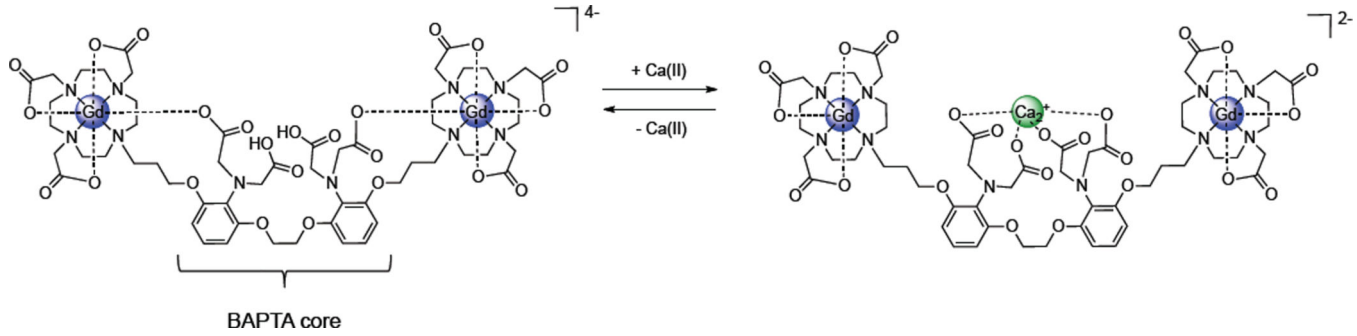

Figure 59.

The Ca(II)-sensitive DOPTA-Gd, a *q*-modulated probe, exhibits a 75% increase in relaxivity in the presence of physiologically relevant concentrations of Ca(II).[275,283,288]

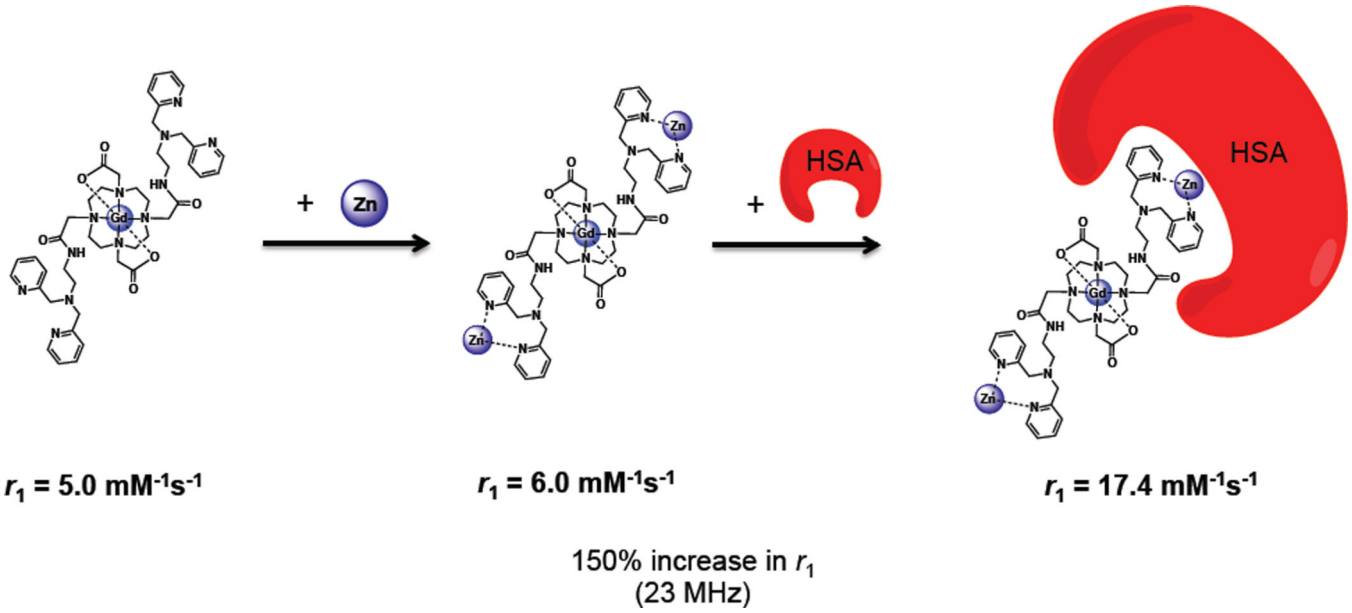

Figure 60.

The relaxivity of the Zn(II) activated Gd-DOTA-diBPEN, a τ_r modulated contrast agent, increases more than 150% upon the addition of Zn(II), in the presence of HSA.[287]

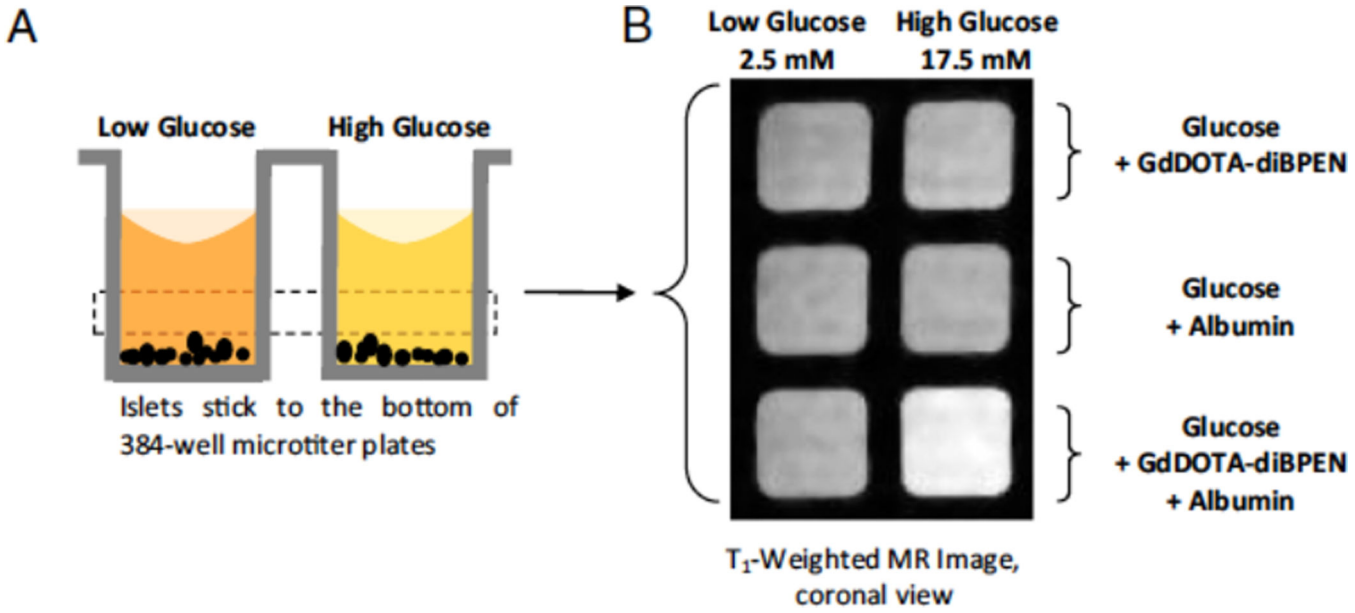

Figure 61.

In an ex vivo experiment, Gd-DOTA-diBPEN was able to detect changes in extracellular Zn(II) concentration following the addition of an insulin-stimulating concentration of glucose to isolated β-islet cells.[292] (Figure reproduced with permission from reference 292. Copyright 2012 Elsevier.)

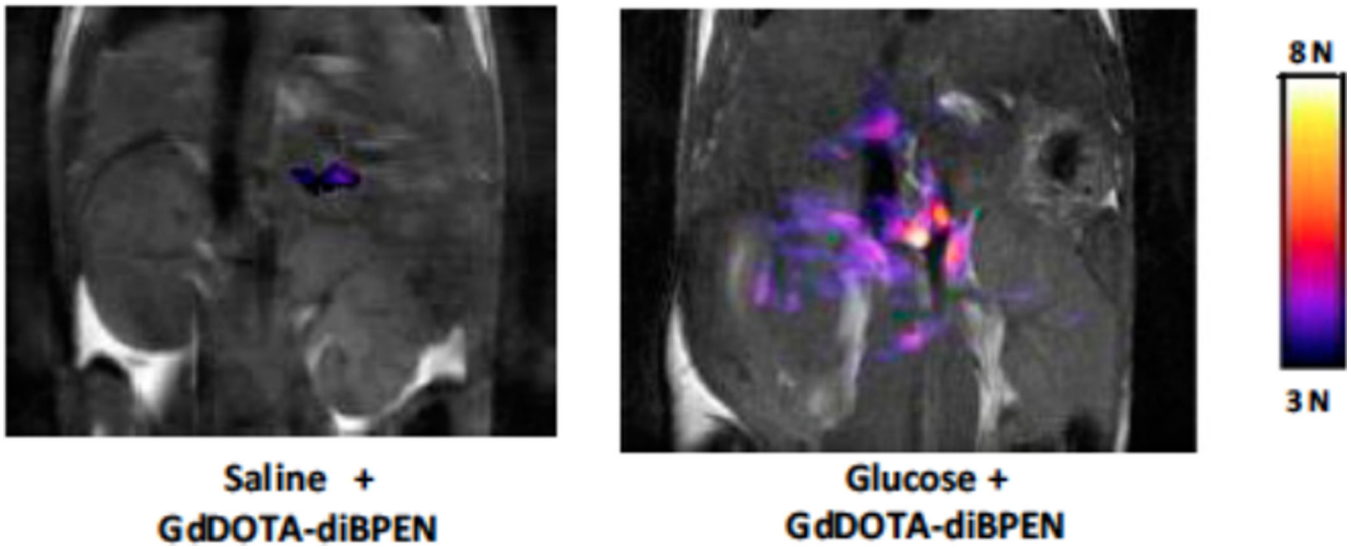

Figure 62.

In vivo images acquired by Sherry et al. of the abdominal region of a 12-week old mouse following IP injection of either saline (left) or glucose (right) and subsequent tail vein injection of the Zn(II)-activated Gd-DOTA-diBPEN.[292] Significant contrast enhancement in the area of the pancreas was observed following the administration of glucose and Gd-DOTA-diBPEN, indicating that the agent is capable of detecting fluctuations in the concentration of Zn(II) associated with insulin release by β-islet cells. (Figure reproduced with permission from reference 292. Copyright 2012 Elsevier.)

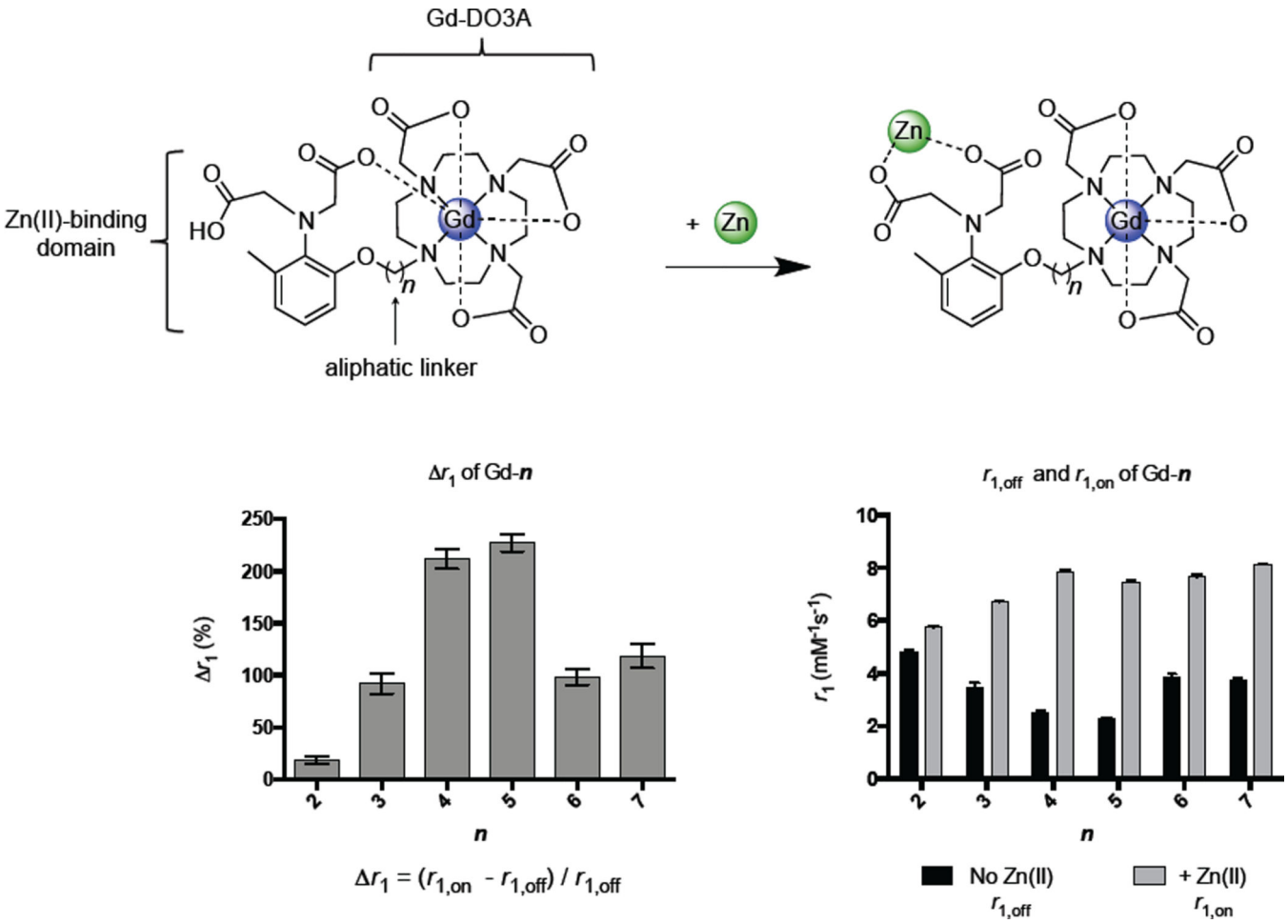

Figure 63.

The Gd-daa-*n* series of Zn(II) activated contrast agents developed by Meade et al. consists of a Zn(II) binding domain conjugated to a Gd-DO3A chelate by an aliphatic linker (top). The change in relaxivity upon the addition of Zn(II) strongly depends on the length of the aliphatic linker, *n*.[274] Figure reproduced with permission from reference 274. Copyright 2013 American Chemical Society.

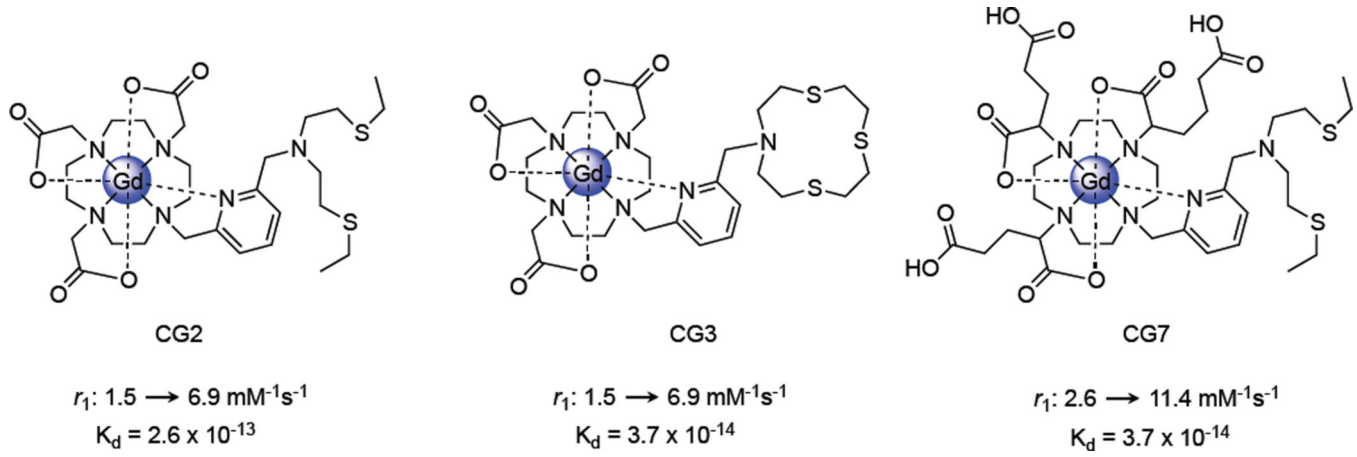

Figure 64.

Copper-activated MR contrast agents developed by Chang et al., which show remarkable affinity and selectivity for copper over other biologically relevant metal cations as well as an extremely large change in relaxivity in response to the presence of copper.[291,302,303]

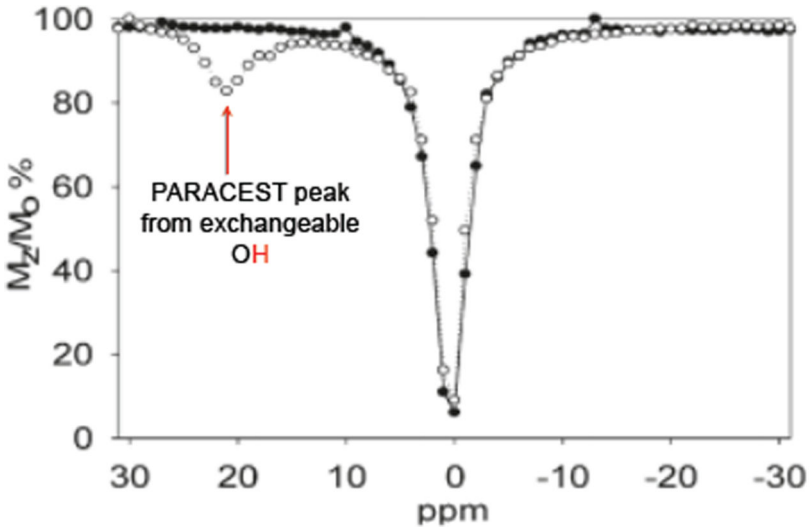

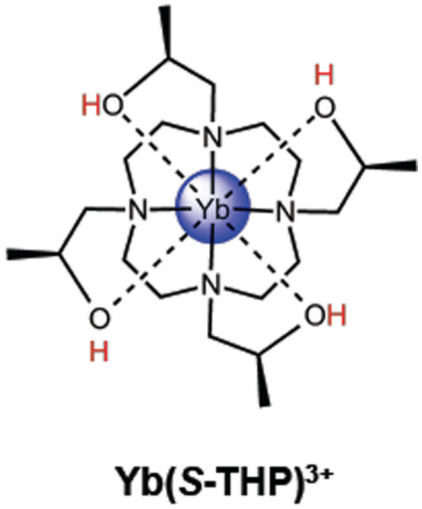

Figure 65.

PARACEST spectrum of 5 mM Yb(*S*-THP)$^{3+}$ at pH 7.0 before (closed circles) and after (open circles) the addition of 10 mM diethyl phosphate (DEP). The PARACEST peak arising from the exchangeable alcohol protons (near 20 ppm) appears only after the addition of DEP.[293–295] (Figure reproduced with permission from reference 294. Copyright 2010 American Chemical Society.)

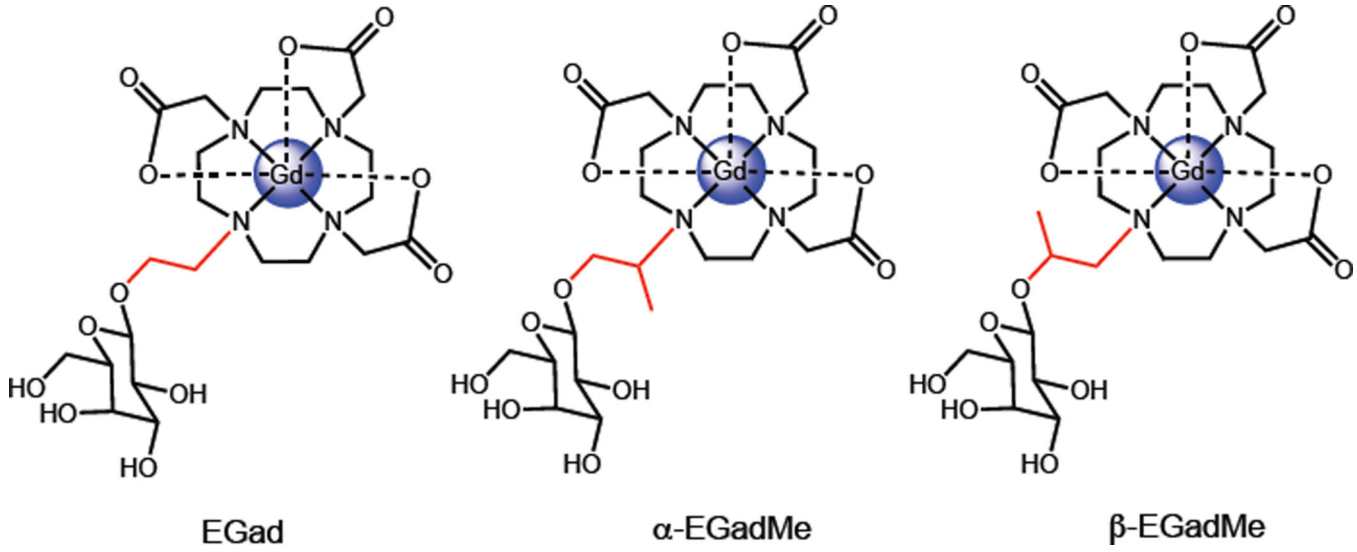

Figure 66.

The EGad series of bioresponsive MRI contrast agents responds to the presence of β-galactosidase.[263–266] The first generation, EGad (left), showed only a 20% increase in relaxivity in the presence of β-gal. The introduction of a methyl group to the linker between the chelate and the sugar moiety, either α (center) or β (right) to the macrocycle, increases this Δr_1 to 40–50%.

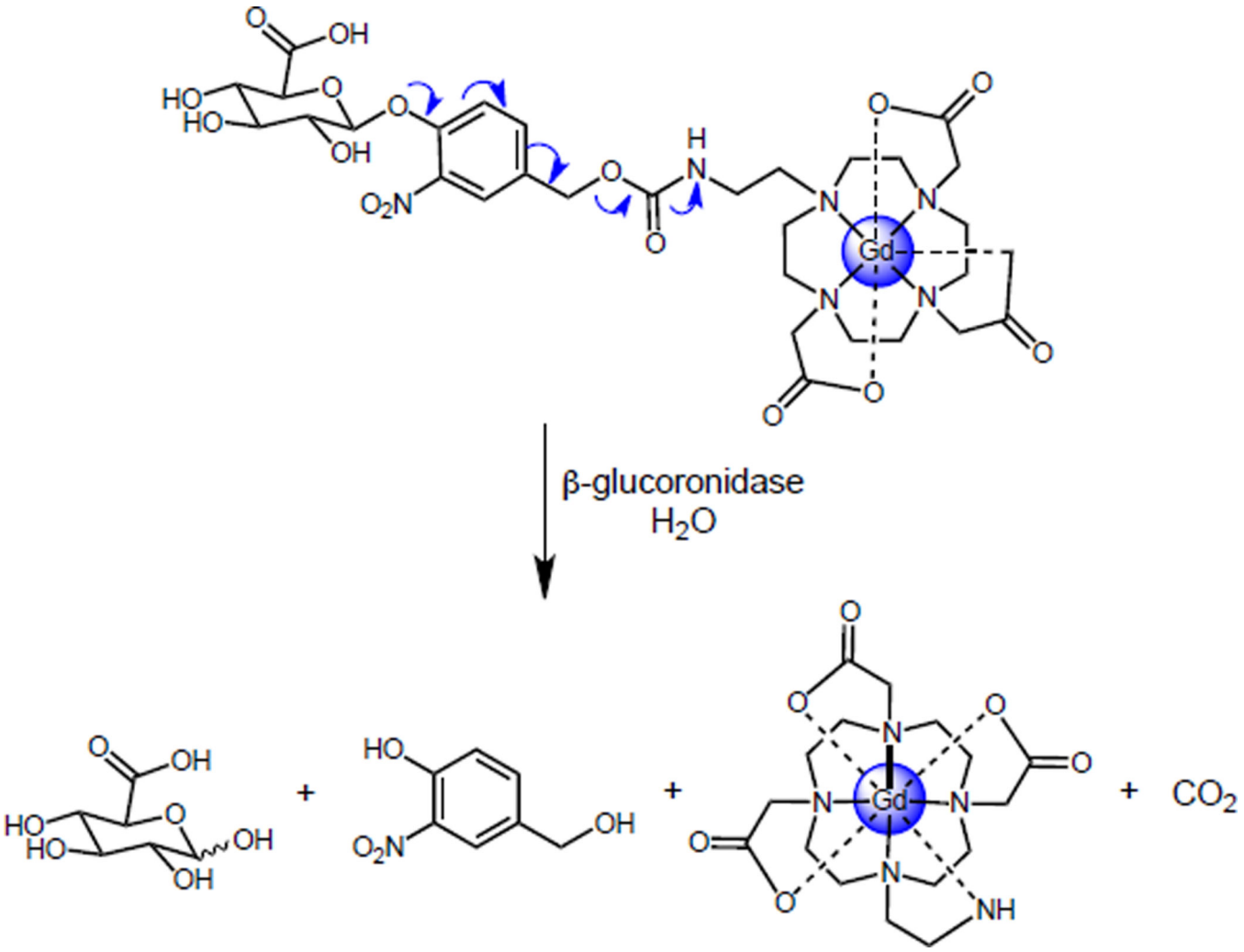

Figure 67.

In the presence of β-glucoronidase, the sugar moiety of the agent depicted is cleaved, initiating an electron cascade that causes the dissociation of the self-immolative linker.[297,299]

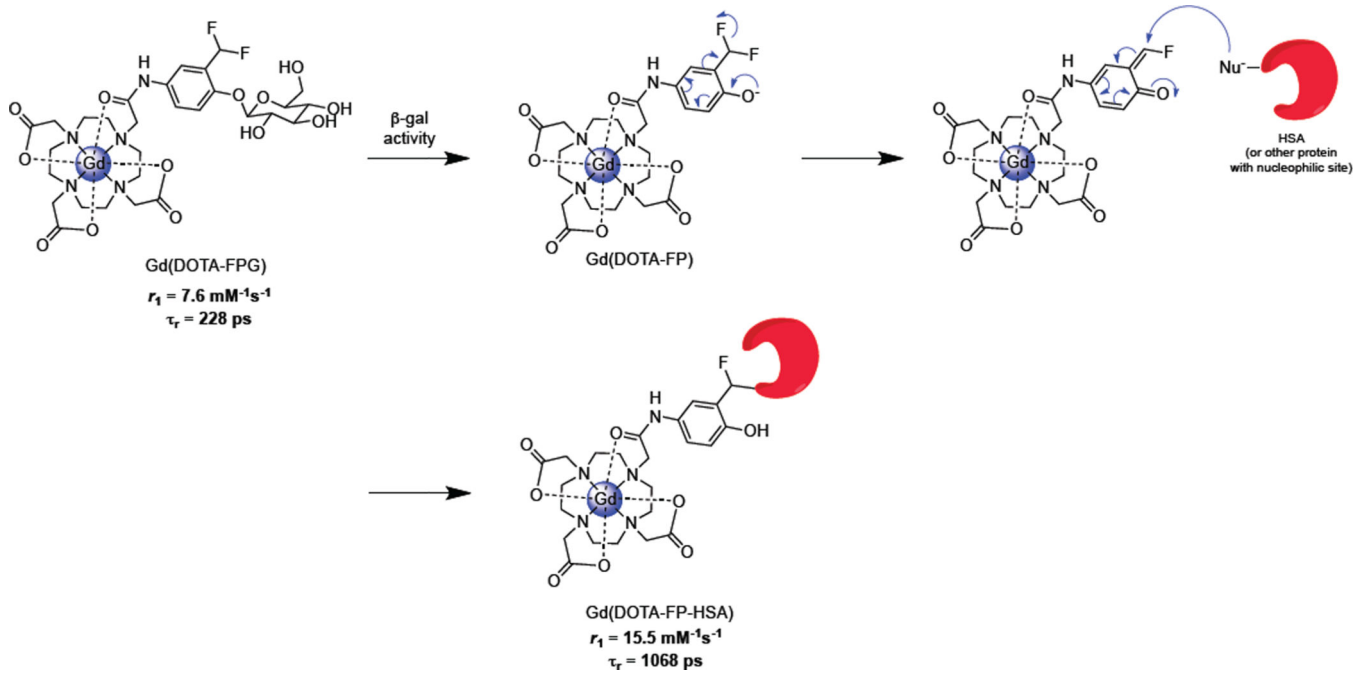

Figure 68.

In the presence of β-galactosidase, the sugar moiety of Gd(DOTA-FPG) is cleaved. Subsequent rearrangement results in the formation of a highly reactive electrophile that is rapidly attacked by a nucleophilic site on HSA (or another available protein) to form a high molecular weight adduct.[299]

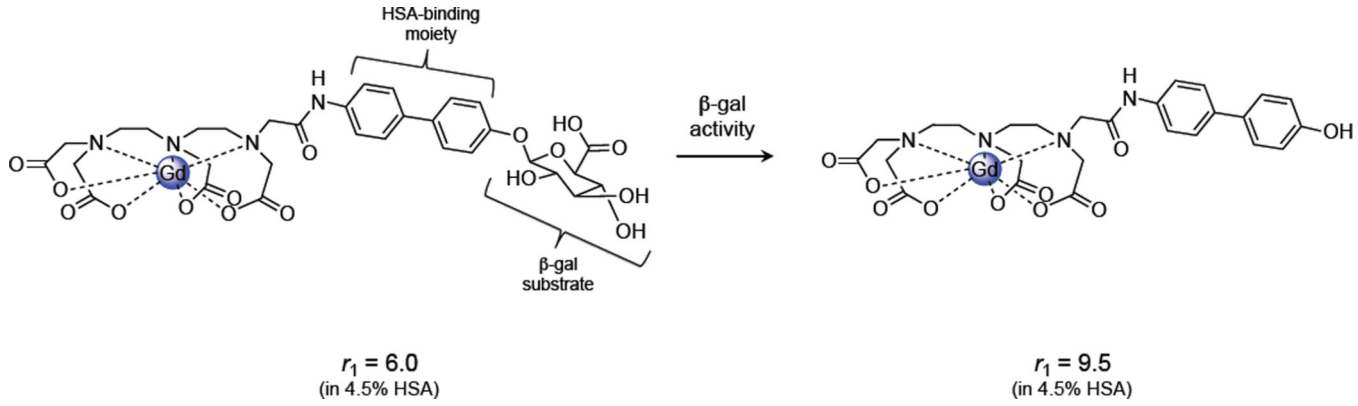

Figure 69.

Following enzymatic cleavage of the sugar substrate, the complex terminates in a hydrophobic biphenyl moiety that has a high affinity for HSA. Once the complex forms a non-covalent adduct with the protein, both the τ_R and the relaxivity of the complex increase.[298]

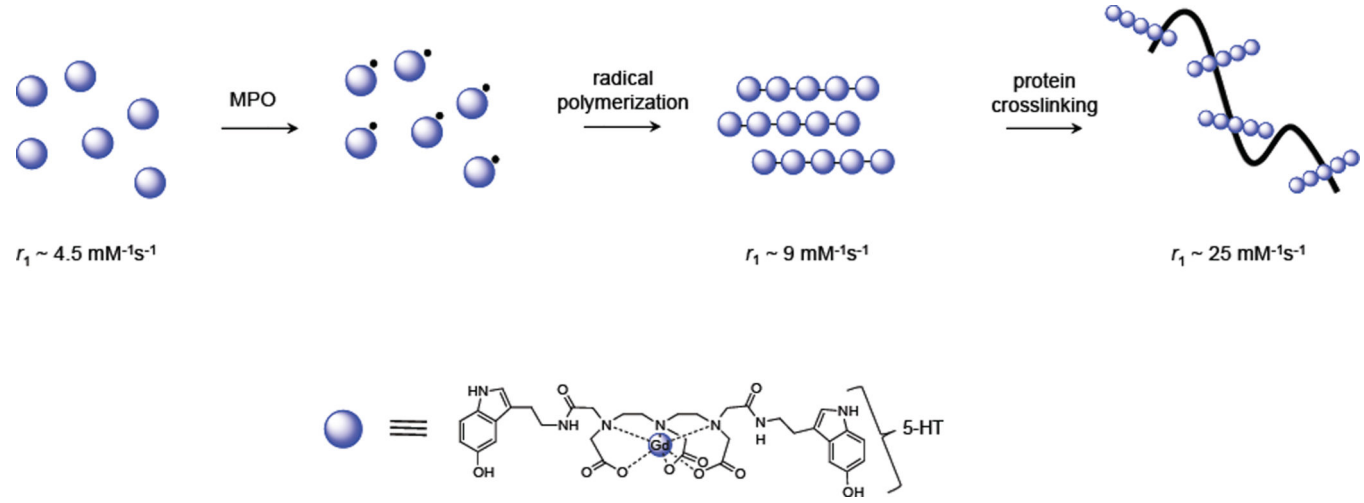

Figure 70.

In the presence of MPO, the 5-HT moieties of Gd-MPO become oxidized and form radicals. Subsequent radical polymerization produces oligomers up to five units long. These oligomers can then become cross-linked through interactions with endogenous proteins, further increasing the molecular weight, and consequently the τ_R and relaxivity, of the contrast agent.[306–309]

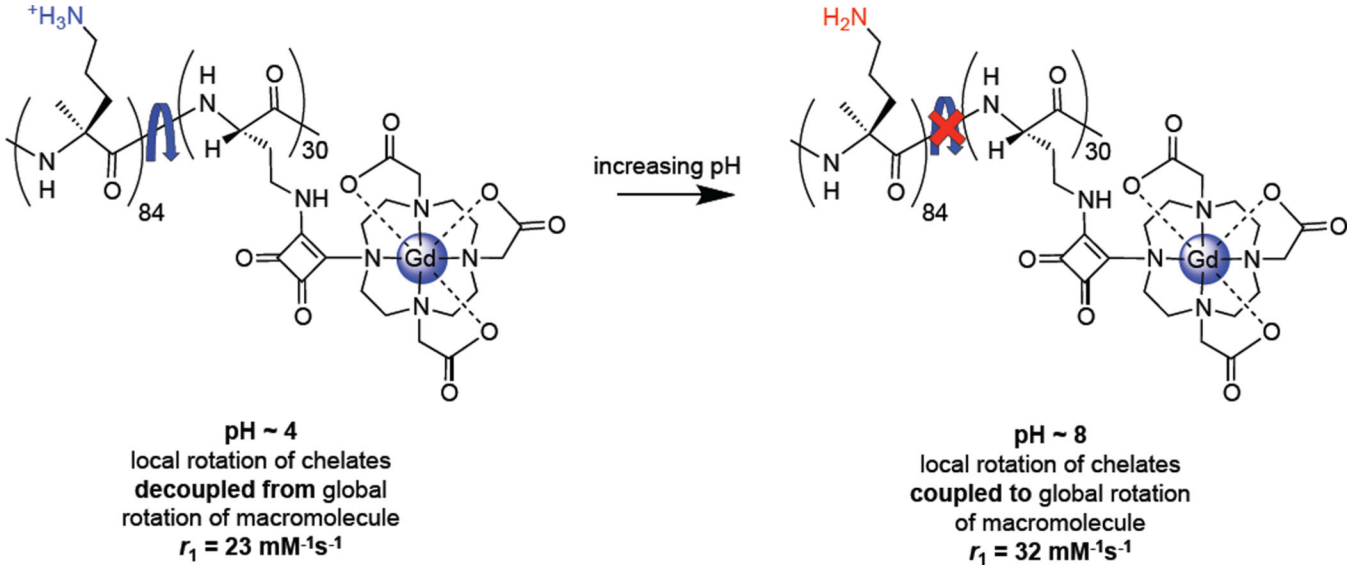

Figure 71.

τ_R-modulated, pH responsive probe developed by Aime et al.[312,316,317] As the pH increases, the peptide structure becomes more rigid, increasing both the τ_R and the relaxivity of the complex.

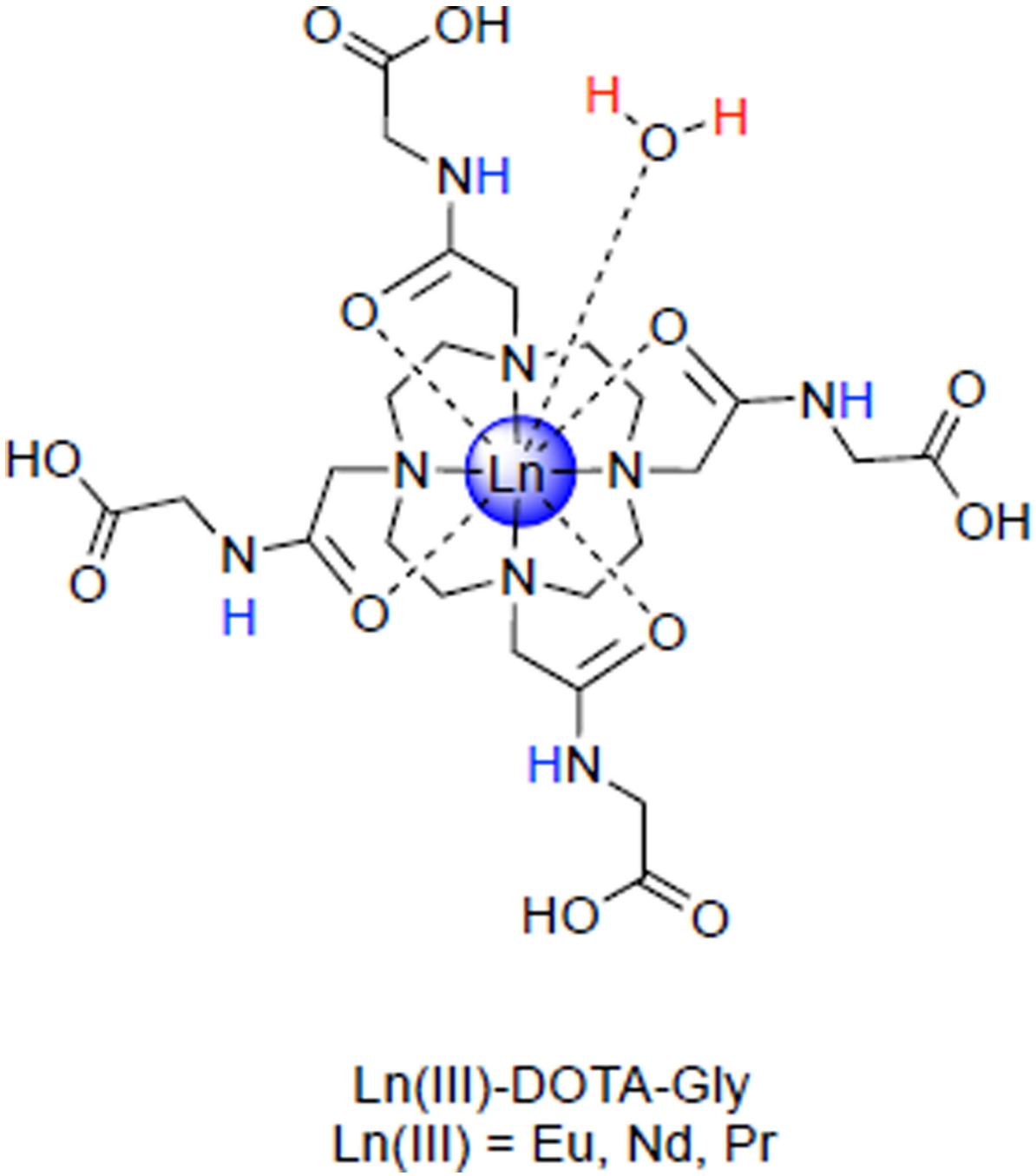

Figure 72.

pH responsive PARACEST probe, Ln(III)-DOTAM-Gly, containing two pools of exchangeable protons: those of the coordinated water molecule (red) and those of the amide groups on the pendant arms (blue). These give rise to two separate PARACEST signals, the intensity of which can be monitored independently to give a ratiometric measure of pH.[318–320]

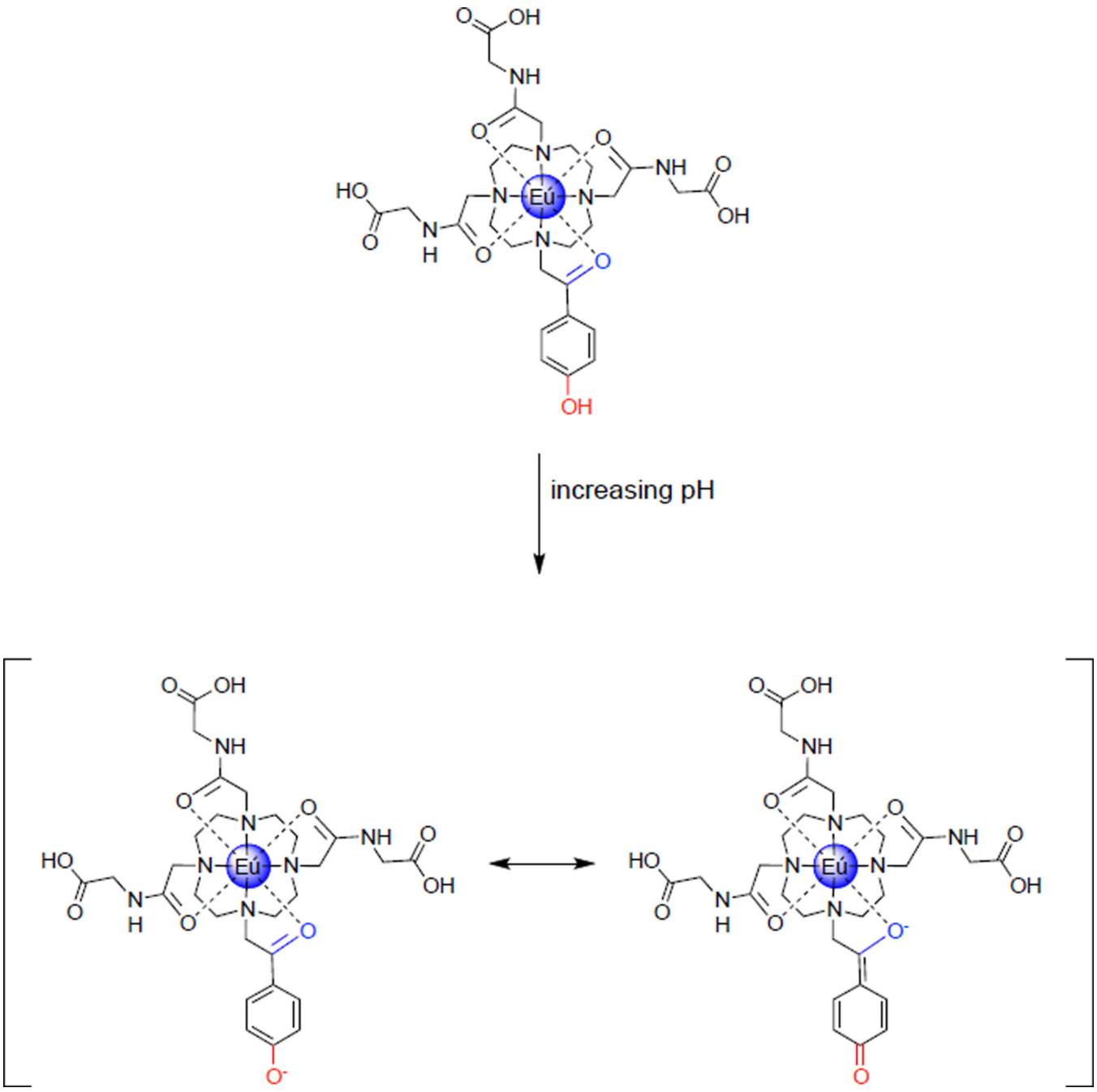

Figure 73.

As the pH increases, the phenol (red) becomes deprotonated (pKa ~6.5–6.7), allowing the complex to adopt a quinone like resonance structure in which the chelating ketone becomes negatively charged (blue), dramatically altering the coordination environment about the lanthanide center. This in turn changes both the frequency and the intensity of the PARACEST signal from the coordinated water molecule, allowing for ratiometric determination of pH from interrogation of a single pool of protons whose PARACEST signal is significantly shifted from the bulk water resonance.[318]